Digital Coherent Receivers for Passive Optical Networks

Domaniç LAVERY

A thesis submitted to the University College London (UCL) for the degree of Doctor of Philosophy

Optical Networks Group
Department of Electronic and Electrical Engineering
University College London (UCL)

September 2013

I, Domaniç Joseph Peter Lavery, confirm that the work presented in this thesis is my own. Where information has been derived from other sources, I confirm that this has been indicated.

Abstract

THE WORK presented herein explores the use of digital coherent receivers in loss-limited transmission with a view to implementation in a 100 km long-reach passive optical network (LR-PON) with a net data rate of 10 Gbit/s per optical network unit.

Optical power receiver sensitivity limits are investigated for C-band coherent receivers. Coherent-enabled advanced (amplitude, phase, and polarisation) modulation schemes are characterised in terms of electronic and optical bandwidth requirements and power efficiency to determine the optimum modulation format for a high capacity LR-PON. Including the net coding gain achievable with forward error correction, the high power efficiency of polarisation switched (PS) quadrature phase shift keying (QPSK) enables an experimental demonstration of 4 photons/bit receiver sensitivity, while polarisation division multiplexed (PDM) QPSK enables transmission with 5 photons/bit sensitivity; a 0.5 dB power penalty. Nevertheless, PDM-QPSK is identified as the optimum modulation format for coherent LR-PON, due to its 1.25 dB bandwidth efficiency advantage over PS-QPSK.

A coherent access network architecture is developed using 10 Gbit/s PDM-QPSK channels in a wavelength division multiplexed configuration. Multiple access is achieved by using the frequency selectivity of the coherent receiver to provide gain to the channel of interest. Combined with high receiver sensitivity, this demonstrates the feasibility of colourless network operation supporting 1024 channels. In bidirectional transmission, crosstalk from backscattering of optical power is mitigated using the receiver frequency selectivity and by using pulse shaping to restrict the optical channel bandwidth. A reflection-to-signal power ratio of 18.5 dB is tolerated without penalty.

Practical realisation is addressed by exploring low complexity, multiplier-free digital signal processing (DSP) algorithms for adaptive channel equalisation; algorithms are identified that can be used without penalty. Finally, to address issues of integration, tunable local oscillator lasers, suitable for monolithic integration, are investigated. The receiver DSP is modified to overcome the additional intensity noise from these lasers. In this scenario, the reduced receiver sensitivity would still enable an LR-PON with 128 channels.

Acknowledgements

WITH the utmost sincerity, I wish to thank my academic supervisors, Dr. Seb J. Savory and Prof. Polina Bayvel, for sharing their unique knowledge, experience and insight throughout my time at UCL. Indeed, without their support and guidance, none of this work would have been possible. I also wish to express my gratitude for being given the opportunity to pursue this Ph.D and for their faith in my ability undertake research; it has been amongst my most enjoyable and rewarding experiences.

I would like to thank Drs. Benn C. Thomsen and Robert I. Killey who have both been so generous with their time, particularly BCT for explaining and rectifying many lab related issues (phase bias ground loops, to name a memorable one).

For so much (too much to describe here) I thank Drs. Carsten Behrens and David S. Millar (perhaps foremost for their patience in introducing me to DSP), Drs. Sergejs Makovejs, Enrico Torrengo and Robert Maher (for introductions to the many and varied experimental techniques in communications research) and Dr. José Mendinueta (for your unforgettably kind welcome on my first day at UCL, and for this beautiful thesis template). Thanks also to Dr. Kai Shi and David J. Ives for discussions on the origin and nature of RIN and to Milen Paskov for discussing early drafts of this thesis.

For the loan of the low noise figure EDFA (chapter 3), thanks are due to the Optoelectronics Research Centre, University of Southampton; particularly Prof. Periklis Petropoulos and Dr. Sheng Liu for explaining the finer details of this amplifier.

I would also like to thank the financial contributors, without whom this work could not have been undertaken; namely the Engineering and Physical Sciences Research Council (EPSRC) and Oclaro Inc. who sponsored the CASE studentship. Additional thanks are extended to Oclaro for the use of their DS-DBR laser (chapter 5).

My family have offered me unceasing support throughout my studies, and this stage has been no exception. My parents, Bernard and Pirlanta, and my wife, Zoë, know that they will have my love and gratitude, always.

Finally, I thank the members of the ONG for their kindness and friendship, which has made the last few years so splendid. I take this opportunity to especially thank the newer members of the optical networks group for many a good discussion (academic or otherwise, usually over coffee) and I wish them all the very best of luck in all their endeavours.

Contents

List of Figures

List of Tables

1 Introduction

CONSUMER demand for high data rate communications has grown exponentially over the last three decades. Recent forecasts indicate that annual, global, Internet Protocol (IP) traffic will reach 828 exabytes (1 exabyte $= 2^{18}$ bytes) in 2014, exceed 1 zettabyte[1] (1 zettabyte $= 2^{21}$ bytes) during 2015, and grow to 1.3 zettabytes by year end 2016 [1]. This estimated usage is actually in excess of the predictions made by the same analysts just a year earlier (767 exabytes in 2014) [2, 3], indicating that this trend shows no sign of abating.

Rapid and continuous development of data-intensive web applications and services has driven this demand, with the most rapid growth area being bandwidth-intensive video-on-demand services; overtaking peer-to-peer networking in 2010 as the single most prevalent internet traffic type, and currently accounting for over 50% of consumer internet traffic [1].

Whilst video-on-demand impacts heavily on core network bandwidth requirements, the ultimate destination for this traffic is in the access network. Access networks must evolve in parallel to core networks in order to match consumer demand. The trend for access networks is well established; consumer bandwidth demand will grow by 50% year-on-year. This trend, dubbed Nielsen's law after the analyst Jakob Nielsen, is shown in Fig. 1.1. Considering just the United Kingdom, 100 Mbit/s broadband connections are currently available, and Fibre to the Node, Curb, Building, or Home

[1] In context, 1 zettabyte per year is approximately ten million simultaneous 25 Mbit/s 1080p video streams.

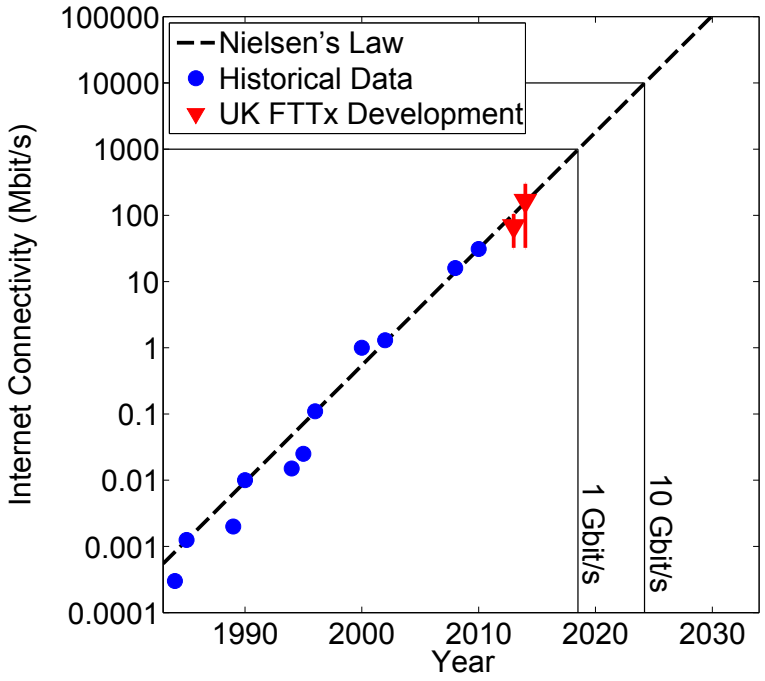

Figure 1.1: Nielsen's law of internet bandwidth: a high-end user's connection speed increases by 50% per year [4]. For reference, the FTTx technologies scheduled for deployment in the United Kingdom over the next two years are also shown [5, 6]. Vertical bars indicate the range of available FTTx connection speeds. The projected connection speeds indicated are for 1 Gbit/s (mid 2018) and 10 Gbit/s (early 2024).

(FTTx) deployments in 2014 will see this at least double [5]; in line with Nielsen's projections. It is then compelling to ask: when will Gigabit/s transceivers be required for consumer deployments? The projection indicates that 1 Gbit/s will be required by mid 2018, followed by 10 Gbit/s early in 2024 (indicated on Fig. 1.1) suggesting the imperative for research in this area.

1.1 Introduction to passive optical networks

1.1.1 The requirement for optical access networks

Since its inception in the 1960s, the continuing development of the internet has been driven, symbiotically, by new applications and increases in bandwidth. In its early years, the internet was mainly used for data sharing in research and academia. However, with the introduction of email in the 1970s, and the World Wide Web in the 1990s, personal and commercial uses followed. At the end of the 20th century, the internet protocol was carried on ordinary copper (twisted pair) phone lines, originally designed for voice band signal transmission. For this reason, when using voice modems, connection speeds were limited to 56 kb/s per channel. The 1980s saw the introduction of the integrated services digital network (better known as ISDN), which combined three channels to

achieve a 144 kb/s (64+64+16 kb/s) symmetric (upstream/downstream) data rate [7].

For transmission over copper pairs, the fundamental limitation in data rate is line attenuation, which is proportional to the square root of the modulated frequency. This property results in the achievable data rate reducing with transmission distance. Coaxial cables offer a stopgap solution to this problem, as they have a wider usable bandwidth, with lower attenuation. The standard for cable communications is the data over cable service interface specification (DOCSIS, 1997), the most recent iteration of this standard enables typical downstream data rates of between 160 Mb/s and 320 Mb/s, which is achieved using combined amplitude and phase modulation, and shared between multiple users through power splitting [7].

To go beyond these data rates, the cable lengths must be shortened; reducing the line attenuation. To achieve this, optical fibres, which have relatively low attenuation, can be used for transmission to, or close to, a customer premises, before retransmission over a short cable link. These are collectively known as FTTx schemes.

There are two optical network architectures which can be used for FTTx distribution; Passive Optical Networks (PONs) or Active Optical Networks (AONs). The AON incorporates network elements for actively routing, amplifying, or otherwise repeating an optical signal. These include, but are not limited to, optical burst switching [8], Erbium Doped Fibre Amplifiers (EDFAs), and Optical-Electrical-Optical conversion (OEO). Conversely, a PON does not include any of these network elements, being instead limited to distribution using, for example, Arrayed Waveguide Gratings (AWGs) and passive splitters.

The relative advantages of each architecture are clear. On the one hand, the AON is able to route optical signals on any wavelength to any receiver with negligible loss of signal power. The cost for this is the requirement of electrically powered remote nodes, whereas a PON requires power only at each transceiver location. The disadvantage of a PON is that fibre attenuation and splitter loss limit both the reach and capacity of the network.

While AONs offer advantages in terms of capacity, if the fibre attenuation can be overcome with sufficiently sensitive receivers then PONs offer the potential for significant cost savings [9], making them ideal for multiple users. It is this economic element which drives research in PONs. The following section describes how a PON can be used to increase network capacity, and shows some standardised PON architectures, noting the achievable capacity in each case.

1.1.2 Topology of an access network

The telecommunications network has been designed with a hierarchical structure such that the majority of traffic routing is confined to the ‘backbone network’, with metropo-

litan area networks (or 'metro networks') connected to the backbone network through a point of presence (POP). In turn, the metro network carries traffic through to customer (subscriber) premises via access nodes. How these network elements are connected in practice is down to individual network design choices; there are several network topologies which can be used, and some of these are shown in Fig. 1.2.

Figure 1.2: Example metro/access network architectures by Saleh and Simmons (1999) [10] ©IEEE (1999). In this work, the focus is on the passive tree network for access (top left).

Access networks comprise the section of a communications infrastructure that connects customers to internet carriers and onto the wider network. This section of the network covers a large area and, as such, equipment such as routers or repeaters will be located away from the point of presence/central office. This incurs not only a real estate cost, but also the operational cost of maintaining the real estate which houses the remote node. Therefore, entirely passive networks are favoured for use in optical access.

In 1995, the Full Service Access Network (FSAN) consortium was formed with the objective of standardising the requirements of PON architectures for optical access. The first standard ([11], 2001-2006), the ATM PON (APON) and the derived standard, the Broadband PON (BPON). Although the line rates in the standard are flexible, the specified maximum downstream data rate for a BPON is 1244.16 Mb/s, however commercial deployments have mainly used the configuration shown in Table 1.1 [12]. In this architecture, capacity is divided between multiple users using Time Division Multiplexing (TDM). A power splitting network architecture is specified for these PONs; a schematic is shown in Fig. 1.3.

To increase capacity beyond BPON, the Gigabit-Capable Passive Optical Network (GPON) recommendations were developed ([13], 2003-2008). A typical GPON

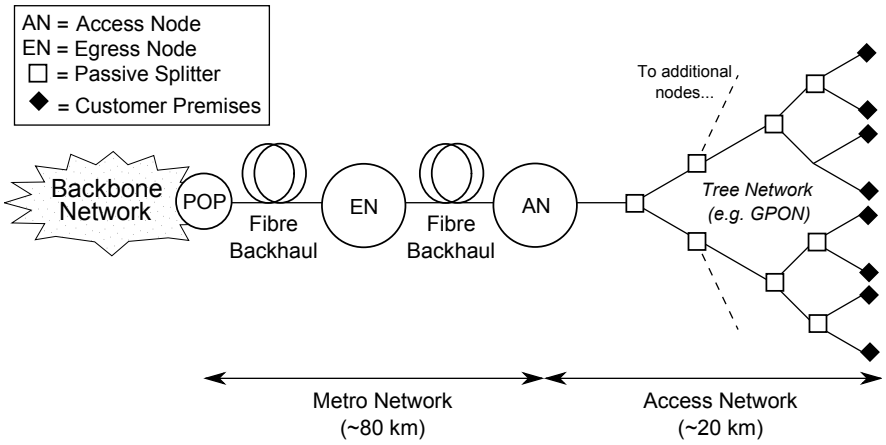

Figure 1.3: Passive tree access network (e.g. GPON) and metro network.

employs a 1:32 split ratio (32 subscribers from one access node) offering an aggregate capacity of between 1 and 2 Gbit/s, divided between individual subscribers using time division multiplexing. The transceiver technology is not specified as part of the GPON standard, however deployments have exclusively employed direct detection receivers. Beyond the GPON specification, work has begun on the XG-PON (10 Gbit/s PON), ([14], 2010) to meet increased bandwidth demands.

Thus far, all the architectures described are power splitting PONs; that is, a passive splitter is used to divide the signal equally to all customer premises (Fig. 1.3). Therefore, the receiver requires a minimum optical signal power to operate without error (the receiver sensitivity), such that the optical power budget – the total power which can be assigned for transmission and signal splitting – is reduced by $10\log_{10}(N)$ dB for an ideal splitter, where the number of subscribers is N. This makes the power sensitivity of the receiver a critical factor for PON [7].

Improvements in receiver sensitivity reduce the lower bound on the required received power for error-free transmission. This additional power can be used either to increase the maximum reach of a communications link, or to divide the signal amongst individual subscribers in a PON. It is the balance between these two parameters that is of interest in a FTTx scenario. The next subsection describes methods for increasing loss budget, and how this impacts on network architecture.

Table 1.1: TYPICAL PON SPECIFICATIONS

	A/BPON	GPON	XG-PON
Standard	ITU-T G.983	ITU-T G.984	ITU-T G.987
Downstream Data Rate (Gb/s)	0.622	2.488	9.9528
Upstream Data Rate (Gb/s)	0.155	1.244	2.488
Reach (km) [max]	20	20 [60]	20 [60]
Split ratio [max]	1:32	1:32 [1:128]	1:64 [1:256]

1.1.3 Long-reach PON architectures

In 2003, a greatly simplified access network was proposed and subsequently developed, where the subscriber premises are directly connected to the POP, removing the metro network entirely [15, 16, 9]. This network architecture is shown schematically in Fig. 1.4. The feasibility of this network architecture (termed the Long-Reach Passive Optical Network (LR-PON)) was established by 2009 [9]. However, to maintain a high split ratio (1:1024, compared with the typical 1:32), it was found that a midspan amplifier, prior to the passive split, was necessary to compensate for splitter loss. Additionally, due to the use of a single intensity modulated wavelength channel, the *aggregate* downstream capacity was limited to 10 Gbit/s. Crucially, capacity is divided between all the subscribers on the network (a contended data rate).

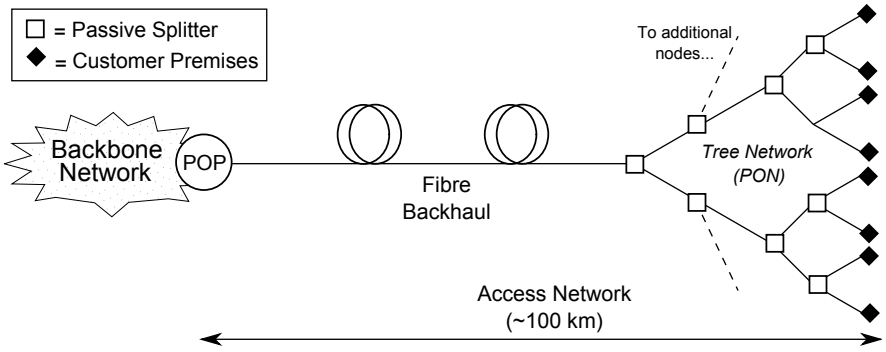

Figure 1.4: Long reach passive optical access network.

Extending the reach of optical access networks beyond the 20 km specified by the GPON standard has the potential to significantly cut operational costs through network consolidation. However, this is not a completely new idea. The amended GPON standard permits the use of a reach extender to enable standards-compliant transmission over 60 km while doubling the split ratio to 1:64 [17] (or even 1:128 as permitted by the original standard [18]). An example of an extended-reach GPON employing a midspan EDFA is shown in Fig. 1.5(a). The difficulty with this approach is that the aggregate capacity of the network (2.4 Gbit/s symmetric upstream/downstream) does not change as, ultimately, all the Optical Network Units (ONUs) are served by a single wavelength pair modulated using TDM.

One approach to remove the requirement of midspan amplification is to split the signal after the fibre backhaul by using an AWG, as in [19]; avoiding penalties due to passive splitting while effectively dedicating a wavelength to each ONU, as shown in Fig 1.5(b). The disadvantage of this approach is that it colours the network, reducing the options for reconfigurability and presenting a challenge for inventory and deployment. For example, each transmitter needs to operate on a wavelength which is locked to the passband of the AWG, while the upstream channel from an ONU must be matched to its particular port on the AWG. This problem can be overcome to some extent through

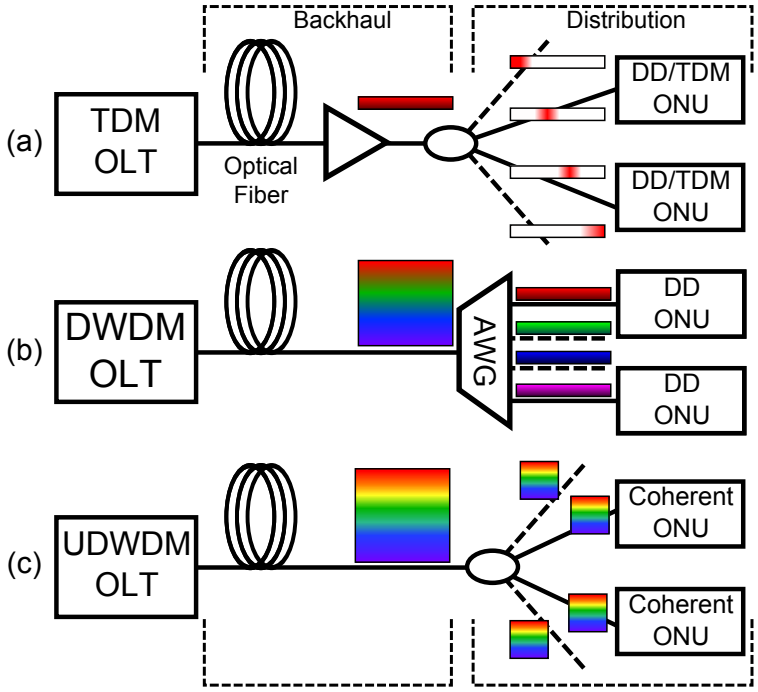

Figure 1.5: Long-reach PON architectures. The backhaul section is typically 80-90km with a passive distribution section of 10-20km. (a) TDM-PON (for a GPON, the entire fibre length is limited to 60 km), (b) WDM-PON, (c) coherent UDWDM-PON.

the transmission of a seed comb (several Wavelength Division Multiplexing (WDM) channels equally frequency spaced) from the Optical Line Terminal (OLT) which is remodulated (usually using a reflective semiconductor optical amplifier) at the ONU for upstream transmission, thereby avoiding the need for *a priori* knowledge of the network configuration. (Having a colourless [wavelength-independent] ONU solves inventory issues, because every ONU is identical.) However, the additional noise added to the carrier through amplification and remodulation dramatically reduces the power budget of the upstream signal. Conveniently, because the seed wavelength is generated at the OLT, homodyne coherent detection is used in this case to overcome these additional losses [20]. This also means that an advanced modulation format (such as Quadrature Phase Shift Keying (QPSK)) can be used for upstream transmission, reducing the electrical bandwidth requirements of the transmitter [20].

The reach and capacity limits of these Direct Detection (DD) receivers for optical access have recently been explored without resorting to remodulation techniques. The hybrid WDM-TDM network is effectively a combination of the architectures shown in Fig 1.5(a) and (b). Here, the ONU is made colourless by incorporating a piezo-electrically controlled tunable laser for upstream transmission. Recent work demonstrated impressive reach (100 km) and split ratios of 1:512 per wavelength when using 32-channel WDM; effectively supporting up to 16384 ONUs on a single PON [21, 22]. Due to the low sensitivity of direct detection receivers, the signal required multiple regenerations using EDFAs at a local exchange meaning that only the dis-

tribution section of the network was truly passive. With this configuration, not all of the economic benefits of long reach can be realised because the local exchange is still required to house equipment such as optical amplifiers and AWGs. Additionally, because the network is still based on TDM, the data rate per user is limited to 20 Mbit/s (each WDM channel carries 10 Gbit/s).

1.1.4 Coherent receivers for passive optical networks

In submarine systems, the move from 10 Gbit/s channels to 40 Gbit/s and beyond was enabled by the use of coherent detection [23]. Indeed, phase- and polarisation- diverse coherent receivers (section 2.3) enable the use of modulation schemes (section 2.2) such as polarisation-division-multiplexed quadrature phase shift keying (PDM-QPSK) which takes advantage of all dimensions available for data transmission in a single mode optical fibre (phase and amplitude on both polarisations), enabling a reduction in optical and electrical bandwidth requirements. This is in contrast to direct detection receivers (on which optical access is currently based) which can only detect amplitude modulated signals. With the binary format On-Off Keying (OOK) in particular, the large optical bandwidth requirements incur a penalty in uncompensated transmission due to chromatic dispersion (see section 2.4.1) meaning that the data rate when using OOK is not scalable.

It was recently suggested that coherent networks (networks using coherent receivers and advanced modulation formats) would be an economically feasible way to increase network capacity, even if this involved optically complex coherent receivers at the ONU (for example, [24, 25, 26]). There are several engineering challenges associated with this approach. Specifically, it is important to reduce the optical complexity of the coherent receiver sufficiently to enable implementation in an access network. Further, it is not sufficient to use the coherent receiver as implemented in long-haul networks; the receiver must be redeveloped to be tolerant to the noise sources that are unique to access networks (see chapters 2 and 5).

The proposed architecture, Fig 1.5(c), involves transmission of an Ultra Dense Wavelength Division Multiplexing (UDWDM) source[2] from the OLT and a passive midspan split such that each wavelength is simultaneously sent to every ONU. The channel of interest is then selected by retuning the Local Oscillator Laser (LO) in the ONU to generate a frequency offset between the channel of interest and the LO (Table 1.2); this heterodyne[3] receiver provides coherent gain that rejects the adjacent

[2] In this context, UDWDM refers to the number of WDM channels which, for full C-band, would be an order of magnitude greater than the number of channels achievable using direct detection receivers, due to the higher spectral efficiencies achievable with advanced modulation formats. See section 2.2.

[3] Heterodyne receivers simplify the detection process by forcing a frequency offset between signal and LO, which ensures that the signal is all real (a single quadrature). A full description of this technique can be found in [27].

channels while avoiding the use of narrow-band tunable optical filters (the mathematical basis for this effect is described in section 2.3.1). The upstream channels are generated by splitting the LO for reuse as the signal, and frequency converting the signal before modulation and transmission. Provided the LO has tuned to the downstream channel, the upstream comb is automatically fixed to a grid.

This network architecture is completely reconfigurable because all downstream channels are sent to all receivers. For example, if a user wished to increase available bandwidth, additional ONUs could be situated at the access point. Each ONU adds an additional wavelength for communication, effectively scaling capacity at that location. However, the disadvantage of using a colourless splitter is the division of optical power between ONUs. If the power budget is too low to support this, an AWG could be used instead (as in the above scenario), but at the expense of dynamic reconfigurability. A hybrid solution is to use a coarse WDM demultiplexer (an AWG with a high free spectral range) followed by passive splitters. In this way, the network can be partially reconfigured while reducing the required power budget. The potential for such network architectures has been explored in, for example, [28].

A simple example of this approach is coherent OOK [26]. Here, only a single photodiode is required to detect the OOK signal (as in the DD case) however, coherent gain from the LO permits a denser channel spacing than could be realistically achieved with optical filters (for example an AWG) while also being reconfigurable through retuning the LO (see section 2.3.1). An additional advantage of this approach is that the receiver sensitivity can approach the quantum noise limit (see section 2.3.2) without narrow-band optical filters[4].

A more recent example of the coherent approach demonstrated the feasibility of using up to 1024 wavelength channels in the UDWDM configuration to provide 1 Gbit/s/λ over up to 100 km [25]. This was achieved by employing the advanced modulation format QPSK, which encodes twice the information per symbol versus OOK. Through the use of coherent detection, the signal could be subsequently digitised using Analogue-to-Digital Converters (ADCs) and equalised in the digital domain, recovering the State of Polarisation (SOP), which therefore allows an arbitrary SOP to be launched into the fibre. The disadvantage of this approach is that, because the receiver is heterodyne, this requires ADCs that have a higher sampling frequency, greater than twice the symbol rate (see Table 1.2). Note, however, that proof-of-concept, realtime operation of this network has already been demonstrated [29]. It is only a small step from the polarisation-diverse heterodyne coherent solution to a network based on phase- and polarisation-diverse intradyne[5] coherent receivers, which have an intrinsic 3 dB shot noise limited sensitivity

[4]Note that noise from TIAs, finite LO power and LO noise sources all prevent such receivers attaining the theoretical sensitivity limit in practice.

[5]Intradyne in this context means that the frequency offset between signal and LO is not necessarily 0 Hz, and frequency tracking is performed after signal detection. This is the technique used in the work

Table 1.2: REQUIRED COHERENT RECEIVER BANDWIDTHS

Coherent Receiver Type	Intradyne Frequency (IF)	Minimum Photodetector Bandwidth
Homodyne	0	f_B
Intradyne	≈ 0	f_B
Heterodyne	IF $\geq f_B$	$2f_B$

gain over heterodyne receivers due to their measurement of the signal quadrature component [30]. For intradyne coherent reception the frequency offset between the signal and LO is free to vary so long as the sum of the signal and beat frequencies remain within the sampling bandwidth; although in practice this is limited by the algorithm chosen to track the frequency offset in the Digital Signal Processing (DSP). Again, a tunable LO laser can be used to select the channel of interest. Ordinarily, the ADCs in these receivers sample at twice the symbol rate (1 sample/symbol is required to avoid aliasing), resulting in reduced electrical bandwidth requirements when compared to heterodyne receivers. These electrical bandwidth requirements are further reduced when the cardinality of the modulation format is increased (see section 2.2); for example, symmetric 10 Gbit/s/λ has been demonstrated over 100 km using Polarisation Division Multiplexing (PDM)-QPSK at 3.125 GBd (requiring only 3.125 GHz receiver electrical bandwidth) [31]. As in the heterodyne case, equalisation can be applied through the use of adaptive linear digital filters [32]. The downside to this receiver is the optical complexity; requiring a dual-polarisation 90^o optical hybrid to separate the in-phase and quadrature signal components (which is not required for heterodyne receivers), and at least four photodiodes and ADCs (compared to two for heterodyne).

Phase- and polarisation-diversity has previously been explored in the context of receiver sensitivity in [33], where it was shown that a homodyne receiver sensitivity was directly related to the power of the LO, but fundamentally limited by shot noise. This principle applies equally to heterodyne and intradyne receivers, although intradyne receivers have a 3 dB shot noise limited sensitivity gain over heterodyne receivers. It was also shown here that polarisation multiplexing does not affect receiver sensitivity (however, it does reduce transceiver bandwidth requirements). It is a key advantage of all coherent receivers that the coherent gain (and therefore their sensitivity) can be improved by simply increasing LO power; an option not available to direct detection receivers.

Of the LR-PON architectures investigated to date, networks based on heterodyne or intradyne coherent receivers offer the highest data rate per subscriber while being scalable and reconfigurable, although these advantages come at the expense of increased

presented in this thesis.

optical complexity. Notably, the data rate offered in these WDM scenarios is uncontended; in principle, the full data rate on each wavelength is available to each subscriber. In the case of a digital coherent receiver, some optical complexity can be transferred to the digital domain, and examples are provided later in this thesis where the benefits and challenges of an access network based on phase- and polarisation-diverse digital coherent receivers are considered.

1.2 Thesis outline

The remainder of this thesis is organised as follows. Chapter 2 introduces the requisite theory for long reach passive optical networks, coherent optical communications, and the associated digital signal processing. The fundamentals of digital coherent detection are described, with particular emphasis placed on the modulation schemes used herein.

Chapter 3 details research evaluating the power sensitivity limits of a coherent receiver. High-sensitivity modulation formats and receiver preamplification are investigated to increase the sensitivity of a digital coherent receiver. The trade-off between sensitivity and spectral efficiency is explored.

Chapter 4, informed by the results in chapter 3, assesses the feasibility of a wavelength division multiplexed coherent access network operating at 10 Gbit/s per wavelength.

Chapter 5 addresses the use of digital postprocessing in coherent receivers for optical access; algorithms for overcoming receiver impairments are derived and evaluated experimentally. In particular, this chapter deals with noise introduced by the local oscillator in a coherent receiver in the form of phase noise and relative intensity noise.

A summary of this thesis and conclusions are given in chapter 6. In light of these results, suggestions are given for further research in this area.

1.3 Original contributions of this thesis

The original contributions made in the course of the research described in this thesis are summarised as follows.

- Generation, transmission and detection of the power-efficient modulation format PS-QPSK (chapter 3), in collaboration with D. S. Millar, B. C. Thomsen, S. Makovejs and C. Behrens. This work resulted in the following publications [34, 35, 36, 37].

- Experimental demonstration of the sensitivity advantage of optically preamplified coherent receivers using advanced modulation formats and low noise optical

preamplifiers to achieve record receiver sensitivities (chapter 3). (The optical amplifier used in this work was produced independently by the Optoelectronics Research Centre, University of Southampton.) This work resulted in paper [38].

- Identification of the ideal modulation format for use in a coherent long-reach passive optical network. The resulting papers were [39, 40]. (Additional long-haul transmission results reported in [41].)

- The first investigations of phase- and polarisation-diverse digital coherent receivers for access networks, demonstrating the feasibility of both unidirectional and bidirectional transmission of PDM-QPSK at 10 Gbit/s per wavelength in a long reach WDM-PON (chapter 4). This work was completed with E. Torrengo who designed the subcarrier generation scheme and assisted with measurements. The publications which resulted from this work were [42, 31].

- Experimental evaluation of the impact of backreflections on receiver sensitivity in a bidirectional PON, showing the dependence of penalty on channel frequency spacing and the advantages gained by pulse shaping in mitigating the impact of backreflections in a bidirectional PON (chapter 4). C. Behrens and M. Paskov assisted with measurements. The resulting publications were [43] (without pulse shaping) and [44] (with Nyquist pulse shaping).

- Demonstration of the use of a monolithically integrated C-band tunable DS-DBR laser, suitable for deployment in access network scenarios. It was found that this laser exhibits low frequency RIN, therefore this work also details the design, implementation and experimental demonstration of a low-complexity digital filter for mitigating the impact of LO RIN in a coherent receiver with an unamplified front end (chapter 5). These investigations were undertaken with R. Maher and B. C. Thomsen who designed the electronic control for the DS-DBR laser and assisted with measurements of the DS-DBR laser linewidth and RIN, and D. S. Millar who assisted with the development of the digital filters used in this work. The papers resulting from this work are references [45, 46].

- Demonstration of LO laser phase noise measurement technique application to Digital Supermode Distributed Bragg Reflector (DS-DBR) laser for 6 GBd PDM-64QAM transmission (chapter 5). Experimental measurements taken with R. Maher, and simulations conducted with M Paskov. (In publication.)

- Demonstration of low complexity equaliser tap updates for a coherent access network (chapter 5). (As yet unpublished.)

1.4 List of publications

The following is an enumeration of original work published in the course of this research.

1. **D. Lavery**, R. Maher, M. Paskov, B.C. Thomsen, P. Bayvel, S.J. Savory, "**Coherent detection of 6 GBd DP-64QAM using a 1.4 MHz linewidth tunable laser**", IEEE Photonics Technology Letters (volume and paper number pending).

2. D. Cardenas, D. Madan, S. Win, **D. Lavery**, S. J. Savory, "**Fixed point and power consumption analysis of a coherent receiver for optical access networks implemented in FPGA**", Mo.3.C.4 in Proceedings of European Conference on Optical Communications 2013.

3. **D. Lavery**, M. Paskov, S. J. Savory, "**Spectral shaping for mitigating backreflections in a bidirectional 10 Gbit/s coherent WDM-PON**", OM2A.6 in Proceedings of Optical Fiber Communication Conference 2013.

4. D. S. Millar, **D. Lavery**, R. Maher, B. C. Thomsen, S. J. Savory, "**A Baud-rate sampled coherent transceiver with digital pulse shaping and interpolation**", OTu2I.2 in Proceedings of Optical Fiber Communication Conference 2013.

5. **D. Lavery**, R. Maher, D. S. Millar, B. C. Thomsen, P. Bayvel, S. J. Savory, "**Digital coherent receivers for long-reach optical access networks**", IEEE Journal of Lightwave Technology, **31** 4 (2013).

6. **D. Lavery**, R. Maher, D. S. Millar, B. C. Thomsen, P. Bayvel, S. J. Savory, "**Demonstration of 10 Gbit/s colorless coherent PON incorporating tunable DS-DBR lasers and low-complexity parallel DSP**", PDP5B.10 in Proceedings of Optical Fiber Communication Conference 2012.

7. **D. Lavery**, C. Behrens, S. J. Savory, "**On the impact of backreflections in a bidirectional 10 Gbit/s coherent WDM-PON**", OTh1F.3 in proceedings of the Optical Fiber Communication Conference (OFC) 2012.

8. C. Behrens, **D. Lavery**, S. J. Savory, "**Long-haul WDM transmission of PDM-8PSK and PDM-8QAM with nonlinear DSP**", OM3A.4 in proceedings of the Optical Fiber Communication Conference (OFC) 2012.

9. **D. Lavery**, S. Liu, Y. Jeong, J. Nilsson, P. Petropoulos, P. Bayvel, S. J. Savory, "**Realizing high sensitivity at 40 Gbit/s and 100 Gbit/s**", OW3H.5 in proceedings of the Optical Fiber Communication Conference (OFC) 2012.

10. **D. Lavery**, C. Behrens, S. J. Savory, "**A comparison of modulation formats for passive optical networks**", Optics Express, **19** 26 (2011).

11. **D. Lavery**, C. Behrens, S. Makovejs, D. S. Millar, R. I. Killey, S. J. Savory, P. Bayvel, "**Long-haul transmission of PS-QPSK at 100 Gb/s using digital backpropagation**", IEEE Photonics Technology Letters, **24** 3 (2012).

12. C. Behrens, **D. Lavery**, D. S. Millar, S. Makovejs, B. C. Thomsen, R. I. Killey, S. J. Savory, P. Bayvel, "**Ultra-long-haul transmission of 7×42.9 Gbit/s PS-QPSK and PM-BPSK**", Optics Express, **19** 26 (2011).

13. **D. Lavery**, C. Behrens, S. J. Savory, "**A comparison of modulation formats for passive optical networks**", Tu.5.C.5 in Proceedings of European Conference on Optical Communications 2011.

14. C. Behrens, **D. Lavery**, D. S. Millar, S. Makovejs, B. C. Thomsen, R. I. Killey, S. J. Savory, P. Bayvel, "**Ultra-long-haul transmission of 7×42.9Gbit/s PS-QPSK and PM-BPSK**", Mo.2.B.2 in Proceedings of European Conference on Optical Communications 2011.

15. D. S. Millar, **D. Lavery**, S. Makovejs, C. Behrens, B. C. Thomsen, P. Bayvel, S. J. Savory, "**Generation and long-haul transmission of polarization-switched QPSK at 42.9 Gb/s**", Optics Express, **19** 10 (2011).

16. **D. Lavery**, E. Torrengo, S. J. Savory, "**Bidirectional 10 Gbit/s long-reach WDM-PON using digital coherent receivers**", OTuB4 in Proceedings of Optical Fiber Communication Conference 2011.

17. **D. Lavery**, M. Ionescu, S. Makovejs, E. Torrengo, S. J. Savory, "**A long-reach ultra-dense 10 Gbit/s WDM-PON using a digital coherent receiver**", Optics Express, **18** 25 (2010).

18. S. Makovejs, D. S. Millar, **D. Lavery**, C. Behrens, R. I. Killey, S. J. Savory, P. Bayvel, "**Characterization of long-haul 112Gbit/s PDM-QAM-16 transmission with and without digital nonlinearity compensation**", Optics Express, **18** 12 (2010).

Papers Accepted for Publication:

1. P.M. Anandarajah, R. Zhou, R. Maher, **D. Lavery**, M. Paskov, B.C. Thomsen, S.J. Savory, and L.P. Barry, "**Gain switched multi-carrier transmitter in a long reach UDWDM PON with a digital coherent receiver**", Accepted for publication in OSA Optics Letters.

2. M. Paskov, **D. Lavery**, S.J. Savory, "**Blind equalization compensating for in-phase/quadrature skew in the presence of Nyquist filtering**", Accepted for publication in IEEE Photonics Technology Letters.

3. R. Zhou, P.M. Anandarajah, R. Maher, M. Paskov, **D. Lavery**, B.C. Thomsen, S.J. Savory, and L.P. Barry, "**Long reach 6 $\times$ 40-Gb/s PDM-16QAM coherent DWDM-PON with injected gain switched comb source**", Accepted for publication in IEEE Photonics Technology Letters.

Submitted Papers:

1. R. Maher, **D. Lavery**, M. Paskov, P. Bayvel, S.J. Savory, B.C. Thomsen, "**Fast wavelength switching 6GBd dual polarization M-QAM digital coherent receiver**", Submitted to IEEE Photonics Technology Letters.

2 Theory

INTRODUCED in chapter 1, the Long-Reach Passive Optical Network (LR-PON) has the potential to increase capacity over the currently installed fibre networks. In doing so, it also increases the reach of the access network; potentially up to 100 km. In order to support this long reach with increased capacity, multiple wavelength channels are transmitted to high sensitivity coherent receivers, which detect and demultiplex the transmitted signals. Considering this, the theory of the coherent LR-PONs is very different to the conventional Gigabit-Capable Passive Optical Network (GPON), for example. This chapter outlines the requisite theory for the work detailed in this thesis.

Section 2.1 introduces the two main channel impairments present in a passive optical network: loss and scattering. The advanced modulation formats required to take advantage of the diversity of the coherent receiver are discussed in section 2.2. The structure of the phase- and polarisation-diverse coherent receiver itself is described in section 2.3. The theoretical basis for the receiver sensitivity and frequency selectivity is also described in this section. Finally, the Digital Signal Processing (DSP) used for demodulating coherently received signals is detailed in section 2.4.

2.1 Channel impairments in a PON

The propagation of light through Single-Mode Fibre (SMF) is well understood, and the equations governing this propagation can be used when modelling transmission systems and when compensating for channel impairments. The performance of conventional

Passive Optical Network (PON) architectures is determined by the loss (or power) budget, which is, in turn, determined by receiver sensitivity and transmission losses. The physical origin of these losses are due to absorption and scattering in the optical fibre, and this is addressed below.

Attenuation

Let $A(z)$ be the complex amplitude of the optical field envelope at a certain distance, z, inside the fibre. Using this notation, linear channel impairments can be expressed through the following equation [47]

$$\frac{\partial A}{\partial z} = -\alpha A(z) \tag{2.1}$$

where α, is the fibre attenuation coefficient. This ordinary differential equation solves as follows

$$A(z) = A_0 \exp(-\alpha z) \tag{2.2}$$

where A_0 is the complex field at the input to the fibre ($z = 0$). Equation (2.2) indicates that the loss of optical power in a fibre is exponential with distance. For SMF, $\alpha_{dB} = 0.2$ dB/km, which relates to the linear α as $\alpha_{dB} = 10\alpha \log_{10}(e)$.

Rayleigh scattering and optical return loss

In bidirectional transmission systems, signal reflections from the upstream path can enter the the downstream receiver (or vice-versa) and lead to crosstalk between the downstream channels and the scattered upstream channel. There are two principal reasons for this to occur. The first is return loss from connectors and splices, such as at the output of the transmitter or at the input to the midspan splitter in the PON architectures shown in chapter 1. As these reflections are caused by discrete optical components or splices, the reflections occur at discrete points along the transmission path.

Continuous reflections can be caused by Rayleigh scattering, which is a form of linear scattering that affects the propagation of light through a medium with particle size much smaller than the wavelength of the light [48].

For a steady signal input power, the reflected fraction of the signal power at a distance, L with end coupler reflectance, R, takes the following form [49]

$$\begin{aligned} r_0(L,R) &= \frac{\eta}{\beta\nu}\left(1 - e^{-2\beta L}\right) + Re^{-2\beta L} \\ &= r_0(L,0) + Re^{-2\beta L} \end{aligned} \tag{2.3}$$

where η is the fibre-specific backscatter parameter (W/J), β is the attenuation coefficient (Np/km), and ν is the group velocity of light in optical fibre (km/s). For reference, as before, the attenuation coefficient in dB/km is $\alpha = 10\beta \log_{10} e$ (dB/km).

2.2 Advanced modulation formats

In the following chapters, emphasis is placed on the use of advanced modulation formats for increasing both receiver sensitivity and the total information content of an optical signal. The following describes the mathematical origin, as well as the encoding chosen, for each modulation format. The sensitivity formulae for all modulation formats considered in this thesis are given in appendix A.

2.2.1 Phase shift keying

Consider an optical carrier represented by the complex field

$$s(t) = |A(t)|e^{j\theta(t)} \tag{2.4}$$

where $|A(t)|$ is the carrier envelope, $\theta(t)$ is the carrier phase and $j = \sqrt{-1}$. A modulation applied to the phase of the carrier (Phase Shift Keying (PSK)) would then be represented by

$$\begin{gathered} s(t) = |A(t)|e^{j(\theta(t)+2\pi D_\phi(t)/M)} \\ D_\phi \in 1...M \end{gathered} \tag{2.5}$$

where $D_\phi(t) \in \mathbb{N}$ represents the data and M is the number of phase levels used to encode data; $\log_2(M)$ bits are encoded in each symbol period. In the work described in this thesis, the cases of M =2, 4 and 8 (Binary Phase Shift Keying (BPSK), Quadrature Phase Shift Keying (QPSK) and 8PSK) are considered. The resulting modulation can be visualised on an Argand diagram, where the sample of each symbol is represented by a single data point; this is often called a constellation diagram. Ideal constellation diagrams for the above formats are shown in Fig. 2.1.

2.2.2 Quadrature amplitude modulation

To further increase the information carried in each symbol period, the amplitude of the carrier can also be modulated in combination with phase; this modulation format is known as Quadrature Amplitude Modulation (QAM). For square QAM, as shown in Fig. 2.2, where the total number of constellations points, N^2, is an even power of 2, this

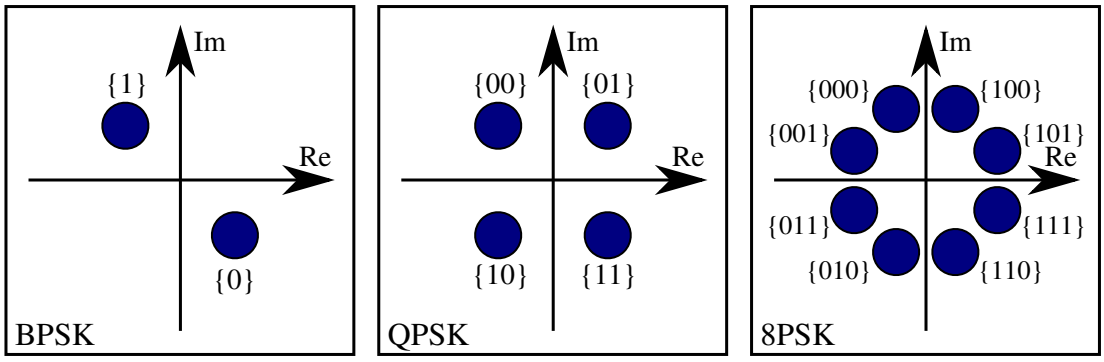

Figure 2.1: Constellations and bit to symbol mapping for 2, 4 and 8-*ary* PSK.

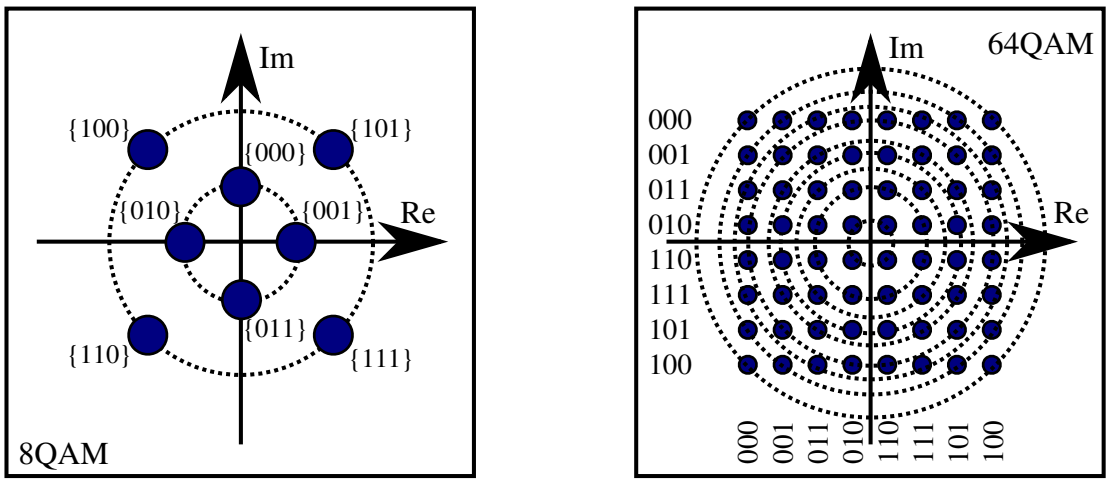

Figure 2.2: Constellations and bit to symbol mapping for 8 and 64-*ary* QAM. Rings of constant magnitude are shown by the dashed lines.

is better expressed in Cartesian co-ordinates

$$s(t) = [D_I - (N+1)/2] + j[D_Q - (N+1)/2] \qquad D_I, D_Q \in 1...N \tag{2.6}$$

Here, $D_I, D_Q \in \mathbb{N}$ are the modulated in-phase and quadrature data, and $2\log_2(N)$ bits are encoded in each symbol period. In the work described in this thesis, 8-*ary* QAM (chapter 3) and 64-*ary* QAM (chapter 5) are investigated (3 and 6 bits/symbol/polarisation, respectively). Note that 4QAM and QPSK are equivalent.

2.2.3 Transmission in orthogonal polarisations

For optical fibres which permit transmission using the two orthogonal polarisation states of light (such as standard single mode fibre) it is possible to transmit information using both polarisation states. Where the two polarisations are treated as statistically independent channels, this approach is termed Polarisation Division Multiplexing (PDM). A common example of this is PDM-QPSK, where QPSK symbols are transmitted in each

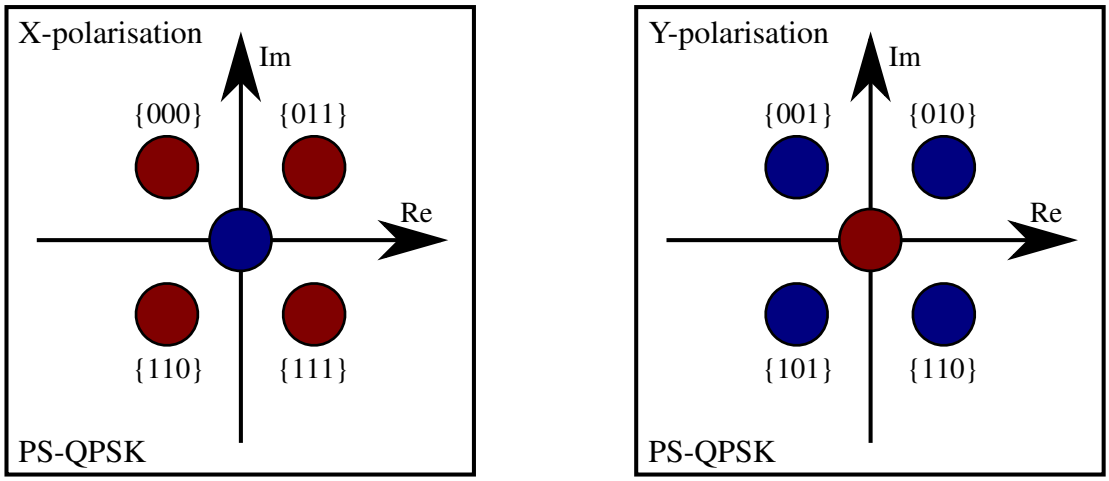

Figure 2.3: Constellations and bit to symbol mapping PS-QPSK. The colours indicate symbols from the same polarisation, and the central constellation point corresponds to the symbol where the data is in the orthogonal polarisation state.

orthogonal polarisation, thus doubling the data rate when compared to transmission of QPSK on a single polarisation.

It is also possible to encode data by modulating the State of Polarisation (SOP) of light directly. Polarisation switching (PS), for example, is where a single bit of information is encoded on which of two orthogonal polarisation states the signal occupies (i.e. is the signal X- or Y-polarised?). The information encoded per symbol is the same for a polarisation switched signal as for an On-Off Keying (OOK) signal.

The information per symbol can be increased by combining polarisation switching with another modulation format, such as QPSK. The constellation for this modulation format, Polarisation Switched (PS)-QPSK, is shown in Fig. 2.3. This modulation format is noteworthy as it has been shown theoretically to enable the highest receiver sensitivity of any modulation format in a four-dimensional channel [50]. This format is therefore investigated in the context of receiver sensitivity in chapter 3.

2.2.4 Gray coding

Where possible, for the modulation formats shown above, the symbols have been Gray coded. That is, the data encoded by adjacent symbols differs only by one bit (a Hamming distance of one). This is important, because the most likely errors caused by Gaussian noise are due to the erroneous selection of the adjacent constellation point [51]. Examples of two and three bit Gray codes are shown in Table 2.1. It can be seen from this table that, indeed, only one bit changes changes between adjacent ‘symbols’. For the standard binary encoding of N bits, at least one, and up to a maximum of N bits will change between adjacent symbols, resulting in a higher bit error probability than for Gray coding.

Table 2.1: GRAY CODING: 2- AND 3-BIT EXAMPLES

Decimal	Binary	2-bit Gray	3-bit Gray
0	000	00	000
1	001	01	001
2	010	11	011
3	011	10	010
4	100	-	110
5	101	-	111
6	110	-	101
7	111	-	100

Where Gray coding has not been possible, for example 8QAM, there is a small sensitivity penalty. This is reflected in the theoretical sensitivity curves shown in Fig. 2.4. (See appendix A and section 2.3.2 for formulae used to calculate these curves.)

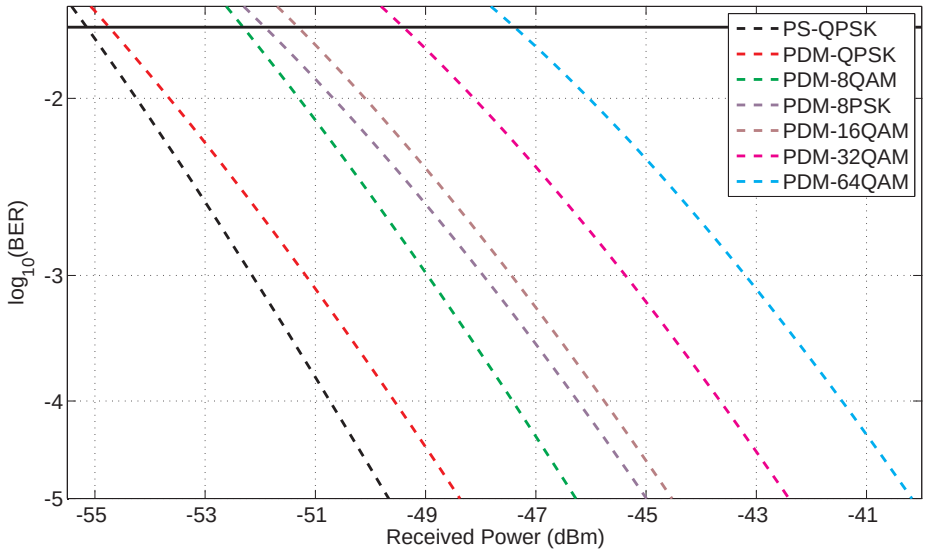

Figure 2.4: Theoretical shot-noise sensitivity limits for various modulation formats at 12.5 Gbit/s detected using a coherent receiver. The power sensitivity limit for each format directly depends upon their individual noise sensitivities, detailed in the appendix. For reference, a BER of 2×10^{-2} is highlighted by the solid black line. See appendix A for the formulae used to calculate these curves.

2.2.5 Transmitter design

Mach-Zehnder modulator

The fundamental component used for high bandwidth optical modulation in this work is the Mach-Zehnder Modulator (MZM). The MZM operates by splitting light into two isolated optical paths, with an electrode in one, or both, paths which changes the relative velocity of the light in each of the two arms via the electrooptic effect. The

result is that, at the output of the modulator, there is a variable interference when the two paths are recombined [52]. The schematic for the MZM is shown in Fig. 2.5.

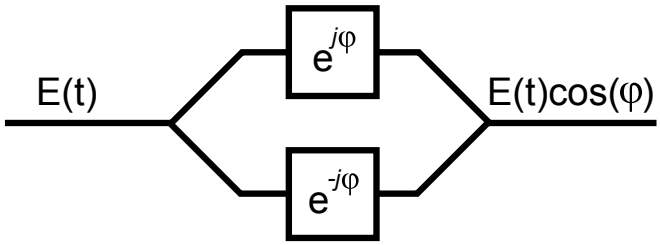

Figure 2.5: A push-pull Mach-Zehnder modulator.

The transfer function of this modulator is given by

$$E_{\text{out}}(t) \propto E_{\text{in}}(t)\cos\left(\phi(t)\right) \tag{2.7}$$

where $E_{\text{in}}(t)$ and $E_{\text{out}}(t)$ are the input and output electric fields, respectively, and the phase shift, $\phi(t) \propto V(t)$, the modulator driving voltage [53]. As a result of the transfer function, equation (2.7), this device can modulate the amplitude of a lightwave generating, for example, OOK. It can also be used to generate a phase modulated signal however, due to the cosine dependence of the modulated phase, only the real or 'in-phase' part of the signal can be modulated. Therefore, this modulator can generate formats such as BPSK (see Fig. 2.1(a)).

In-phase and quadrature (IQ) modulator

To overcome the limitations of a MZM, equation (2.7), a nested Mach-Zehnder interferometer structure can be designed which contains two parallel MZMs for modulating the in-phase and quadrature phase of an optical signal, as shown in Fig. 2.6. The orthogonality of each arm of this modulator is ensured by inserting a 90^o phase shift in one arm before signal recombination. This structure, termed either a triple MZM or

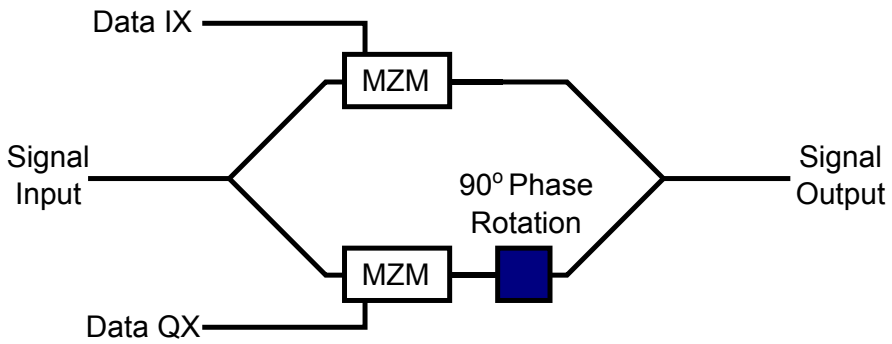

Figure 2.6: An IQ modulator; a nested Mach-Zehnder structure for modulating the in-phase and quadrature phase of an optical signal. The electrical data signals, Data IX and QX, modulate the in-phase and quadrature components of an optical signal, respectively.

'IQ' modulator, combines the transfer function of two MZMs, equation (2.7), and has

the following transfer function

$$\begin{aligned} E_{\text{out}}(t) &\propto E_{\text{in}}(t)\left[\cos\left(\phi_I(t)\right) + j\cos\left(j\phi_Q(t)\right)\right] \\ &= E_{\text{in}}(t)\sqrt{\cos^2\left(\phi_I(t)\right) + \cos^2\left(j\phi_Q(t)\right)}\exp\left(j\,\text{atan2}\left[\cos(\phi_I(t)), \cos(\phi_Q(t))\right]\right) \end{aligned} \tag{2.8}$$

where $\phi_I(t)$ and $\phi_Q(t)$ are the phase shifts modulated on the in-phase and quadrature arms of the IQ modulator, respectively, and the function $\text{atan2}(a,b)$ returns the polar angle of an arbitrary complex number $a+bj$. Equation (2.8) demonstrates that an arbitrary amplitude and phase can be achieved using an IQ modulator. This enables the generation of modulation formats with multiple phase levels (for example QPSK) or multiple amplitude and phase levels (for example QAM). This modulator structure is used experimentally as part of the transmitter used for generating all the modulation formats detailed in this thesis (chapters 3-5).

Generalised four dimensional modulator

The IQ modulator can modulate the phase and amplitude of a single polarisation of a signal. However, each dimension of an optical signal can be modulated independently by using four parallel MZMs nested in an interferometric configuration, Fig. 2.7. In

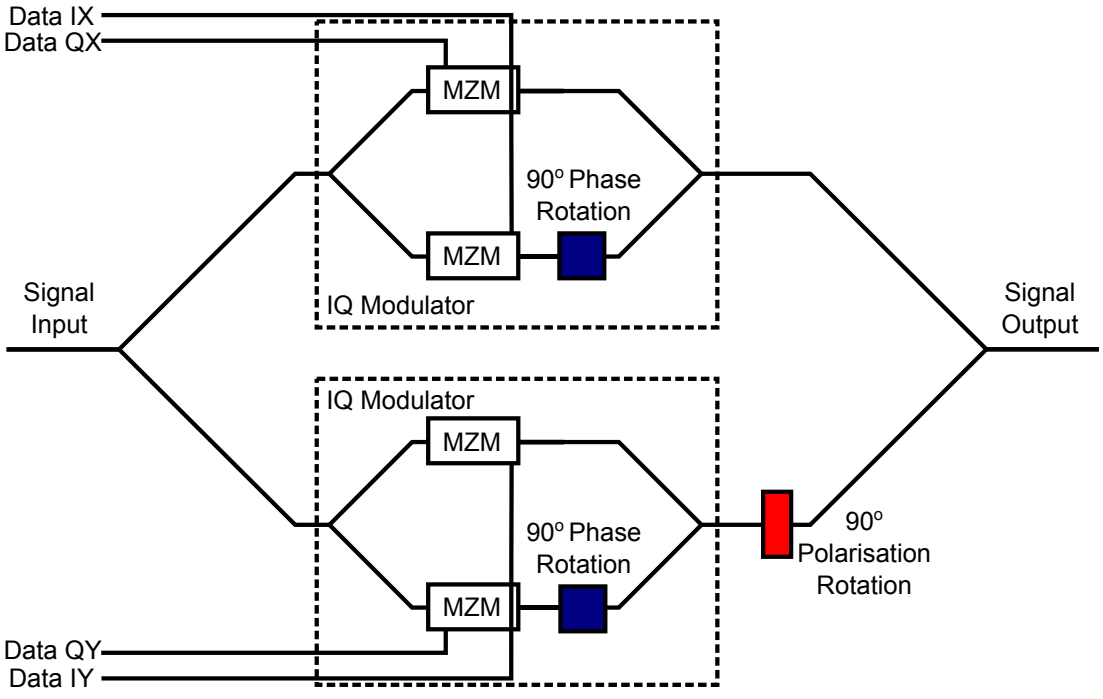

Figure 2.7: A four dimensional modulator incorporating nested Mach-Zehnder interferometers and four Mach-Zehnder modulators. Key: MZM - Mach-Zehnder Modulator, I/Q - in-phase/quadrature, X/Y - polarisation state.

this configuration, each polarisation is modulated independently using an IQ modulator. The two IQ modulators shown in Fig. 2.7 have the same transfer function. However, the

90^o polarisation rotation in one arm prior to the signal being recombined means that the second IQ modulator encodes data on an orthogonal polarisation state to the first IQ modulator. Therefore, the four MZMs can modulate the four dimensions of the optical field[1].

2.3 Phase- and polarisation-diverse coherent receiver

Conventional optical receivers, single photodiodes, can measure only the amplitude of a signal. Coherent receivers additionally measure the signal phase allowing the use of advanced modulation formats, which can combine amplitude and phase modulation. Additionally, using Polarisation Beam Splitters (PBSs) in both the signal and Local Oscillator Laser (LO) paths, the polarisation information of a signal can also be recovered. Further, by digitally sampling the electrical output from each photodiode (as shown in Fig. 2.8), DSP can be used to aid with data recovery [54].

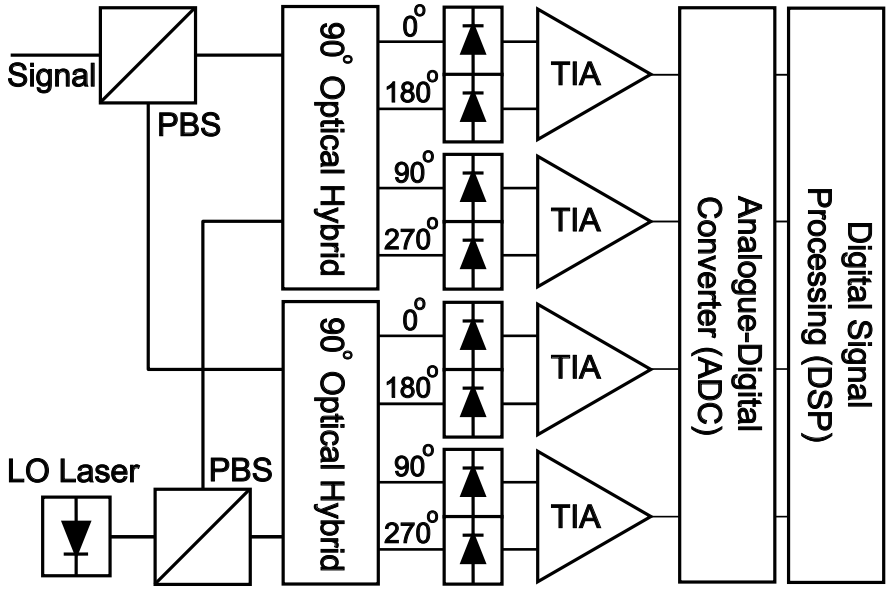

Figure 2.8: A phase- and polarisation-diverse digital coherent receiver using balanced transimpedance amplifiers (TIA) for common mode rejection. The LO laser provides a CW reference signal which produces an intermediate beat frequency when combined with the signal. Using this method of signal detection, all four dimensions of the optical field can be recovered.

In addition to enabling the use of advanced modulation formats, coherent receivers have many other properties which make them attractive for use in passive optical networks, such as high sensitivity and frequency selectivity. These advantages become clear when considering the mathematical basis for (intradyne) coherent detection, as follows.

[1]When investigating polarisation multiplexed modulation formats experimentally, it is not always possible to produce the four electrical driving signals required by this modulator. An alternative technique for emulating the output of this modulator using only two driving signals is discussed in section 3.1.1.

Consider the phase- and polarisation-diverse receiver structure shown in Fig. 2.8. An optical signal is split into two orthogonal polarisation states using a PBS, the two outputs of which enter two 90° optical hybrids. The frequency of Continuous Wave (CW) light from a local laser (the LO) is tuned close to the wavelength of the signal and undergoes a similar process but enters the second input of each 90° optical hybrid.

Each of the outputs from the 90° optical hybrid, as shown in Fig. 2.8, has a second matched output which is phase shifted by π relative to the first output, and can also be detected. The output from the first optical hybrid (first polarisation) measures the beat product between signal and LO as the sum of their fields. The current measured on each photodiode after the optical hybrid is then given by

$$\begin{aligned} i_{I\pm}(t) &\propto \frac{1}{2}|E_{LO}(t)|^2 + |E_s(t)|^2 \pm 2\Re\left[E_s(t)E_{LO}^*(t)\exp(j\Delta\omega_{s-LO}t)\right] \\ i_{Q\pm}(t) &\propto \frac{1}{2}|E_{LO}(t)|^2 + |E_s(t)|^2 \pm 2\Im\left[E_s(t)E_{LO}^*(t)\exp(j\Delta\omega_{s-LO}t)\right] \end{aligned} \tag{2.9}$$

where, on the left hand side of the equation, I indicates the in-phase component (first pair of photodiodes), Q indicates the quadrature component (second pair of photodiodes) and $+$ and $-$ distinguish between the two outputs of each pair of photodiodes. On the right, $E_s(t)$ and $E_{LO}(t)$ are the (baseband) signal and LO fields, respectively, and $\Delta\omega_{s-LO} = \omega_s - \omega_{LO}$ is the relative frequency between signal and LO. The functions $\Re$ and $\Im$ mean 'the real part of' and 'the imaginary part of', respectively. Differentially amplifying the output of each photodiode pair removes the direct detection terms

$$i_I(t) = i_{I+}(t) - i_{I-}(t) \propto \Re\left[E_s(t)E_{LO}^*(t)\exp(j\Delta\omega_{s-LO}t)\right] \tag{2.10}$$

$$i_Q(t) = i_{Q+}(t) - i_{Q-}(t) \propto \Im\left[E_s(t)E_{LO}^*(t)\exp(j\Delta\omega_{s-LO}t)\right] \tag{2.11}$$

and similarly for the second polarisation, resulting in the full optical field being translated into the electrical domain.

2.3.1 Frequency selectivity

One of the key advantages of coherent detection, particularly in an access network scenario (see chapter 4), is frequency selectivity. An optical fibre has a transmission window which spans more than 400 nm (50 THz), however, optical networks typically limit transmission to only one or two bands within this window for convenience of sourcing equipment, as well as network management. Here, the C-band (conventional transmission band, 1530–1565 nm, approximately 5 THz) is considered, which matches the gain profile of an Erbium Doped Fibre Amplifier (EDFA).

Even within this smaller window, there is still ample bandwidth to simultaneously

transmit multiple channels across a range of wavelengths, and this process is termed Wavelength Division Multiplexing (WDM). At the receiver, it is desirable to demultiplex these channels such that only one channel is converted into the electrical domain within each receiver. Conventionally, a frequency selective device such as an arrayed waveguide grating or Fabry-Perot filter is used for this procedure. However, from equations (2.10-2.11), it can be seen that the LO can be used as a narrow optical filter. Begin by summing the differentially amplified outputs from the two photodiodes

$$i(t) = i_I(t) + ji_Q(t) \propto E_s(t)E_{LO}^*(t)\exp(j\Delta\omega_{s-LO}t) \tag{2.12}$$

which, assuming the frequency offset between signal and LO is small, simply becomes the baseband equivalent

$$i(t) \propto E_s(t)E_{LO}^*(t) \tag{2.13}$$

Now, assume a second channel, field E_{s2}, enters the coherent receiver with a frequency $\omega_{LO} + \delta\omega$. The resulting electrical signal for this channel is

$$i(t) \propto E_{s2}(t)E_{LO}^*(t)\exp(j\delta\omega t) \tag{2.14}$$

where $\delta\omega$ is a frequency offset term, which determines the frequency of phase rotations of the second signal, relative to the LO. If the beat frequency, $\delta\omega$, is outside the electrical bandwidth of the receiver then this will lead to the second channel, E_{s2}, being rejected through low-pass filtering. This is of fundamental importance when considering an Ultra Dense Wavelength Division Multiplexing (UDWDM) transmission system, as in chapter 4, for two reasons. Firstly, it enables the reception of a single channel from a WDM source without filtering and, secondly, it allows the receiver to tolerate reflections due to Rayleigh backscattering in bidirectional transmission (see section 4.3).

2.3.2 Sensitivity

Receiver sensitivity is a measure of tolerance to noise for a particular detection scheme. In an optical system, this noise could arise from the Amplified Spontaneous Emission (ASE) from optical amplifiers, for example, or from receiver noise sources such as shot noise. Consider the case of a signal degraded by such an Additive White Gaussian Noise (AWGN) source.

When a signal is degraded by noise, it is conventional to express the signal quality in terms of the Signal-to-Noise Ratio (SNR). In optical communications, it is more convenient to define an Optical Signal-to-Noise Ratio (OSNR), which is the SNR normalised over a fixed bandwidth. For historical reasons, this bandwidth is normally

12.5 GHz (0.1 nm). The OSNR is defined as follows

$$\mathrm{OSNR} = (\mathrm{B_{sig}}\gamma_b)/(2\mathrm{B_{ref}}) \tag{2.15}$$

where γ_b is the SNR per bit, $\mathrm{B_{sig}}$ is the total signal data rate and $\mathrm{B_{ref}}$ is the reference bandwidth. When the term γ_b is obtained, the relationships between OSNR and Bit Error Rate (BER) can be readily calculated (for signals modulated using only amplitude and phase, these are the standard formulae from Radio Frequency (RF) communications, as in [51]). For the modulation formats considered herein, these are given in appendix A. Using these formulae, the relative OSNR requirements to achieve a particular BER for different modulation formats can be calculated. Knowledge of the relationship between OSNR and BER provides a benchmark performance against which experimental results can be compared. The direct measurement of OSNR is used in this thesis in section 5.3.

Consider, now, the scenario where the signal is impaired only by receiver noise sources, and that the two polarisations of the coherent receiver can be treated as independent channels if separated optically at the receiver[2] [33]. The contribution of each noise source within a coherent receiver can be calculated as follows.

Begin by considering a single polarisation coherent receiver (i.e. no polarisation beam splitter), and start with the sum of the photodiode outputs as in equation (2.13), but scale by the photodiode responsivity, R, to give the (complex) current

$$\begin{aligned} i_c(t) = i_I(t) + i_Q(t) &= RE_s(t)E_{LO}(t) \\ &= R\sqrt{P_sP_{LO}} \end{aligned} \tag{2.16}$$

where the detector responsivity, R, can be defined as follows

$$R = \frac{\eta e}{hf} \tag{2.17}$$

and, here, η is the photodiode quantum efficiency, e is the charge of an electron, h is Planck's constant and f is the frequency of the optical signal.

In the process of photodetection, due to the Poisson distributed arrival times of photons, the conversion of incident photons into electrons introduces a noise term called shot noise. The spectral noise density (shot noise) is described by the Schottky formula [55]

$$S_{shot} = 2eI_R \tag{2.18}$$

where e is the fundamental electronic charge and I_R is average received photocurrent. In

[2]This approach assumes an ideal polarisation beam splitter used when separating polarisations of the signal incident on the coherent receiver.

the case of a coherent receiver, the LO shot noise dominates, and is given by the term

$$\sigma_{shot}^2 = 2eR\frac{P_{LO}}{2}\frac{B}{2} \tag{2.19}$$

where the LO laser power is halved when dividing the laser output between the in-phase and quadrature of the coherent receiver.

The power spectral density of the noise due to the amplified spontaneous emission factor of an optical preamplifier is as follows.

$$S_{ase} = hfn_{sp}(G-1) \tag{2.20}$$

where B is the symbol rate, B/2 is the noise bandwidth, n_{sp} is the spontaneous emission factor for an optical preamplifier, G is the amplifier gain and P_{LO} is the power of the local oscillator laser. Due to the noise sources being present on both I and Q photodiodes,the effective noise is doubled.

$$\sigma_{beat}^2 = 4eR\frac{\eta n_{sp}(G-1)}{2}\frac{B}{2}\frac{P_{LO}}{2} \tag{2.21}$$

Therefore the total noise current is given by

$$\sigma_t^2 = \sigma_{shot}^2 + \sigma_{beat}^2 \tag{2.22}$$

The electrical signal-to-noise ratio which results is simply the ratio of the mean square signal current to the mean square noise currents

$$\gamma_s = \frac{\overline{i_c^2}}{2\sigma_t^2} \tag{2.23}$$

Consider the case where no preamplifier is used ($G = 1$), and where the power of the local oscillator laser is large ($P_{\mathrm{LO}} \to \infty$). The result is that the receiver approaches the following shot noise limit

$$\gamma_{s,shot} = \frac{\eta P_s}{hfB} \tag{2.24}$$

Now consider the use of an optical preamplifier such that $G \gg 1$, generating a high power signal which overcomes the limits of the quantum efficiency of the receiver photodiodes. In this case, the receiver enters the regime of the LO-ASE beat noise limit

$$\gamma_{s,beat} = \frac{P_s}{hfn_{\mathrm{sp}}B} \tag{2.25}$$

Note that, for an ideal amplifier (3 dB noise figure), $n_{\mathrm{sp}} = 1$. Also note that, for an ideal photodiode, $\eta = 1$. Therefore, in the idealised limits (the 'quantum limit'), the beat

noise limit is equal to the shot noise limit, and this limit is given by

$$\gamma_{s,limit} = N_p \tag{2.26}$$

where N_p is the number of received photons per symbol. Using the formulae from appendix A, the theoretical power sensitivity limits can be calculated for the shot noise limited scenario, equation (2.24), the beat noise limit, equation (2.25) and the quantum limit, equation (2.26). These three results are relied upon in chapter 3 when evaluating the sensitivity of a digital coherent receiver using different modulation formats. The quantum limits for the modulation formats considered herein are shown in Fig. 2.4. This result is used in chapters 4-5.

2.4 Digital signal processing

The digitised signal obtained after the Analogue-to-Digital Converters (ADCs) in a coherent receiver may be distorted. This is due largely to impairments in the optical channel, for example ASE, chromatic dispersion, fibre nonlinearity, polarisation mode dispersion and Polarisation Dependent Loss (PDL). In addition, there can be distortions added in the transmitter (e.g. Inter-Symbol Interference (ISI) due to limited electrical bandwidth) and at the receiver (e.g. quantisation noise due to the Effective Number of Bits (ENOB) of the ADCs). Finally, there can be distortions intrinsic to the optical source itself, for example laser linewidth (induces phase noise), frequency stability and Relative Intensity Noise (RIN).

Distortions must either be compensated or managed at the receiver in order to recover the transmitted signal. As coherent receivers can be used to fully recover the state of an optical field (see section 2.3), this information can be passed on to a digital postprocessing module so that more complex techniques can be used to recover the signal than could otherwise be employed in the optical domain. One approach to recovering the transmitted signal would be to calculate the inverse of the optical channel and apply this as a filter to the received samples. There are two reasons why this does not occur in practice, a) the particular transfer function of the optical channel is not a parameter of interest (only the transmitted data is important), so it would be computationally expensive to compute this value, b) the channel response is time-varying, and so a time-varying (adaptive) filter is required to recover the transmitted signal.

In this work, a modular approach to DSP was taken such that each channel impairment is compensated separately; possible because feedforward algorithms were used. A generic example of digital postprocessing is outlined in Fig. 2.9. In general, a signal is sampled by the ADCs (or subsequently resampled) at 2 samples per symbol. Each of

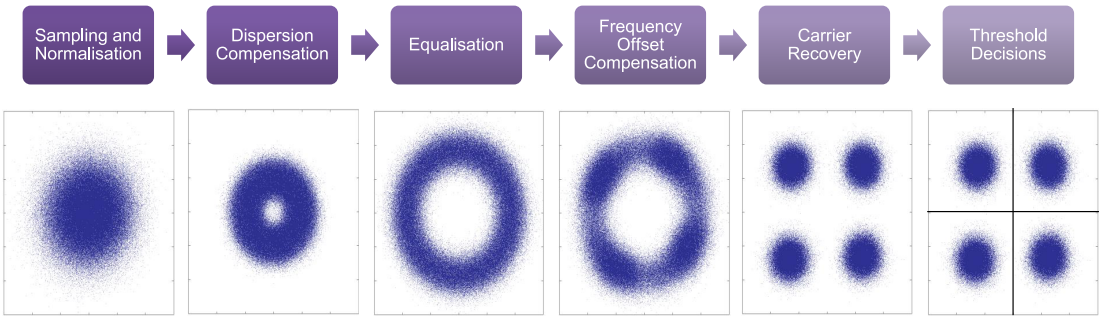

Figure 2.9: An example of a modular approach to digital compensation of channel impairments and subsequent carrier and data recovery. Constellations shown are taken from an experimental data set: PDM-QPSK at 10.7 GBd after 2000 km SMF.

the digital signal streams (4 in the case of a phase- and polarisation-diverse coherent receiver) is normalised to compensate for any discrepancy between the responsivity of each photodiode, and phase shifted to compensate for the relative delays in the optical hybrids. To compensate for chromatic dispersion, where required, a Finite Impulse Response (FIR) filter is applied, as described in section 2.4.1. To enable the polarisation state of the signal to be tracked, and to find the optimal sampling instant, an equaliser is employed as described in section 2.4.2. Carrier recovery is then performed; first by removing any constant phase offset (due to the difference in frequency between the signal and LO) and then by tracking the phase variations due to laser linewidth. Both are described in section 2.4.3. Finally, the data is recovered by making hard decisions on the received signal. In this work, the implementation of error correcting codes is not explored, however the use of forward error correction is assumed, such that a particular bit error rate threshold can be assumed to be error free (section 2.4.4).

2.4.1 Chromatic dispersion compensation

Consider the impact of chromatic dispersion in the absence of loss and fibre nonlinearity. This can be modelled by the following equation, where β_2 is the dispersion coefficient [47]

$$\frac{\partial A}{\partial z} = -j\frac{\beta_2}{2}\frac{\partial^2 A}{\partial t^2} \tag{2.27}$$

This is now a linear equation and can be solved analytically by taking the Fourier transform as follows

$$\frac{\partial}{\partial z}G(z,\omega) = -j\frac{\beta_2}{2}\int_{-\infty}^{\infty}\frac{\partial^2 A}{\partial t^2}\exp(j\omega t)\,dt \tag{2.28}$$

$$\Rightarrow \frac{\partial}{\partial z}G(z,\omega) = j\frac{\beta_2}{2}\omega^2 G(z,\omega) \tag{2.29}$$

using the identity $f'(t) = jw\mathcal{F}(w)$ to solve to Fourier transform in equation (2.28). Equation (2.29) is now a differential equation which is solved to give the frequency domain transfer function

$$G(z,\omega) = \exp\left(j\frac{\beta_2}{2}\omega^2 z\right) \tag{2.30}$$

The all-pass filter $1/G(z,\omega)$ is then the compensating filter for this dispersion. This filter is difficult to implement digitally [32], but it can be shown that transforming back to the time domain yields a FIR filter which can compensate large accumulated dispersion [32]

$$g(z,\omega) = \sqrt{\frac{-j}{2\pi\beta_2 z}}\exp\left(\frac{jt^2}{2\beta_2 z}\right) \tag{2.31}$$

where $g(z,\omega)$ is the time domain impulse response, which is infinite in duration, as it passes all frequencies for a finite sampling frequency; this introduces aliasing of the signal. A practically implementable FIR filter can be designed (with a truncated response), where the taps weights are given by

$$a_n = \sqrt{\frac{-j}{2\pi\beta_2 z}}\exp\left(\frac{jk^2}{2\beta_2 z}\right) \tag{2.32}$$

and

$$-\left\lfloor\frac{N}{2}\right\rfloor \leq k \leq \left\lfloor\frac{N}{2}\right\rfloor \tag{2.33}$$

for $N \in \mathbb{N}$ and

$$N = 2\left\lfloor\frac{|D|\lambda^2}{2cT^2}\right\rfloor + 1 \tag{2.34}$$

where λ is the optical wavelength, T is the reciprocal of the sampling frequency, and c is the speed of light. The dispersion parameter is related to the second order propagation constant as $D = -2\pi c\beta_2/\lambda^2$ This FIR filter is used to compensate for dispersion in section 3.3, where high symbol rate signals are investigated. For the remainder of the thesis, low symbol rates (<6 GBd) are used. For a maximum transmission distance of 100 km, assuming SMF dispersion of 17 ps/nm/km, and a wavelength of 1550 nm, 3 FIR filter taps[3] are required to compensate dispersion, which can be achieved using a short adaptive equaliser[4].

[3]For transmission of 3 GBd PDM-QPSK, which is investigated throughout this thesis, only a single filter tap is required to compensate dispersion.

[4]Throughout this thesis, 5 equaliser filter taps are used in order to ensure compensation of transmission

2.4.2 Equalisation

The primary purpose of digital equalisation in passive optical networks is to approximate the inverse channel response such that the polarisation state of the signal can be recovered. The method of equalisation varies depending on the modulation format used and on the tolerable level of complexity. However, the following algorithms all use Multiple Input Multiple Output (MIMO) filtering to recover the polarisation state, as shown in Fig. 2.10. Additionally, all the filters implemented for the experiments described in this thesis assume two samples per symbol oversampling, to enable the equaliser to recover the ideal sampling phase[5].

All the equalisers described here are of the class of blind, adaptive, property restoral filters [56]. Such filters adapt their tap weights after each iteration based on the output of an error function. This error function is a measure of the deviation from the property that the equaliser aims to restore; a property which can be determined *a priori* if the modulation format is known. It has been shown that such adaptive filters can obtain the inverse channel response when restoring a known signal property [56].

The following algorithms are those which are used in the experiments detailed in chapters 3–5. For all of these equalisers, the tap weights are updated without knowledge of the transmitted symbols (i.e. using a blind update algorithm).

(i) Godard algorithm for constant modulus formats

The Godard algorithm [57], also known as the Constant Modulus Algorithm (CMA), is often used for formats where the envelope of the signal is a constant. This is the property which the algorithm seeks to restore. Due to its reliable convergence, this algorithm can also be used for other modulation formats as a method for pre-convergence of a subsequent equaliser. In the experimental work detailed herein, this algorithm is always used for equalisation of polarisation multiplexed QPSK. It is also used for PDM-8PSK when investigated in section 3.2.

In order to recover the state of polarisation of a signal using this algorithm, the filter must be adapted such that signal power can be exchanged between the two polarisations; a MIMO configuration. The algorithm is as follows. First the filter is applied to each polarisation (in the first instance, these filters can be initialised to delta functions for the through terms, and zeros for the cross polarisation terms)

$$x_{out}(k) = \mathbf{h}_{xx}^{H}\mathbf{x}_{in} + \mathbf{h}_{xy}^{H}\mathbf{y}_{in}$$
$$y_{out}(k) = \mathbf{h}_{yx}^{H}\mathbf{x}_{in} + \mathbf{h}_{yy}^{H}\mathbf{y}_{in}$$

where $\mathbf{h}_{out,in}$ is a filter with subscripts indicating the input and output polarisation

impairments.

[5]For realtime detection, a discrete clock recovery module is often used to track the sampling phase, relaxing the phase noise tracking requirement on the equaliser.

state, superscript H indicates the element-wise complex conjugate transpose (Hermitian conjugate) of the input vectors, and $x_{out}(k)$, $y_{out}(k)$ are the kth outputs on the X and Y polarisations, respectively. In discrete terms, the filters are applied as a time-domain convolution, for example

$\mathbf{h}_{xx}^{H}\mathbf{x}_{in} = \sum_{n=0}^{N-1} h_{xx}^{*}(n)x_{in}(k-n)$

where N is the filter length (following [32]). This is shown schematically in Fig. 2.10.

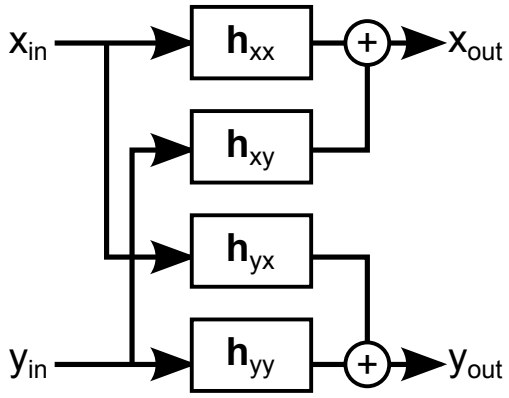

Figure 2.10: Structure of a 2×2 MIMO equaliser.

The calculation of the error term distinguishes the equalisation algorithms which follow. For the CMA, the X and Y polarisation error terms, $e_{x,y}$ are calculated as follows

$e_x \leftarrow 1 - |x_{out}|^2$

$e_y \leftarrow 1 - |y_{out}|^2$

where the left arrow indicates the assignment operator (e.g. the variable e_x takes the value $1 - |x_{out}|^2$). As defined, the error function targets a unit modulus.

The final stage in the adaptive algorithm is the filter tap updates.

$\mathbf{h}_{xx} \leftarrow \mathbf{h}_{xx} + \mu e_x \mathbf{x}_{in} x_{out}^{*}$

$\mathbf{h}_{xy} \leftarrow \mathbf{h}_{xy} + \mu e_x \mathbf{y}_{in} x_{out}^{*}$

$\mathbf{h}_{yx} \leftarrow \mathbf{h}_{yx} + \mu e_y \mathbf{x}_{in} y_{out}^{*}$

$\mathbf{h}_{yy} \leftarrow \mathbf{h}_{yy} + \mu e_y \mathbf{y}_{in} y_{out}^{*}$

These updated taps are then used for the next iteration of filtering.

(ii) Polarisation directed equalisation

Polarisation directed equalisation is based on the CMA, and only varies in the generation of the error function [58]. This algorithm was designed for use with the modulation format PS-QPSK, where the sum of the modulus of each polarisation is a constant (power is present only in one polarisation in each symbol period). Therefore, this equaliser seeks to restore this property with the following adaptation to the CMA error function.

if $|x_{out}| > |y_{out}|$ **then**
  $R_x \leftarrow 1$
  $R_y \leftarrow 0$
else
  $R_x \leftarrow 0$
  $R_y \leftarrow 1$
end if
$e_x \leftarrow R_x - |x_{out}|^2$
$e_y \leftarrow R_y - |y_{out}|^2$

This algorithm is used in sections 3.2 and 3.3 for equalisation of PS-QPSK.

(iii) Phase decision equalisation

While the format BPSK is, in fact, a constant modulus format, it is not sufficient to use the unmodified CMA due to the π phase margin between constellation points, which results in an unequal distribution of power present in each quadrature [59]. The equaliser can be assisted by making decisions on the phase of each symbol, as described in [60]. Here, phase estimation is used as follows

$x_{out} \leftarrow x_{out} e^{-j\phi_x}$
$y_{out} \leftarrow y_{out} e^{-j\phi_y}$
$e_x \leftarrow e^{j\phi_x}(\mathrm{sgn}(\Re(x_{out})) - x_{out})$
$e_y \leftarrow e^{j\phi_y}(\mathrm{sgn}(\Re(y_{out})) - y_{out})$

where ϕ_x and ϕ_y are the phase of the signal (x and y polarisations) as determined by the Viterbi and Viterbi algorithm (see section 2.4.3), and sgn is the signum operator

$$\mathrm{sgn}(x) = \begin{cases} -1 & \text{if } x < 0 \\ 0 & \text{if } x = 0 \\ 1 & \text{otherwise} \end{cases} \tag{2.35}$$

This algorithm measures the deviation in phase from the nearest symbol (± 1), and returns that information to the equaliser update algorithm. The algorithm is used for equalising PDM-BPSK in section 3.2.

(iv) Equalisation for M-*ary* QAM

The modulation format M-*ary* QAM does not have a constant modulus except in the special case of QPSK (i.e. 4QAM). Nevertheless, it is possible to use the constant modulus algorithm for pre-convergence of the equaliser taps [56]. However, to fully converge the equaliser for QAM, it is necessary to use an equalisation algorithm tailored to QAM, such as radially directed equalisation [61]. Physically, this corresponds to making a

decision on the ring (expected radius) of the signal, and then calculating the deviation from this ring in order to derive an error metric. Therefore, this equaliser is distinguished by its error function, which is as follows:

if $|x_{out}| < T_1$ **then**
  $R_x \leftarrow R_1$
else if $|x_{out}| > T_1$ **and** $|x_{out}| < T_2$ **then**
  $R_x \leftarrow R_2$
  $\{...\}$
else
  $R_x \leftarrow R_n$
end if
$e_x \leftarrow R_x - |x_{out}|^2$

and similarly for the y-polarisation, where T_n is the n$^{\text{th}}$ threshold level, R_n is power of the n$^{\text{th}}$ QAM ring and the algorithm assumes n rings. This algorithm is used for the equalisation of PDM-8QAM in section 3.2 (CMA used for preconvergence). In section 5.3, the equalisation of PDM-64QAM is assisted using this algorithm. To ensure equaliser convergence, the taps are preconverged using first the CMA, and then this radially directed algorithm, but assuming a three modulus signal. Final equalisation is achieved using a decision directed equaliser (error term is the deviation from the closest symbol) interleaved with a decision directed phase estimator as described in section 2.4.3(iii) [61].

2.4.3 Carrier recovery

The combined linewidth of the signal laser and the LO within a coherent receiver is translated into phase noise. This is because linewidth adds an uncertainty in frequency and, therefore, phase, leading to a time varying phase component. Lasers are often considered to have Lorentzian power spectral density [62] and the corresponding phase noise is assumed to follow a Wiener-Lévy random walk process [63], however, it should be noted that there are cases where these assumptions are not valid (such as for the laser used in chapter 5). Using the random walk assumptions, it is possible to compensate for phase noise digitally and outlined here are the algorithms used throughout this work.

These algorithms are collectively known as Carrier Phase Estimation (CPE), or carrier recovery, and are the methods by which the phase of a received carrier is calculated such that, subsequently, the modulated phase component can be obtained. Broadly, they all operate by removing the modulation before estimating the phase.

(i) Viterbi and Viterbi

First proposed in 1983, the Viterbi and Viterbi algorithm describes a class of nonlinear phase estimation techniques for constant modulation phase modulated formats (M-*ary* PSK) [64]. By raising the digitised symbols to the M$^{\text{th}}$ power, the modulation can be removed, and the phase estimated independently. If an M-PSK signal is modulated as follows[51]

$$s(t) = A\cos\left[2\pi f_c t + \frac{2\pi}{M}m\right], \qquad m = 1,2,\ldots,M \tag{2.36}$$

where f_c is the carrier frequency, then the equivalent digitised signal after a coherent receiver can be represented as a complex number, Z

$$Z(k) = e^{j(\frac{2\pi}{M}m+\phi(k))} + n(k) \tag{2.37}$$

where $n(k)$ is the channel noise, $\phi(k)$ is the phase noise and m is the PSK symbol. By raising the complex numbers to the power M, the modulated component becomes $2\pi m$, which is always a multiple of 2π and, therefore, evaluates to a unit constant in equation (2.37). Hence, a phase estimate can be found at a certain point in time, c, by averaging the phase over a window of size $2w$

$$\phi(c) = \frac{1}{M}\left[arg\left(\sum_{n=c-w}^{c+w} Z_n^M\right)\right] \tag{2.38}$$

This algorithm is used for phase estimation of PDM-QPSK throughout this thesis (chapters 3-5), and for PDM-8PSK in section 3.2. Note that a similar algorithm can be employed for frequency offset (intradyne frequency) estimation. After the M$^{\text{th}}$ power nonlinearity has been applied, the frequency offset can be estimated from the peak of the Fourier transform of the signal.

(ii) Polarisation-switched Viterbi and Viterbi

For polarisation-switched QPSK, the signal of interest is only present in one of two orthogonal polarisation states at a time. However, it is possible to track phase changes by making a decision on the polarisation state of the signal in each symbol slot before phase estimation [34]. The phase estimation comprises the Viterbi and Viterbi algorithm operating on a stream of symbols obtained after a decision on the polarisation state. This decision is as follows:

if $|x_{out}| > |y_{out}|$ **then**
  $S \leftarrow x_{out}$
else

$S \leftarrow y_{out}$
end if

where S is the sample used for phase estimation. This algorithm is used in sections 3.2 and 3.3 for carrier phase estimation in a PS-QPSK receiver.

(iii) Phase estimation for high order QAM

There are several methods of carrier recovery which are applicable to QAM. One commonly used example is the least mean squares carrier tracking method outlined in [61].

In this work, M-*ary* QAM where M>4 is addressed twice in this thesis. First, sensitivity measurements are taken for PDM-8QAM in section 3.2. Subsequently, the modulation format PDM-64QAM is employed to test the efficacy of a laser linewidth compensation scheme, section 5.3.

When using 8QAM, the transmitter and local oscillator laser linewidths were sufficiently low (100 kHz) that it was only necessary to modify the standard Viterbi and Viterbi algorithm by first making decisions on the ring (i.e. the amplitude of the signal) and using this information to remove the QAM modulation. The resulting symbols were then recovered as for the Viterbi and Viterbi algorithm.

For 64QAM, decision directed phase estimation was used. Here, decisions are made on all the symbols within a phase estimation window. Each symbol is then rotated to remove the modulation, and the resulting samples are then averaged over the window, as in the the Viterbi and Viterbi algorithm. The phase estimate is then fed back to the next sample window to ensure the accuracy of subsequent decisions [65].

Cycle slips and failure of carrier recovery

Using the techniques described above, incorrectly identifying the phase of a carrier can, over the course of several symbols, lead to a discontinuity in the estimated phase and therefore subsequent symbols are misclassified. This is known as a cycle slip, and will cause symbol misclassification to occur consecutively until the receiver is reset [63]. In an installed system, resetting the receiver will lead to a break in service, which is not satisfactory behaviour. Differential encoding can overcome this problem by encoding data on the phase difference between two symbols, rather than the absolute phase of each symbol. In doing so, the information received is dependant only on the phase of the currently detected symbol and the previously detected symbol. This is discussed in the following section.

2.4.4 Data recovery and error correction

Differential encoding and decoding

Discussed herein is differentially coded QPSK, although differential coding can be applied equally to other phase modulated signals. To differentially encode a stream of QPSK symbols, the following logical formula can be employed [66]:

$$\begin{aligned} I_k = &\ \overline{a}_k\overline{b}_k\overline{I}_{k-1} + \overline{a}_k b_k Q_{k-1} + a_k\overline{b}_k\overline{Q}_{k-1} + a_k b_k I_{k-1} \\ Q_k = &\ \overline{a}_k\overline{b}_k\overline{Q}_{k-1} + \overline{a}_k b_k\overline{I}_{k-1} + a_k\overline{b}_k I_{k-1} + a_k b_k Q_{k-1} \end{aligned} \tag{2.39}$$

This can be implemented in hardware with a minimum number of logic gates by using the simplified formula [66]:

$$\begin{aligned} I_k = &\ \overline{a_k \oplus b_k} \cdot \overline{b_k \oplus I_{k-1}} + (a_k \oplus b_k) \cdot \overline{b_k \oplus Q_{k-1}} \\ Q_k = &\ \overline{a_k \oplus b_k} \cdot \overline{b_k \oplus Q_{k-1}} + (a_k \oplus b_k) \cdot (b_k \oplus I_{k-1}) \end{aligned} \tag{2.40}$$

where the k^{th} input bits are a_k and b_k and the k^{th} output bits are I_k and Q_k for the in-phase and quadrature components, respectively. Subsequent decoding of a differentially coded signal can be performed in several ways. Optical decoding can be employed where a signal is delayed by one symbol and superimposed with the subsequent symbol. The resulting field is that of the symbol before differential encoding. An alternative is to coherently detect the optical field and then apply the aforementioned process digitally to the field of the recovered symbols. This is the approach used for recovery of a QPSK in the presence of high phase noise; section 5.2.1.

Table 2.2: LOGIC FOR DIFFERENTIAL ENCODING

Data $a_k b_k$	Phase Difference $\Delta\theta$	Output Logic $p_k q_k$
00	180°	$\overline{p}_{k-1}\ \overline{q}_{k-1}$
01	90°	$q_{k-1}\ \overline{p}_{k-1}$
10	270°	$\overline{q}_{k-1}\ p_{k-1}$
11	0°	$p_{k-1}\ q_{k-1}$

As previously noted, for differentially encoded data the output logic is dependant on the phase transitions (i.e. the phase differences). This property is expressed in Table 2.2 [66]. The disadvantage of this encoding is that, to a first approximation, every bit error incurs a second, correlated error in the following symbol due to the differential encoding between two symbols. However, after this point the symbols can be classified correctly, even in the presence of a cycle slip. The mathematical basis of this problem is discussed in detail by Taylor [63]. Theoretically, error correcting codes can be designed which treat pairs of errors as a single error thereby negating the penalty for differential

decoding; albeit for additional computational complexity [67].

Forward error correction

Sensitivity gains can be achieved through the use of Forward Error Correction (FEC). The principle of FEC is that, by transmitting additional coded information with the data, the signal can be decoded such that all the transmitted data can be recovered (without retransmission) even in the presence of errors. (This technique is not unique to coherent detection schemes, and can equally be applied to direct detection systems.)

In this work, it is the application of FEC, rather than the operating principle of error correcting codes, which is of importance. However, it should be noted that individual codes have different constraints on the distribution and proportion of errors; usually that errors be independent and identically distributed. As the noise sources in this work do follow a Gaussian distribution; the errors can, therefore, be considered to be independent and identically distributed. A possible exception would be in the case of high nonlinearity, as in section 4.1.2, however it is clear that, even in this scenario, about the FEC limit of interest the dominant noise source is AWGN.

In the FEC process, there are a certain number of bits transmitted, n, of which k are usable and $(n-k)$ are discarded after error correction. The value $\frac{k}{n}$ is termed the *code rate* and is a measure of the redundancy used for FEC. Examples of error correcting codes are provided in Table 2.3. An increase in coding overhead can improve the

Table 2.3: ERROR CORRECTING CODES

Code Name	Decision	Overhead (code rate)	BER Corrected Below 10^{-15}
RS(255,239) [68]	Hard	7% (0.935)	1.0×10^{-4}
Interleaved BCH [68]	Hard	7% (0.935)	1.3×10^{-3}
Continuously Interleaved BCH [69]	Hard	7% (0.935)	4.5×10^{-3}
BCH Product Code [70]	Hard	20% (0.833)	1.1×10^{-2}
Continuously Interleaved BCH [69]	Hard	20% (0.833)	1.5×10^{-2}
Interleaved BCH [68]	Hard	25% (0.8)	1.3×10^{-2}
BCH(144,128)×BCH(256,239) [71]	3-bit Soft	25% (0.8)	2.0×10^{-2}
Turbo Product Code [72]	Soft	15% (0.870)	1.8×10^{-2}

performance of FEC; i.e. a higher BER can be corrected to error free. The particular code implementation can also change the performance of the error correction (although the reason for this is outside the scope of this discussion), as can changing the decision type.

At the output of the receiver DSP a decision has to be made on the received bit, $r \in 0, 1$. This is a hard decision, and there are several FEC codes which can correct errors after hard decisions.

It is also possible for the receiver to provide an estimate on the certainty of the received bit (in the case of a digital coherent receiver, this probability is based on the output of the DSP); this is a soft decision. For example, one received data bit in a 3-bit soft decision would take the possible values $r \in 000, 001, 010, 011, 100, 101, 110, 111$, where the most significant bit is the hard decision equivalent bit and the subsequent bits provide probability information (000 and 111 are 'definitely' 0 or 1 bits, respectively). As additional information regarding the signal quality is retained, there is a potential improvement in the efficacy of FEC, but the cost is increased DSP complexity due to the processing of the additional, probability information [69].

Chapter 3 investigates the sensitivity limits when using a coherent receiver in a passive optical network. Soft decision FEC is assumed (unless otherwise noted), as this has the a higher net coding gain than hard decision FEC [71]. For subsequent chapters, the target BER for a particular FEC code is noted.

Orthogonalisation and clustering algorithms

In section 5.3.3, 64QAM signals are generated in order to determine the efficacy of a linewidth reduction scheme. With the large number of constellation points, the modulator bias must be exactly tuned to avoid modulation distortions; inevitably, without automatic bias control, minor distortions will be present. The following two algorithms are used for ensuring the orthogonality of the received constellation (in-phase and quadrature) and that modulation distortions can be overcome using nonlinear decision boundaries.

While optical signals can suffer from distortions due to AWGN, it is also possible that non-deterministic effects can affect signal quality. For example, an imbalance in the power in the quadrature and in-phase components of a QAM signal could be caused through imbalance in the modulator biases. In section 5.3, such small imbalances are corrected through the Gram-Schmidt Orthogonalisation Procedure [73].

The algorithm for implementing this procedure takes a set of nonorthogonal samples and transforms them to a set of orthogonal samples. Following the notation in [73], for a received signal with in-phase and quadrature components r_I and r_Q, respectively, the orthogonalised signal components, I^o and Q^o are given by

$$\begin{aligned} I^o(t) &= \frac{r_I(t)}{\sqrt{P_I}} \\ Q'(t) &= r_Q(t) - \frac{\rho r_I(t)}{P_I} \\ Q^o(t) &= \frac{Q'(t)}{\sqrt{P_Q}} \end{aligned} \tag{2.41}$$

where $\rho = E\{r_I \cdot r_Q(t)\}$ is the correlation coefficient, $P_I = E\left\{r_I^2(t)\right\}$, $P_Q = E\left\{Q_I'^2(t)\right\}$

and $E\{\cdot\}$ is the expectation operator.

The second algorithm used is the k-means clustering algorithm[6] [74]. This algorithm iteratively tracks the displacement of constellation points from their optimal position by treating each cluster of constellation points as a two dimensional Gaussian with a variable mean. Another way of viewing this algorithm is that it moves the effective decision boundaries to their optimal position, instead of, for example, using rectangular decision boundaries, making it ideal for QAM where modulation distortions are present [75]. Again, this algorithm is used in section 5.3, for optimising the detection of 64QAM signals.

[6]This is a simple well-known algorithm from the field of machine learning, and so is not repeated in detail here.

3

Approaching the limits of receiver sensitivity

THE FUNDAMENTAL power sensitivity limit of an optical receiver is determined by several factors. The choice of modulation format used for communication impacts directly on receiver sensitivity; as noted in section 2.2, the transmitted constellation points can be arranged in such a way as to encode more information in a symbol period, or to increase the Euclidean distance between points to reduce the probability of a bit being received in error in the presence of noise. For a coherent receiver, the primary receiver noise source is shot noise (or quantum noise), as described in section 2.3.2, which arises due to the Poisson distribution of the arrival time of incident photons.

Considering this, this chapter details an investigation into methods for approaching the sensitivity limit of coherent optical receivers, beginning with section 3.1, which details the theoretical and experimental sensitivity advantages of coherent detection, and the further gains which can be made using optical preamplifiers.

For reasons of transceiver electrical (and optical) bandwidth efficiency in a PON, it is important to minimise the bandwidth required to modulate at a particular data rate, while not compromising on receiver sensitivity. Section 3.2 details the use of advanced modulation formats with coherent receivers and investigates how judicious selection of a modulation format can give sensitivity gains, spectral efficiency gains, or both.

Throughout, the significance of high performance FEC is considered. The recently

developed error correcting codes listed in section 2.4.4 provide a particular net coding gain for a fixed coding overhead, which can be used to estimate the receiver performance after error correction is applied.

Finally, section 3.3 describes an experiment which combines the above techniques to demonstrate, for the first time, a receiver operating at 40 Gbit/s with a sensitivity below 4 photons/bit[1] at a BER of 4.5×10^{-3}. This result is compared to other recent sensitivity experiments in terms of sensitivity and data rate.

3.1 Coherent receivers and optical preamplification

One of the great advantages of coherent receivers is that they recover the full optical field (section 3.2), enabling the use of advanced modulation formats which utilise all four dimensions available for transmission through an optical fibre. Additionally, if ADCs are employed within the coherent receiver, DSP can be used to manipulate the digitised information and undo transmission and modulation distortions affecting the optical signal. It is these properties combined that allow digital coherent receivers to enable both high capacity and high receiver sensitivity.

3.1.1 Receiver sensitivity using PDM-QPSK

The format PDM-QPSK, which carries 4 bit/symbol, is a good example of a format which can be detected with a high sensitivity using coherent receivers (section 2.2). This format is an ideal starting point for investigating receiver sensitivity as its generation and digital processing requirements are well established. The following details a series of experiments which use PDM-QPSK to investigate coherent receiver sensitivity. Shown in Fig. 3.1 is the experimental configuration used for generating PDM-QPSK.

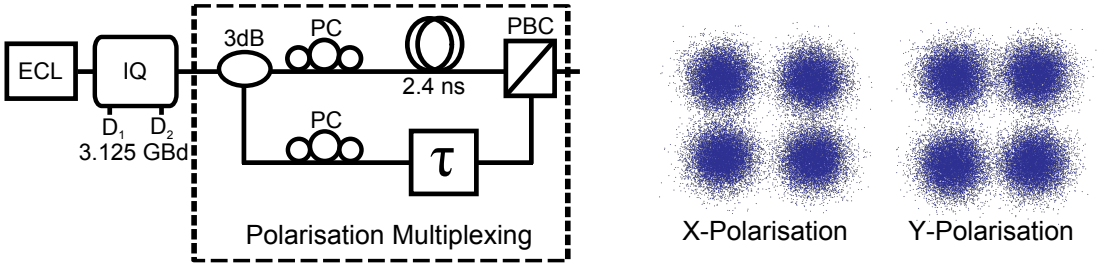

Figure 3.1: The experimental transmitter configuration for the generation and transmission of PDM-QPSK. Shown on the right are example constellations with a BER of 3×10^{-3}.

An External Cavity Laser (ECL) (wavelength 1550 nm, linewidth ∼100 kHz) was modulated using an IQ modulator, which was driven with two decorrelated Pseudo-

[1]This sensitivity is given net of a 7% FEC overhead.

Random Binary Sequences (PRBS) of length $2^{15} - 1$ at a frequency of 3.125 GHz. This resulted in a single polarisation QPSK signal with a symbol rate of 3.125 Gbaud.

To obtain polarisation multiplexing in a practical system, the outputs from two such modulators would be combined in orthogonal polarisations. However, for experimental convenience, the optical output from the modulator was sent to a stage which emulates polarisation multiplexing. It does so by equally splitting the signal into two optical fibres, each containing a delay line and a Polarisation Controller (PC). The delay in one arm is varied such that the two arms are delayed relatively by an integer number of symbols. The two arms are then recombined in orthogonal polarisations using a Polarisation Beam Combiner (PBC).

The resulting format emulates PDM-QPSK at 3.125 Gbaud (12.5 Gbit/s). This data rate was chosen as it enables transmission at 10 Gbit/s with a 25% overhead reserved for FEC. Using this coding overhead, the target BER is 2×10^{-2} (assumed herein) for soft decision FEC (section 2.4.4).

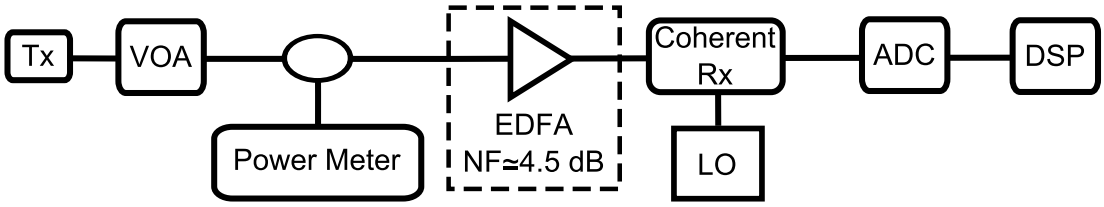

Figure 3.2: Experimental configuration for measuring the sensitivity of a digital coherent receiver. A Variable Optical Attenuator VOA was used to set the power to the receiver. Where noted, an EDFA was used to amplify the optical signal prior to detection.

Shown in Fig. 3.2 is the experimental configuration used for evaluating the sensitivity of the digital coherent receiver; this is the configuration which was used for the subsequent work in this chapter, unless otherwise noted. Note that a second ECL was used as the LO, that the signal from the ADCs was resampled at 2 samples/symbol and that the DSP was performed offline using the techniques described in section 2.4.

It was noted in section 2.3.2 that the sensitivity limits for a phase- and polarisation-diverse coherent receiver with and without preamplification converge on the same value; that is, the shot noise limit. However, this analysis neglects receiver noise sources which have a greater impact at low incident optical power (such as quantisation noise from the ADC, or noise from the TransImpedance Amplifiers (TIAs) after the photodiodes). Therefore, preamplification will improve performance. Fig. 3.3 shows the results of this investigation.

For ideal preamplification, the amplifier noise figure must be 3 dB (the quantum limit, see section 2.3.2). When using an amplifier with a $\simeq 4.5$ dB noise figure, the penalty is measured to be 1.8 dB from the quantum limit at the FEC limit. It can also be seen that the use of an EDFA improves sensitivity by 7.2 dB versus the scenario without preamplification. The reason for the 9 dB penalty versus the shot noise limit

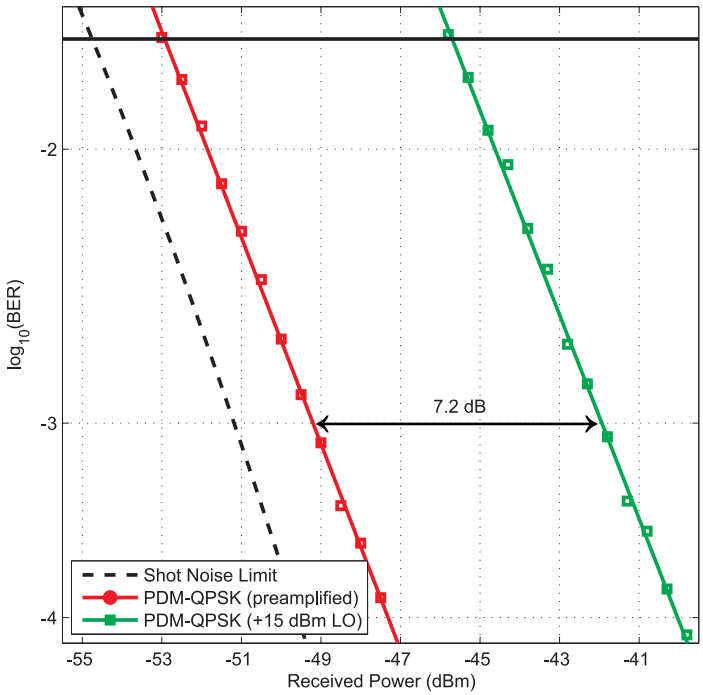

Figure 3.3: Experimentally measured sensitivity and sensitivity gain obtained through optical preamplification of a coherent receiver [31]. Across all measured optical input powers, the measured sensitivity improvement for 12.5 Gbit/s PDM-QPSK was 7.2 dB. For reference, the dashed black line shows the theoretical shot noise limited sensitivity (see appendix A) for 12.5 Gbit/s PDM-QPSK, and the solid black line indicates the 2×10^{-2} BER.

(equal to the quantum limit in this scenario) without preamplification can be attributed to loss in the optical hybrid, the quantum efficiency of the photodiodes and the limited ADC resolution.

3.2 Advanced modulation formats for PON

3.2.1 Polarisation-switched QPSK

It has been previously shown that different modulation formats exhibit different tolerances to noise [50]. Improved performance can be attributed to a greater distance (Euclidean distance) between constellation points, minimising the probability of bit errors. There are many formats (particularly square QAM) where a rigorous analysis has been performed in two dimensions (phase, amplitude), however, the optical channel supports four dimensions (phase and amplitude on both the X- and Y-polarisations), and so if all four dimensions are modulated independently then the minimum distance between constellation points must be also be determined in four dimensions in order to calculate the expected sensitivity.

For polarisation multiplexed formats, the second polarisation can be treated as an independent channel as the statistics of the noise on the second polarisation are

decoupled from the first, so the effective sensitivity does not change. However, when the polarisation state is modulated, as is the case for polarisation-switched quadrature phase shift keying (PS-QPSK), the knowledge of the permissible symbols can be used to improve the receiver sensitivity. In fact, the asymptotic (high OSNR) sensitivity advantage of PS-QPSK over PDM-QPSK is 1.76 dB, reducing to 0.5 dB at a BER of 2×10^{-2}[50]. The transmitter structure for generating PS-QPSK is show in Fig. 3.4. This is the transmitter configuration used throughout this chapter. PS-QPSK simply

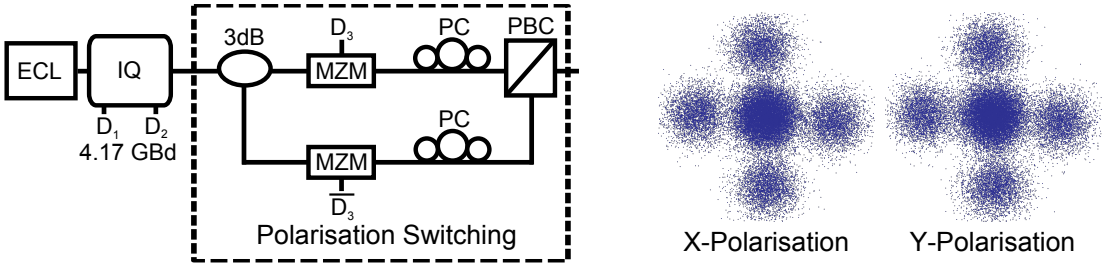

Figure 3.4: The experimental transmitter configuration for the generation of PS-QPSK at a symbol rate of 4.17 GBd (12.5 Gbit/s). Shown on the right are example constellations with a BER of 3×10^{-3}.

consists of QPSK being present in one of two orthogonal polarisation states in each symbol period. As such, it carries three bits of information per symbol (two in phase, one in polarisation). PDM-QPSK by comparison carries four bits of information per symbol. The method for generating this format is shown in Fig. 3.4. Essentially, a single polarisation QPSK symbol is generated using an IQ modulator, and this is polarisation switched by splitting the signal equally into two optical fibres, each containing a MZM acting as an intensity modulator. These are driven symbol-synchronously to extinguish one arm when the other is in a transmit state. The two signals are recombined in orthogonal polarisations such that there is power in only one polarisation in each symbol slot.

3.2.2 Modulation formats for sensitivity limited applications

Pulse position modulation

Historically, there have been several attempts at producing modulation formats for high sensitivity applications. One such modulation format is Pulse Position Modulation (PPM), which has for many years been deployed for use in deep-space optical communications [76]. The details of this format are given in appendix A; here an overview of the properties of this format are given.

PPM is an amplitude modulation format where the optical power can only exist in one of M time slots, encoding $\log_2(M)$ bits of data per M time slots. In such a system, the noise power of a slot can be averaged over the entire symbol, resulting in an

increased sensitivity [77]. The compromise is that the data rate, for a fixed slot rate, is reduced by a factor of $\log_2(M)/M$, making the modulation format unsuitable for high data rate communications.

Having said this, Liu *et. al.* [78, 79] investigated the possibility of encoding phase information with the burst of photons used for the PPM symbol; in this case combining PDM-QPSK and 16-*ary* PPM. In this configuration, each symbol carries 4 bits from PDM-QPSK and 4 bits from 16-PPM. In order to carry the same information using PPM alone would require 256-PPM, meaning that this combined modulation format offers a 16-fold reduction in bandwidth requirements. The disadvantage of this approach is that correct decoding of the QPSK information is dependent on correct decoding of the PPM information, and so the theoretical performance of this format (dubbed PQPPM) is dependent on a combination of the respective sensitivities of the underlying formats.

This combined modulation format exhibits a 2.9 dB sensitivity gain over PDM-QPSK at a BER of 10^{-3}. However, a simple calculation shows that, even as a combined modulation format, the bandwidth expansion factor makes this format prohibitive for the 10 Gbit/s access network considered in chapter 4. For example, 16-*ary* PQPPM would require a bandwidth of 25 GHz to encode 12.5 Gbit/s; 8 times greater than the requirements for PDM-QPSK.

More recently, still, the possibility of combining other formats with PPM was investigated [80]. In this work, the relative asymptotic sensitivity performance was evaluated theoretically for several formats based on PPM, using the state of polarisation and signal phase as degrees of freedom. However, as this work only investigated the asymptotic (i.e. low BER) performance of the formats. For communications systems incorporating FEC, the relationship between modulation format and sensitivity is less straightforward. In any case, there is still a significant bandwidth expansion factor, which makes these formats less attractive for implementation in PONs.

A comparison of PS-QPSK, PDM-BPSK and PDM-QPSK

It is of interest to see how PS-QPSK compares to other modulation formats in a typical PON scenario. In this section, PS-QPSK is compared to PDM-BPSK and PDM-QPSK in terms of receiver sensitivity performance. PS-QPSK and PDM-QPSK are generated using the method shown in Figs. 3.4 and 3.1, respectively. PDM-BPSK was generated using a similar method to PDM-QPSK, except the IQ modulator was driven in a push-pull configuration in order to minimise the loss of the generation stage. This generation technique is shown in Fig. 3.5.

The four scenarios considered are with/without receiver preamplification using an EDFA and with/without transmission. Consider the configuration shown in Fig. 3.6 which was used for this investigation. A modulation format (PDM-BPSK, PDM-QPSK,

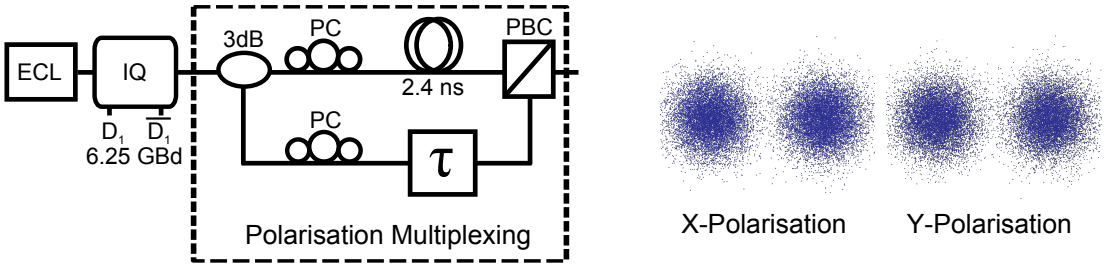

Figure 3.5: The experimental transmitter configuration for the generation of PDM-BPSK at a symbol rate of 6.25 GBd (12.5 Gbit/s). Shown on the right are example constellations with a BER of 3×10^{-3}.

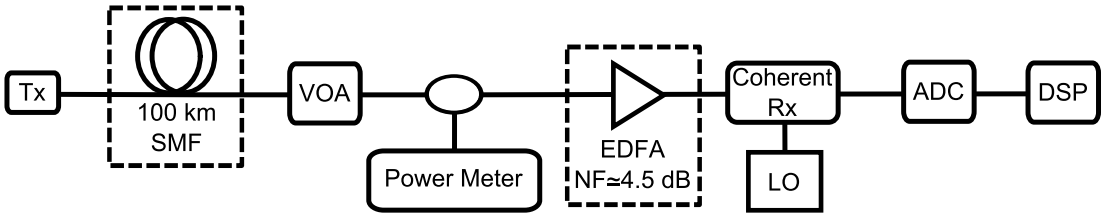

Figure 3.6: The transmission and receiver configuration used to investigate the sensitivity of a coherent receiver when using different modulation formats.

PS-QPSK) was generated using the techniques previously described in the 'Tx' block. Where transmission was tested, the signal was propagated over 100 km SMF, with a measured loss of 0.2 dB/km. A Variable Optical Attenuator (VOA), was used to set the power to the EDFA (where used) or the coherent receiver. This power was measured using a calibrated power meter.

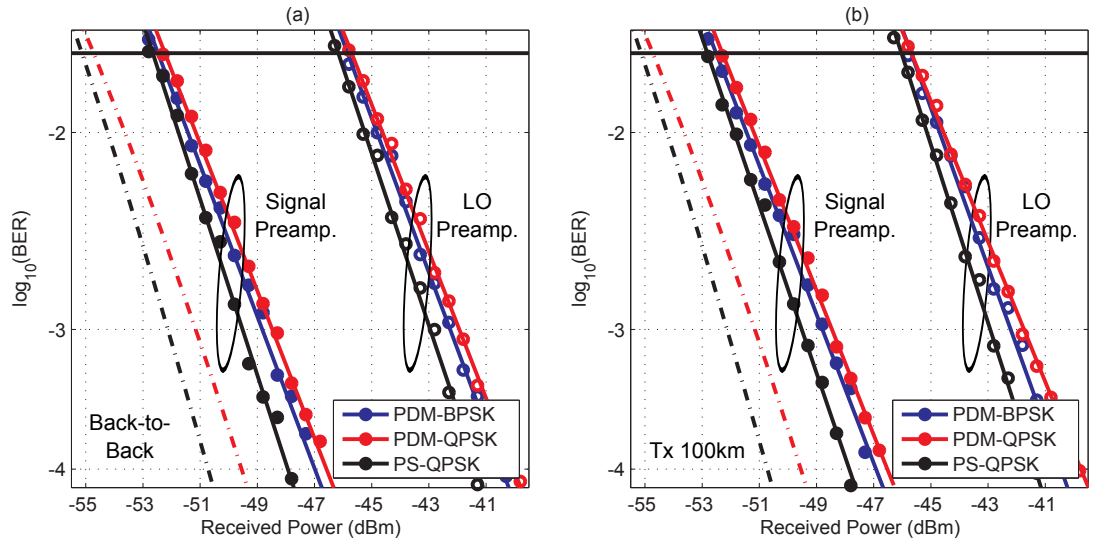

Figure 3.7: Experimental power sensitivities of PDM-BPSK, PDM-QPSK and PS-QPSK at 12.5 Gbit/s. Shot noise limits are shown for PS-QPSK (black dashed line) and PDM-QPSK and PDM-BPSK (red dashed line, note the theoretical receiver sensitivity is the same). Open circles are with LO amplification (to +15 dBm), filled circles are with signal amplification. The advantage of PS-QPSK over the reference formats in (a) back-to-back configuration, is maintained in (b) transmission over a 100 km link (0 dB signal launch power). [39].

The results shown in Fig. 3.7 highlight some of the interesting properties of PS-QPSK which can be advantageous in passive optical networks. Firstly, Fig. 3.7(a) shows that, at a BER of 2×10^{-2}, the back-to-back sensitivity of PS-QPSK exceeds that of PDM-QPSK by 0.5 dB, and of PDM-BPSK by 0.3 dB, with or without signal preamplification. In transmission, as shown in Fig. 3.7(b), the sensitivity advantage is maintained by PS-QPSK; as before, more than 0.3 dB sensitivity advantage is seen over PDM-BPSK and PDM-QPSK.

Note that the sensitivity of PDM-BPSK exceeds the expected sensitivity by 0.2 dB. This sensitivity gain can be attributed to an increased transmitted signal-to-noise ratio, achieved by driving the IQ modulator in a push-pull configuration.

At the FEC limit, the penalty with respect to the shot noise limit is approximately the same for both PDM-BPSK and PS-QPSK (2.4 dB) due to the 0.4 dB difference in the OSNR tolerance of these modulation formats. Should a higher code rate (lower coding overhead) be employed, the advantages for using PS-QPSK increase; at a BER of 10^{-3}, the benefit is 0.7 dB over PDM-BPSK and 1.0 dB over PDM-QPSK.

3.2.3 Sensitivities of spectrally efficient modulation formats

Discussed in the following chapter is the possibility of using Wavelength Division Multiplexing (WDM) to increase the capacity of a PON. When channels are brought closer together in wavelength, such that the symbol rate is of the order of the channel spacing, linear crosstalk between channels impairs transmission performance. However, the data rate can be increased while maintaining the symbol rate if high spectral efficiency modulation formats are employed.

Two such formats, which both carry 6 bit/symbol, are PDM-8PSK and PDM-8QAM. The differences between these formats lie in the arrangement of constellation points; 8PSK consists of 8 equally spaced points on a phasor with constant modulus, whereas 8QAM is essentially two nested QPSK constellations. While the generation of 8PSK is potentially simpler than for 8QAM (due to its constant modulus), both formats have the same electrical bandwidth requirements. Example constellations and experimental configurations are shown in Fig. 3.8.

To generate 8PSK at 12.5 Gbit/s, Fig. 3.8(a), light from an ECL was modulated to generate a QPSK signal (as previously described). This signal was then passed through a phase modulator (denoted ϕ) driven to provide a $\pi/4$ phase shift to the signal; encoding a third bit of data.

The modulation format 8QAM was generated in a similar way, Fig. 3.8(b), except that the QPSK signal was passed through a second IQ modulator which was biased such that the QPSK constellation was mapped to an inner and outer QPSK constellation. Data was encoded on the inner constellation using a third driving signal, and the bias

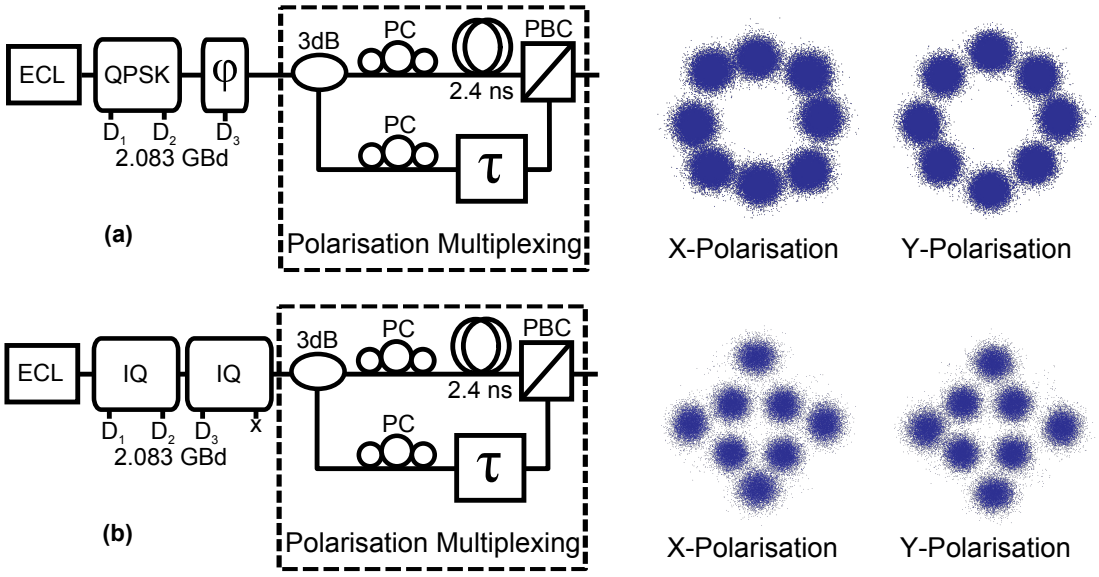

Figure 3.8: Configuration for generation of 12.5 Gbit/s (a) 8PSK, and (b) 8QAM. Shown on the right are example constellations with a BER of 3×10^{-3}.

values were set such that the inner constellation had a $\pi/2$ rotation relative to the outer constellation.

The experimental investigation of sensitivity was undertaken using the receiver preamplified configuration shown in Fig. 3.2.

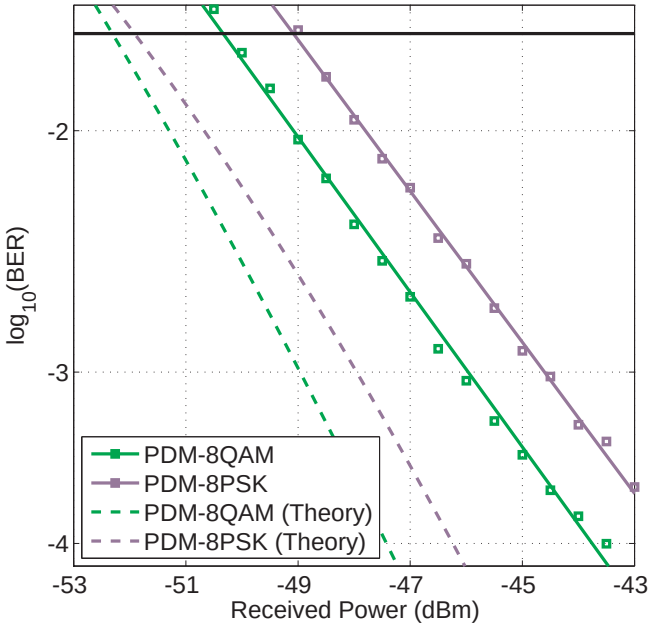

Figure 3.9: The receiver sensitivity achieved using 12.5 Gbit/s PDM-8PSK and PDM-8QAM.

The results from experimentally comparing PDM-8PSK and PDM-8QAM are shown in Fig. 3.9. Additionally shown are the theoretical limits of receiver sensitivity for these two formats (see appendix A). Note, firstly, that PDM-8QAM exhibits a greater sensitivity than PDM-8PSK for all the test powers, in line with theory. This is

due to this increased Euclidian distance between constellation points for 8QAM when compared with 8PSK. However, note that there is an increasing discrepancy between theory and experiment towards the high BER region.

The theoretical curves converge, indicating only a small benefit from using 8QAM but the benefit is more marked in practice. This can be attributed to a greater implementation penalty for 8PSK due to the narrow phase margin between constellation points. Even so, this investigation highlights and confirms 8QAM as a more power efficient format to use in a PON and, therefore, 8QAM will be considered in the following section. This result is used in the following section where the compromise between receiver sensitivity and information content is discussed.

3.2.4 Information-sensitivity trade-off

Intuitively, it might be expected that an increase in the information carried in each symbol period would lead to a degradation in sensitivity. However, Fig. 3.7 shows that this is not necessarily the case. Receivers using PS-QPSK are more sensitive than those using PDM-BPSK, but PS-QPSK carries three bits of information per symbol against only two for PDM-BPSK.

Two formats which carry equivalent information in each symbol period can exhibit very different sensitivities, as shown in the previous section (Fig. 3.9). As such, the correlation between receiver sensitivity and information carried per symbol (sometimes termed constrained capacity) needs to be examined.

Using the transmitter configurations already outlined, and the receiver configuration shown in Fig. 3.2, the sensitivity of a coherent receiver was experimentally obtained using four different modulation formats: PDM-BPSK, PS-QPSK, PDM-QPSK, and PDM-8QAM. The results of this investigation are shown in Fig. 3.10(b) for the preamplified receiver and Fig. 3.10(c) for the receiver without preamplification [40]. Fig. 3.10(a) provides the theoretical limits for reference.

The modulation format PS-QPSK exhibits the highest sensitivity. As such, it is pertinent to ask whether PS-QPSK is the optimum modulation format for loss limited communication, such as in a PON scenario. This figure shows that, with the exception of 8QAM, the relative sensitivity of each format converges at high BERs; mitigating the intrinsic advantages of the more sensitive formats. (This is highlighted in the theoretical curves shown in Fig. 2.4. Here, theoretical curves for higher order square QAM are compared with the reference formats. It can be seen that, again with the exception of 8QAM, the sensitivity of the formats converge at high BERs, albeit more slowly for the higher order formats.)

The experimental sensitivities at the 1.3×10^{-3} and the 2.0×10^{-2} BER limits for FEC (section 2.4.4) are shown against achievable information per symbol for each

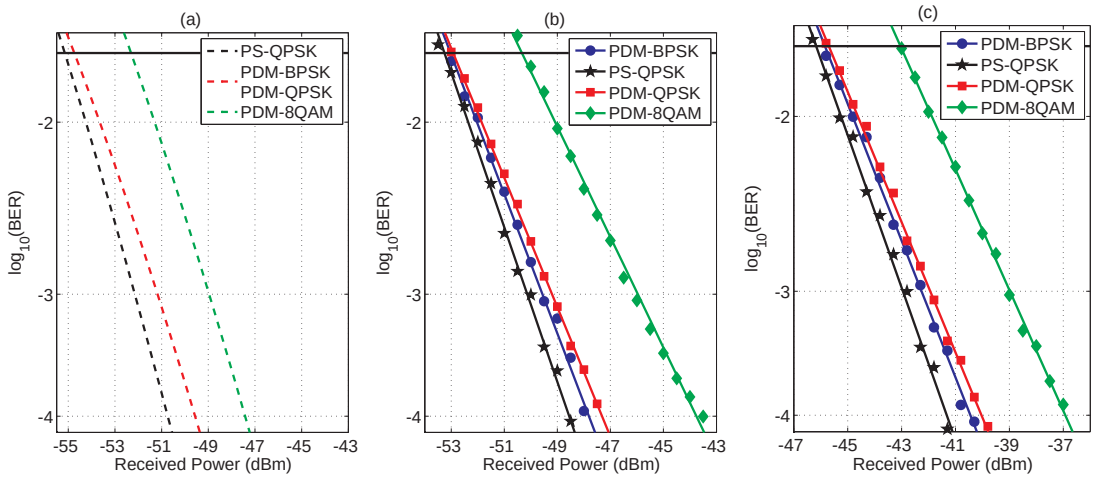

Figure 3.10: Sensitivity of different modulation formats at a data rate of 12.5 Gbit/s. Shown in (a) are the theoretical shot noise sensitivity limits (QPSK and BPSK have the same sensitivity limit). The experimental data points are shown (b) with receiver preamplification and (c) without receiver preamplification. The horizontal black line indicates the 2×10^{-2} FEC limit.

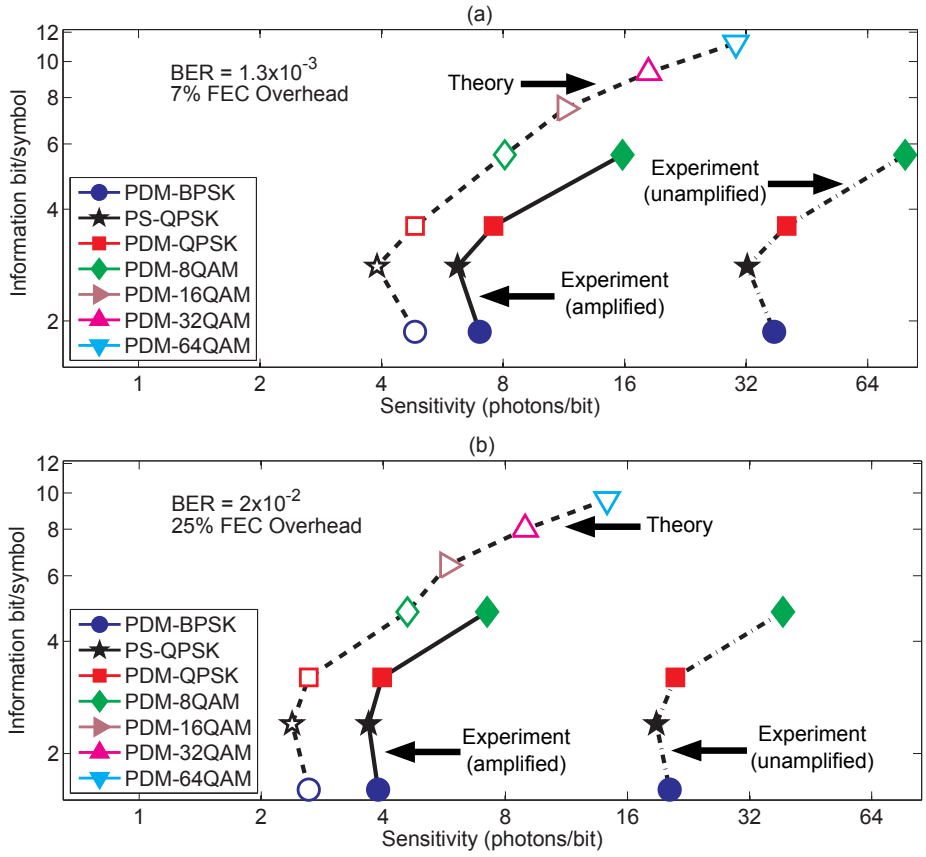

Figure 3.11: Theoretical (open markers) and experimental (filled markers) information per symbol (net of FEC overhead) versus sensitivity for the modulation formats under test. To highlight the trend, theoretical values for higher order QAM are also shown. The sensitivity for each format at a target BER of 1.3×10^{-3} is shown in (a), where a 7% overhead is assumed for FEC. The sensitivity at a target BER of 2×10^{-2} is shown in (b), where a 25% overhead is assumed for FEC.

format in Fig. 3.11. This figure highlights the aforementioned trend of the sensitivities for each format to converge at high BERs.

There are two particularly important results that can be derived from this figure. Firstly, relative sensitivity gain for each format is independent of whether or not the receiver is preamplified. Secondly, the optimum choice of modulation format is strongly dependent on the choice of FEC code. For codes with a high net coding gain, there is very little to choose between the formats in terms of sensitivity, and this is apparent from inspection of Fig. 3.11(b). As such, PDM-QPSK should be favoured over other modulation formats when this is the case, as the required transceiver bandwidth is lower than PS-QPSK for a particular data rate.

However, when FEC with a lower net coding gain is used, then the sensitivities diverge, and it becomes more advantageous to use PS-QPSK, as it offers an expected sensitivity gain of 1 dB over PDM-QPSK and PDM-BPSK. However, this result should be accepted with caution. The 1 dB sensitivity gain of PS-QPSK (c.f. theoretical curves Fig. 3.10(a)) is at the cost of a 1.25 dB (25%) reduction in information content per symbol (constrained capacity), which is important when trying to utilise the full fibre bandwidth available for transmission.

This is a significant result for the investigation of the long reach access network in chapter 4, because it suggests that the power budget increase afforded by PS-QPSK can be exchanged for reduced transceiver bandwidth requirements in both the electrical and optical domains. While the sensitivity gains afforded by PS-QPSK are demonstrably significant in long-haul communications [34], the alternative use of PDM-QPSK reduces transmission reach by between 2.5 km and 5 km in loss-limited transmission systems (assuming SMF loss of 0.2 dB/km); this does not justify the increased bandwidth requirements of PS-QPSK.

3.3 Probing coherent receiver sensitivity limits

As previously noted, the use of optical preamplification can greatly improve the achievable sensitivity of a coherent receiver. It was also noted in section 2.3.2 that this achievable sensitivity could be further improved to approach the shot noise limit as the noise figure of the preamplifier is reduced. This is because the spontaneous emission factor, n_{sp}, would also be reduced, up to a limit of 1 (i.e. a 3 dB noise figure). This motivated an investigation into receiver sensitivity using a 3.25 dB noise figure EDFA as the optical preamplifier. The goal of this work was to experimentally probe the achievable sensitivity limits when using a digital coherent receiver. Additionally, as was noted in section 3.2.2, whilst receiver sensitivity can be traded for bandwidth, for this thesis it is of interest to maintain sensitivity, even for multi-Gigabit/s transmission systems. To emphasise this point, the following experiments are performed at 40 Gbit/s

and 100 Gbit/s.

The experimental configuration used in this investigation is shown in Fig. 3.6; here the EDFA was replaced with a dual stage low noise figure EDFA; details are given in Table 3.1.

Table 3.1: LOW NOISE FIGURE EDFA PARAMETERS

	EDFA 1	**EDFA 2**	**Combined**
Pump Wavelength (nm)	977	977	-
Pump Power (mW)	450	450	-
Erbium Doped Fibre length (m)	7.1	20	-
Small Signal Gain (dB)	-	-	44
Small Signal Noise Figure (dB)	-	-	3.25

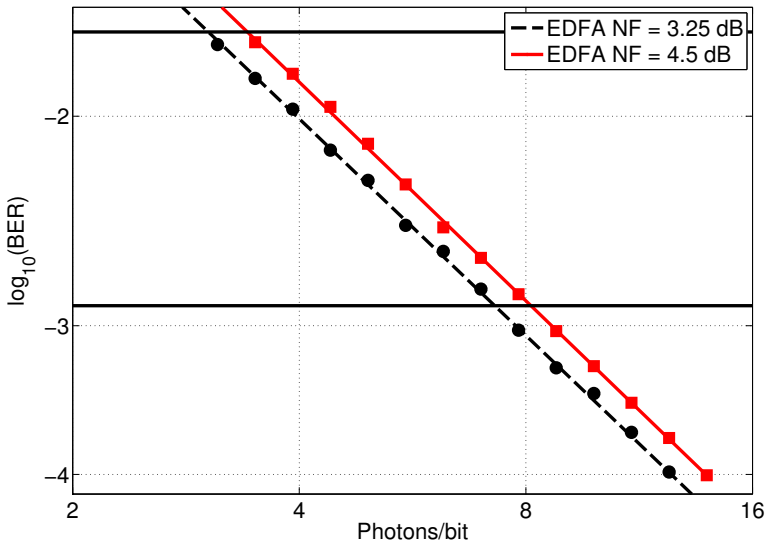

Figure 3.12: The experimental receiver sensitivities when using a 3.25 dB noise figure optical preamplifier and a 4.5 dB noise figure optical preamplifier with the modulation format 28 Gbaud PDM-QPSK. Two FEC limits are highlighted by horizontal black lines: 1.3×10^{-3} and 2.0×10^{-2}. The assumed code rate is 0.8 for the higher BER, giving a net bit rate of 89.6 Gbit/s.

The receiver side DSP required modification to enable transmission at the higher symbol rates, with a chromatic dispersion compensating filter included prior to equalisation, as detailed in section 2.4.

The results of this investigation, shown in Fig. 3.12, highlight the sensitivity gains which can be made when using a low noise figure preamplifier. In this test case, back-to-back 28 GBd PDM-QPSK, the improvement in sensitivity at a BER of 2.0×10^{-2} the gain was 0.6 dB. This shows that, in addition to the use of coherent detection and FEC, an improvement in the noise figure of the optical preamplifier also offers significant sensitivity gains[2].

[2]This is the key result from the work in [38].

The limits of this technique were also investigated, in order to maximise the receiver sensitivity at the highest possible data rate. The optimum choice of modulation format to investigate sensitivity limits would be PS-QPSK however, due to experimental limitations, it was only possible to generate PS-QPSK at 14.3 GBd. As such, 28 GBd PDM-QPSK is included as a high data rate reference point.

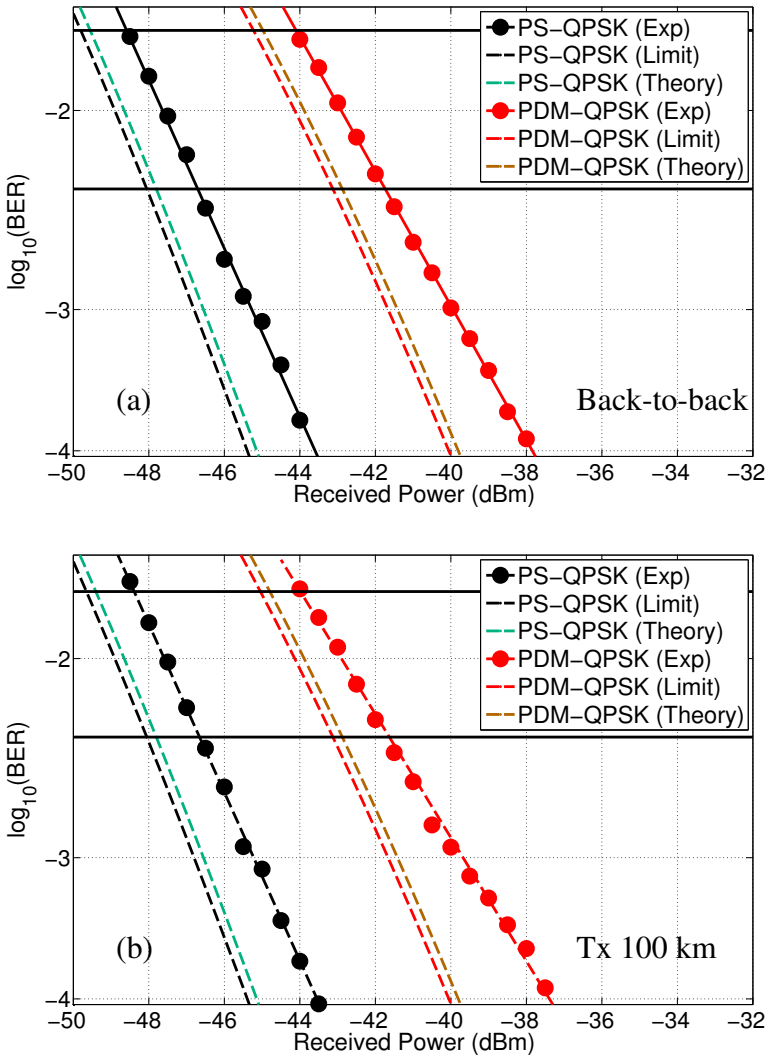

Figure 3.13: Receiver sensitivity of 40 Gbit/s PS-QPSK and 100 Gbit/s PDM-QPSK. The solid black lines highlight the 4.5×10^{-3} and 2×10^{-2} FEC limits. Shown in (a) are the back-to-back sensitivities, while in (b) transmission over 80 km SMF is considered. The shot noise limit (Limit) and the theoretical limit using a 3.25 dB noise figure preamplifier (Theory) are shown as derived from the formulae in appendix A.

Fig. 3.13(a) shows the achievable sensitivities in the back-to-back configuration. Fig. 3.13(b) shows the receiver sensitivity after 100 km transmission. Note that the receiver sensitivity is degraded by less than 0.1 dB at a BER of 2×10^{-2}

It is of interest to compare these results with previously reported high sensitivity receivers; this comparison is made in Fig. 3.14. First, note that research has historically focussed on low data rate channels, such as for deep space communications. Neverthe-

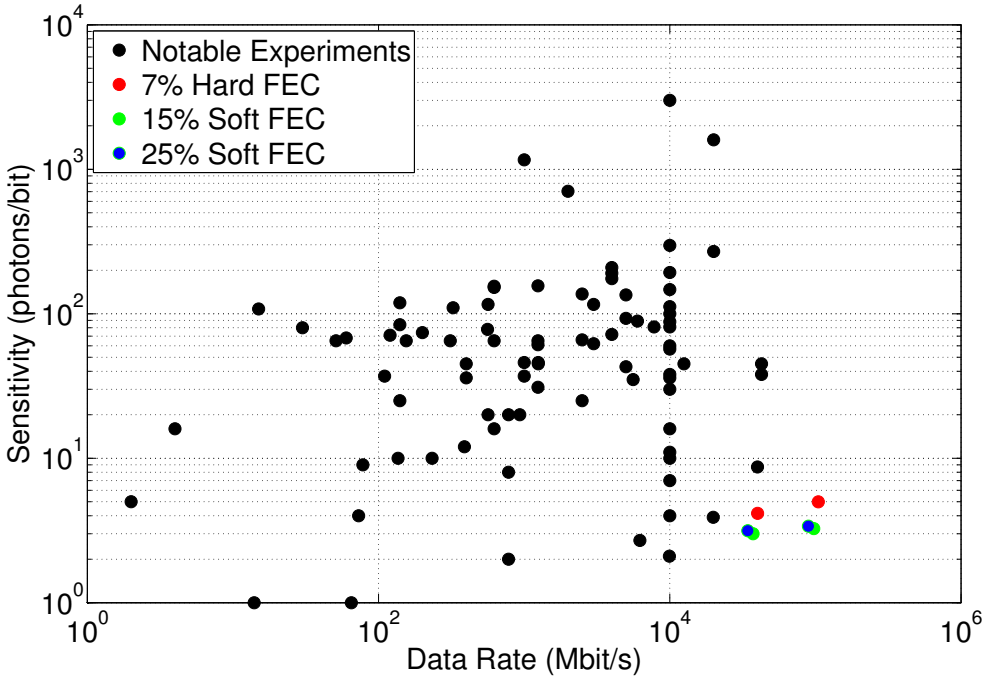

Figure 3.14: Record experimental receiver sensitivities [76, 78, 79, 81] in photons/bit net of coding overhead. The new results from this thesis assume the use of a particular FEC code (see section 2.4.4).

less, chiefly by using PPM, sensitivities better than 5 photons per bit have been reported for data rates below 20 Gbit/s. Gains have also been made when using FEC, however, in isolation, the sensitivity limit is 1 photon/bit [82].

Note that sub 1 photon/bit communications is possible when considering PPM with FEC. However, this is yet to be demonstrated for high data rates. For example, in [83], a sensitivity of 0.5 photons/bit was achieved for a data rate of 781 Mbit/s, but only when accounting for the quantum efficiency of the photodetector.

The work described herein (Fig. 3.14, bottom right) has demonstrated the possibility of using coherent receivers, FEC, and advanced modulation formats to achieve a high sensitivity, without the comparatively large bandwidth expansion of PPM. This enabled the generation and detection of 14.3 GBd PS-QPSK and 28 GBd PDM-QPSK with sensitivities better than 5 photons/bit. However, this analysis makes assumptions on the error correcting code used. Three FEC scenarios are considered; 7% hard FEC with a BER tolerance of 4.5×10^{-3}, 15% soft FEC with a BER tolerance of 1.8×10^{-2} and 25% soft FEC (assumed throughout this chapter) with a BER tolerance of 2×10^{-2} [69, 72, 71].

The key results are then as follows. The highest sensitivity at 40 Gbit/s using PS-QPSK and hard decision FEC is then 4 photons/bit. For 100 Gbit/s PDM-QPSK this rises to 5 photons/bit (7% hard decision FEC). Sacrificing some of the data for additional error correction, the performance can be enhanced to 3 photons/bit for PS-QPSK and 3.3 photons/bit for PDM-QPSK. However, whilst the 25% overhead soft

decision FEC (assumed throughout this chapter) achieves a net data rate of 34 Gbit/s (90 Gbit/s PDM-QPSK), the most advanced soft decision FEC requires only a 15% overhead, achieving 37 Gbit/s (97 Gbit/s PDM-QPSK).

3.4 Summary

The combination of high data rates and the high power sensitivity achievable when using digital coherent receivers is demonstrated. The results in this chapter show the many techniques that can be used to enhance this sensitivity. Notably, this chapter identifies the ideal modulation for use in a 10 Gbit/s/λ UDWDM LR-PON as PDM-QPSK. This result is used in chapters 4-5. The main findings of this chapter are as follows.

- Comparison of the achievable receiver sensitivity when using advanced modulation formats, FEC, and receiver preamplification and a discussion of the trade-off between receiver sensitivity and information content per symbol when selecting advanced modulation formats
- PDM-QPSK identified as the best modulation format for a 10 Gbit/s/λ LR-PON when FEC is employed
- High sensitivity (4 photons/bit) demonstrated when using PS-QPSK at 40 Gbit/s with low noise receiver preamplification (5 photons/bit also demonstrated for PDM-QPSK at 100 Gbit/s)
- Advanced forward error correcting codes could improve the sensitivity in both cases to approximately 3 photons/bit.

4

Coherent access networks

PASSIVE optical networks (PON) are a potentially cost-effective solution for offering Gigabit/s data rates to multiple network subscribers. As described in chapter 1, the long-reach (100 km) PON is particularly economical, because the metropolitan area network can be combined with the access network. However, in order to increase both capacity and reach to implement such a network, the receiver sensitivity must be increased. Chapter 2 detailed the advantages of coherent receivers which make them suitable for use in a PON; notably, high receiver sensitivity. Of additional significance is their compatibility with advanced modulation formats, which reduces the transceiver electrical bandwidth required to achieve a particular data rate, while increasing network capacity.

Using the findings from chapter 3, which determined the optimum modulation format for use in a PON (maximising capacity for a small sensitivity penalty) this chapter experimentally investigates the use of coherent transmission systems for the optical access network. Section 4.1 initially investigates the relationship between receiver sensitivity, network capacity and reach. Beyond this, Section 4.1.2 details investigations seeking the optimal channel spacing in a WDM-PON, while section 4.2 investigates how bidirectional (full duplex) transmission on an optical fibre impacts on optimal channel spacing. Finally, section 4.3 investigates the impact of crosstalk at the Optical Network Unit (ONU) due to Rayleigh backscattering, and how pulse shaping can be used to mitigate this effect.

4.1 Coherent receivers in access networks

4.1.1 Single channel benchmark

In this work, the use of a phase- and polarisation-diverse digital coherent receiver was investigated for high sensitivity reception of optical signals. In chapter 3 it was shown that such receivers offer high sensitivity whilst enabling the use advanced modulation formats. Specifically, it was found that it was possible to achieve a high sensitivity in a narrow optical bandwidth using PDM-QPSK, making it a good choice of modulation format for a 10 Gbit/s PON. Critical in a PON is how that receiver sensitivity impacts on power budget. To investigate this a single PDM-QPSK channel was generated and detected, in order to evaluate the maximum achievable single channel capacity of a coherent PON. The experimental configuration shown in Fig. 4.1 was used to investigate this.

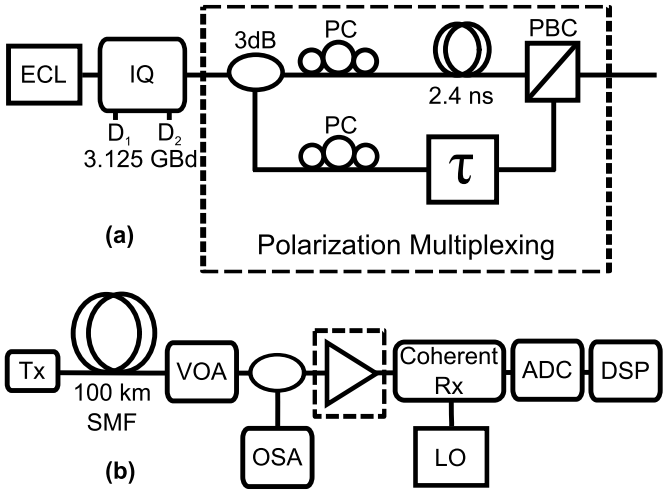

Figure 4.1: Experimental configuration used to investigate the propagation of a single 12.5 Gbit/s QPSK channel over a 100 km SMF. Shown in (a) is the PDM-QPSK generation and in (b) is shown the optical fibre and the digital coherent receiver. The VOA is used to emulate splitting loss and, where noted, the EDFA is used to preamplify the signal.

Using the DSP described in chapter 2, it was possible to transmit over 100 km SMF without penalty versus the back-to-back scenario. With a launch power to the fibre of 0 dBm, the loss budget with preamplification was 52.9 dB at a BER of 2×10^{-2}, and without preamplification this dropped to 45.7 dBm. (This corresponds to 1024 and 256 subscribers, respectively.) Shown below is an analysis of how such a receiver would impact on access network capacity and reach [42, 31, 39].

Fig. 4.2 shows that, even without the use of preamplification, the coherent PON would support a transmission distance of 100 km followed by eight 3 dB splits (256 subscribers). Of course, an increase in launch power would increase power budget and, therefore, this represents only a benchmark of what could be achieved in practice (see following section). For a single channel, the cost associated with an optical preamplifier

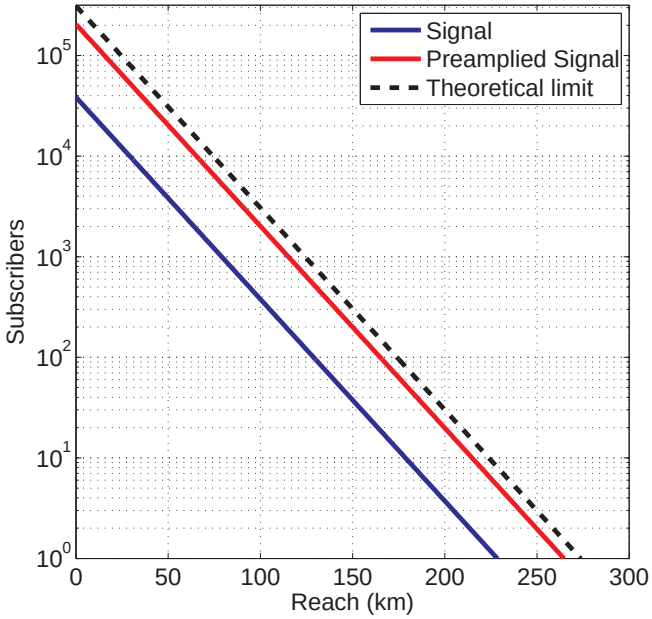

Figure 4.2: Effective number of subscribers who could be connected to a single access network when employing a passive split architecture. The *total* network capacity here would be 10 Gbit/s, which is commensurate with a long-reach PON. The assumed fibre loss is 0.2 dB/km.

before each receiver would be prohibitive. However, considering this scenario for completeness, here it would be possible to transmit over 100 km with a 1024-way split (ten 3 dB splits). Again, this loss budget could be improved by increasing transmission power.

Replacing direct detection transceivers with coherent transceivers would be beneficial but costly. This is because, while the network itself would be greatly simplified, the total network throughput would not necessarily be increased versus, for example, a single OOK channel. The next section addresses the possibility of using wavelength division multiplexing to increase throughput by effectively providing each subscriber with their own dedicated 10 Gbit/s channel.

4.1.2 Optimal frequency grid in a PON

It is common for systems such as the GPON to separate the wavelengths of the upstream and downstream channels [7], however, modulation is still based on time division multiplexing for such networks. More recently, the notion of a true WDM-PON has been explored [7], where the passive split in the tree network (Fig. 1.3) is replaced with an arrayed waveguide grating. This approach is generally used when the receivers in such networks are not frequency selective, and therefore cannot discriminate between wavelengths. This approach necessarily 'colours' the ONUs at the customer premises, and inhibits network reconfiguration.

It is possible to increase the capacity of a PON by using WDM to multiplex channels

in a manner which exploits both the wide bandwidth of an optical fibre and the frequency selectivity of a coherent receiver (see section 2.3.1). The frequency selectivity is crucial as it allows network reconfiguration; that is, the ONUs are not coloured. Such a network could be implemented using the architecture in Fig. 1.4. This network architecture was explored, in this work, through the following experimental investigation.

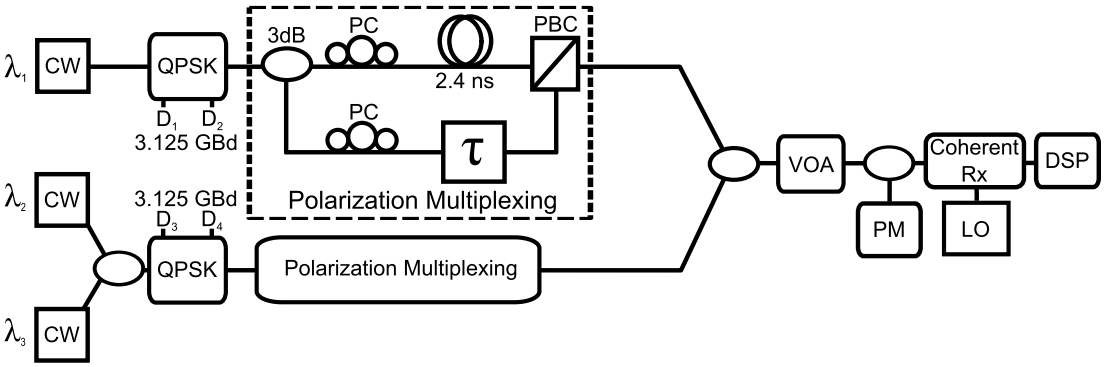

Figure 4.3: Experimental configuration for investigating the impact of channel spacing in a coherent WDM PON. Where transmission was considered, the channels were propagated over 120 km SMF before the power being set with the VOA at the receiver.

Shown in Fig. 4.3 is the experimental configuration used for investigating how channel spacing impacts on receiver sensitivity. It should be noted at this point that the conventional (C) fibre transmission window spans the wavelengths from 1535-1565 nm, which is 5 THz. In order to achieve high capacity, a high channel density is required. Therefore, targeting approximately 1000 channels requires a channel spacing of around 5 GHz. Such dense channel spacings are known as Ultra Dense Wavelength Division Multiplexing (UDWDM). Although there are no formal specifications for UDWDM, there are ITU specifications for dense WDM, where the channel spacings are 50 GHz or 100 GHz, thus, both 5 GHz and 50 GHz channel spacing are investigated here.

Fig. 4.4 shows the experimentally determined impact of channel spacing on receiver sensitivity[1]. Fig. 4.4(a) shows the results from the previous section, adding that there is very little impact on receiver sensitivity for high transmission powers.

Again, for the 50 GHz channel spacing shown in Fig. 4.4(b), high transmission powers have very little impact on receiver sensitivity. However, for the penalty at the FEC limit to be less than 1 dB, the transmission power was limited to 10 dBm per channel. As this is a power-dependent effect, this penalty can be attributed to fibre nonlinearity. Specifically, as this penalty is not present for the single channel case with a 10 dBm launch power, Fig. 4.4(a), this penalty is due to cross phase modulation [84].

Finally, for the target 5 GHz channel spacing shown in Fig. 4.4(c), the use of

[1]Note that these results preceded the other measurements documented in this chapter. There is, consequently, a discrepancy with respect to receiver sensitivity, due to using an LO power of 13 dBm versus 15 dBm. However, these results are self-consistent, and nevertheless show the impact of fibre nonlinearity.

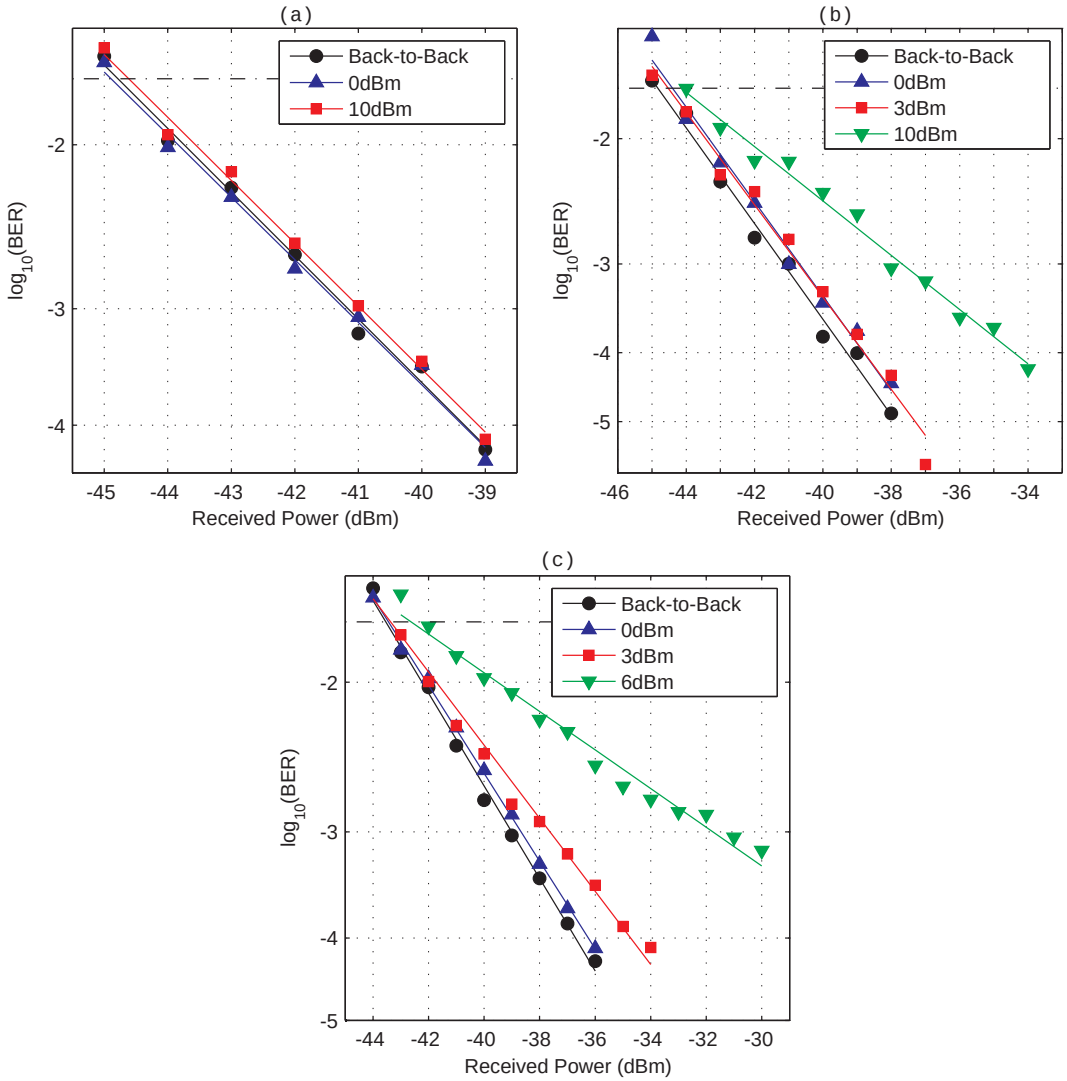

Figure 4.4: Back-to-back and transmission of 3.125 Gbaud PDM-QPSK at different launch powers for (a) single channel (b) 50 GHz channel spacing (c) 5 GHz channel spacing. The 2×10^{-2} FEC limit is indicated by the dashed line. For a 5 GHz grid, the loss budget is 48.6 dB, increasing to 54.0 dB for a 50 GHz grid. In each of the WDM scenarios, the maximum channel power investigated was for a 1 dB sensitivity penalty. [42]

UDWDM increases the impact of fibre nonlinearity; here, to achieve less than 1 dB penalty with respect to back-to-back, the maximum transmission power per channel was reduced to 6 dBm.

Since the penalty at low transmission powers is small for all channel spacings measured, it can be assumed that the analysis in Fig. 4.2 holds. A crude extrapolation of the three channel performance shown here to the many channels expected in a coherent PON shows that the performance of this system would be sufficient to achieve transmission over 100 km with a per user data rate of 10 Gbit/s.

4.2 Passive bidirectional transmission

Whilst a PON-based access network should, by definition, include no active components in the field, capital expenditure can still be reduced by making simplifications to the network structure. Indeed, operational expenditure can also be reduced in this way because the simplified network is easier, and therefore cheaper, to manage.

Considering this, it is advantageous to employ bidirectional (full duplex) transmission such that only a single fibre (rather than a fibre pair) is necessary for each access network. This simplification also halves the required number of passive splitters. The disadvantages of this approach are highlighted in section 4.3, however, in the following section the feasibility of bidirectional transmission is explored.

4.2.1 Feasibility study

Shown in Fig. 4.5 is the schematic of a bidirectional PON incorporating digital coherent receivers. The salient features of this schematic are the frequency plan, the colourless ONUs and the asymmetry introduced by the EDFA at the Optical Line Terminal (OLT). Note that an EDFA at the OLT is a reasonable assumption as it can be used to boost the power of *all* received channels, and so the device cost is averaged over all subscribers.

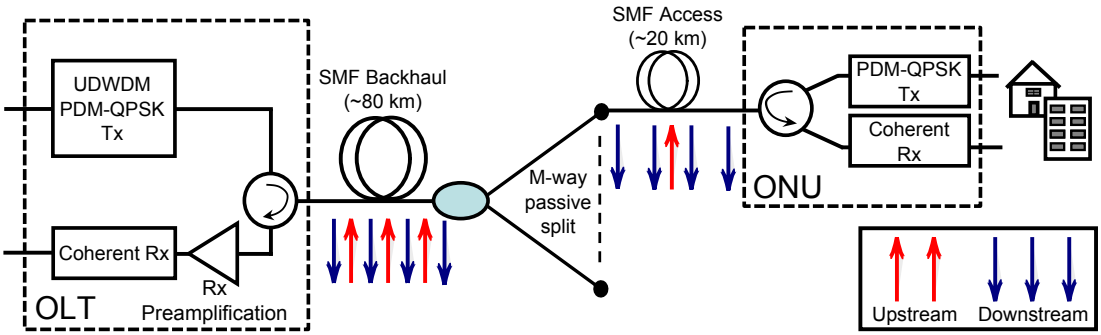

Figure 4.5: Schematic for a bidirectional PON using digital coherent transceivers. The arrows indicate an interleaved upstream/downstream frequency plan.

To investigate the feasibility of this approach, the experimental configuration shown in Fig. 4.6 was used. The aim was to generate five 5 GHz spaced channels which could be transmitted through the fibre in a variety of combinations. In the configuration shown, subcarrier generation is used to generate three 10 GHz spaced channels for the downstream and, separately, two upstream channels with a 10 GHz spacing are transmitted upstream; offset from the downstream channels by 5 GHz. This emulates the frequency plan shown in Fig. 4.5.

Shown in Fig. 4.7(a) are the results of this experiment. The abbreviation US (upstream) indicates the scenario where three channels are propagated through the fibre with two counter propagating, and an EDFA preamplifies the receiver. This emulates

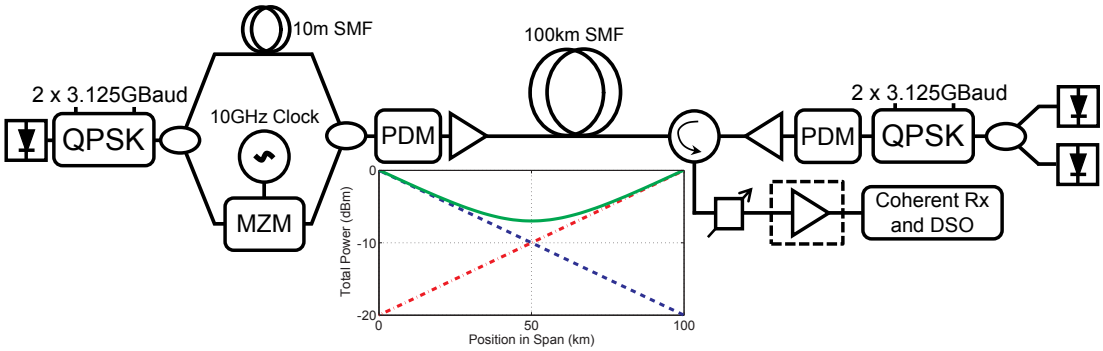

Figure 4.6: Bidirectional LR-PON experimental configuration; the power loss due to splitting in the distribution network is emulated by a variable optical attenuator (placed directly before the receiver as the access span is not being evaluated). The MZM is driven at 10 GHz to generate 20 GHz spaced subcarriers. In the case that five channels are required for downstream only experiments, the upstream is combined with the downstream comb before the span. The subplot shows the expected power at each point in the fibre for any two neighbouring channels in bidirectional transmission at 0 dBm.

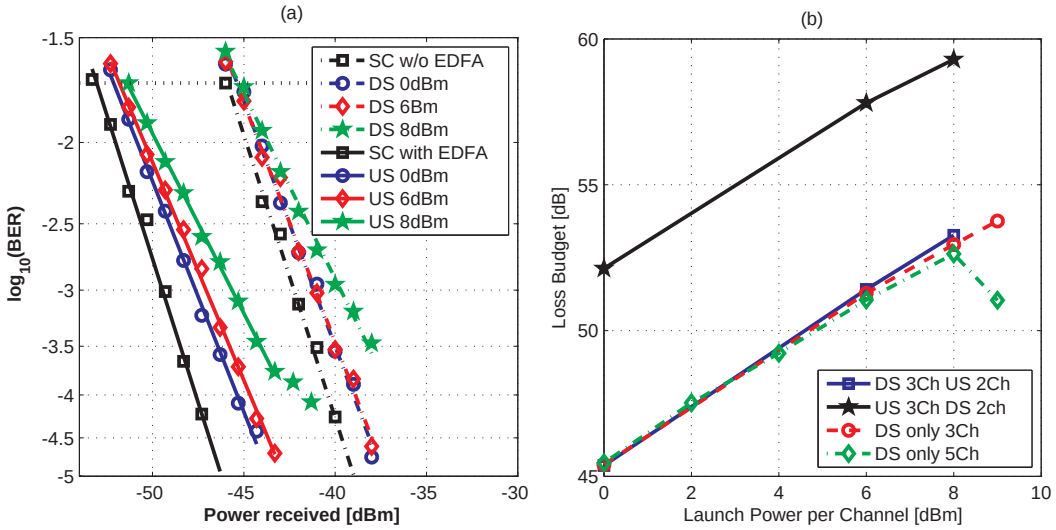

Figure 4.7: (a) The sensitivity measurements for single channel (SC), downstream 3-channel with 2 upstream interfering channels (DS), and upstream 3-channel with 2 downstream interfering channels (US) for different launch powers. The single channel measurements are shown with and without preamplification. All US measurements are with a preamplified receiver. (b) Loss budget at the FEC limit (BER=2×10^{-2}) for different transmission powers in the case of downstream only (5-channels and 3-channels) and the bidirectional US and DS configuration. [31]

OLT operation. Here, the abbreviation DS (downstream) indicates three propagating channels and two counter propagating channels without a preamplifier, emulating ONU operation. It can be seen that, particularly for the upstream, there is minimal impact from the counter propagating channels.

This is made apparent from Fig. 4.7(b) which measures loss budget (at the FEC limit) against launch power for the upstream and downstream configurations. Loss budget increases with launch power up to and including 8 dBm per channel. This

indicates that any channel impairments are not significant in this region. However, it is worth noting that when five 10 GHz spaced channels are copropagated, there is an optimum transmission power of 8 dBm per channel; at 10 dBm, the loss budget decreases. This indicates that, while three channels is a good approximation of the coherent PON, it may be necessary to investigate more channels for higher transmission powers.

It should be noted that nonlinearity in multiple channel UDWDM PON has already been investigated by means of simulation. Here, it was shown that the main nonlinear penalty arises from four-wave mixing due to the short transmission distances involved [85, 86]. Additionally, the relative strength of four-wave mixing products has been investigated for a 1 Gbit/s UDWDM-PON [24]. Here it was shown that the impact of nonlinearity is strongly dependent on the length of the span before the splitter, and the type of fibre used. Further simulations are required to quantify the impact of four-wave mixing for the particular network configuration described herein (discussion in chapter 6), as the increased signal bandwidth (3 GHz) will reduce the relative impact of nonlinearity in the presence of chromatic dispersion.

4.3 Penalty due to backreflections

It is clear from Fig. 4.5 that there are several potential issues with bidirectional transmission, mostly due to reflections. Optical power could be reflected into the receivers (at the OLT and ONU) from fibre splices or the midspan splitter. These reflections would lead to relatively low level backreflections (the splitter for example would attenuate backreflected signals by at least $6\log_2(M)$ dB, where the splitting ratio is 1:M). However, connectors or splices close to the receiver could cause the co-located transmitter to reflect a high power optical signal into the receiver. This is an acknowledged issue for bidirectional PONs, and is termed Near End Crosstalk (NEXT) [7, 87].

In this work, NEXT is investigated in a digital coherent receiver (ONU side) for channel spacings and data rates commensurate with a coherent LR-PON. To a first approximation, backreflected optical power will only be received at the wavelength of the ONU side transmitter. Therefore, a single aggressor channel emulates the backreflection, as shown by the experimental configuration in Fig. 4.8. (This technique has previously been demonstrated for direct detection systems in [88].)

In this experiment, the aggressor channel (denoted λ_2) was held at a fixed power into the receiver, while the power of the signal under test (λ_1) was varied to determine the receiver sensitivity. To remove any high frequency components of the driving signals (such as 12 GHz clock tones from the waveform generator), 7 GHz RF filters were included between the driving signals and the IQ modulators. The frequency spacing between the channels was also varied to investigate how this changes the impact of

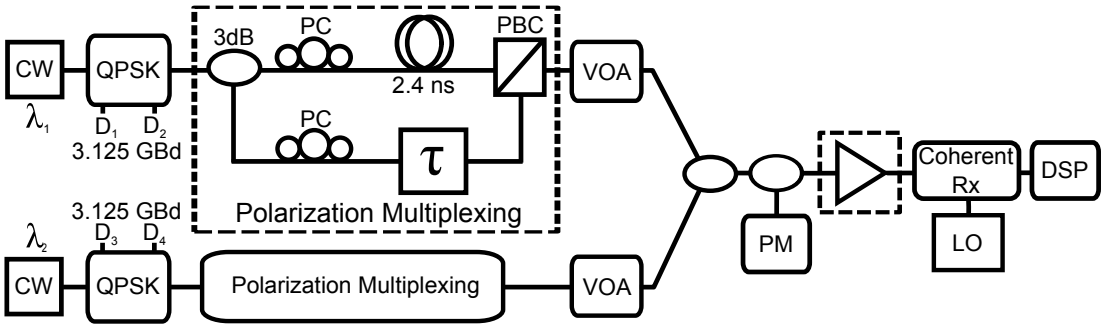

Figure 4.8: Configuration of backreflection experiment. Two PDM-QPSK channels are combined at different channel powers to emulate the effect of the coherent interference characteristic of NEXT. The received power of both channels was measured using an optical power meter (denoted PM). Where noted, the receiver was preamplified using an EDFA.

NEXT.

Shown in Fig. 4.9(a) is the impact of upstream/downstream channel spacing and backreflected power on the efficacy of coherent reception. It is unlikely that an ONU would incorporate any kind of optical preamplifier due primarily to cost. However, for completeness, the case of a preamplified ONU is considered in Fig. 4.9(b).

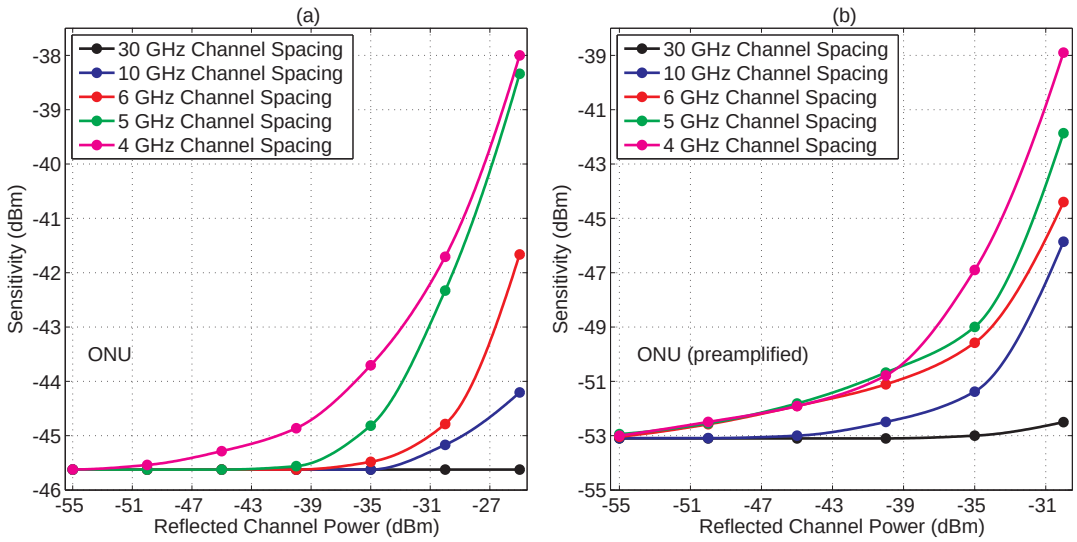

Figure 4.9: Results of an experiment measuring the impact of backreflections (NEXT) on the sensitivity of a receiver in an ONU. The assumed FEC limit is 2×10^{-2}. (a) Single reflected channel at various channel spacings; (b) a similar investigation where an EDFA is used to preamplify the receiver [43].

Note from Fig. 4.9(a) that no sensitivity penalty is observed for 30 GHz spaced channels at any of the received aggressor ('backreflected') powers because the backreflected channel is outside of the receiver bandwidth. Bringing the aggressor within the receiver bandwidth by reducing the channel spacing to 10 GHz, a 1 dB sensitivity penalty occurs when the reflected power is -26.7 dBm. Section 4.1.2 highlighted the attraction of using a 5 GHz separation between upstream and downstream. For this

spacing, the tolerable backreflected power is reduced to -34.2 dBm.

Shown in Fig. 4.9(b) is the sensitivity of the optically preamplified ONU receiver in the presence of backreflections. For a 5 GHz spacing, to ensure a sensitivity penalty of less than 1 dB, the maximum tolerable backreflected power is -46.4 dBm. Importantly, from a system design perspective, this threshold does not vary significantly for the narrower 4 GHz channel spacing or, indeed, the 6 GHz spacing. Further separating the channels to 10 GHz significantly mitigates the impact of backreflections with a tolerance to backreflections of -37.6 dBm at the 1 dB sensitivity penalty threshold. With a 30 GHz channel spacing, the sensitivity penalty is less than 1 dB for all backreflected powers up to the tested power of -30 dBm.

Even with a 30 GHz separation[2] the preamplified receiver is not immune to sensitivity penalty, which can be attributed to the signal receiving reduced gain from the preamplifier relative to the ideal case. For the narrower channel spacings, the penalty stems from spectral overlap leading to crosstalk, and the LO beating with the backreflection leading to a degradation in the effective resolution of the analogue-to-digital converters used at the receiver. Assuming that a significant proportion of the backreflected signal will come from the first connector in the network, it is possible to estimate the impact this would have in a real system.

Consider the typical connector backscattering parameters shown in Table 4.1 (a selection of published values for connector return loss). Using the upper bound for FC/PC connectors, backscattering is approximately -50 dB while for FC/APC connectors this can be reduced to below -60 dB. For a launch power of 0 dBm per channel with a 5 GHz bidirectional channel spacing, Fig. 4.9 shows that backreflections would not impact on system performance at the ONU. Assuming ONU preamplification, the use of FC/PC connectors would incur a 0.6 dB sensitivity penalty. Note further that the preamplified ONU scenario can approximate OLT performance, factoring in the 3 dB additional power due to the received upstream channel having two adjacent backreflected downstream channels.

Table 4.1: CONNECTOR RETURN LOSSES

Connector Type	Typical Return Loss (dB)
Polished Connector	-35 to -50
Ultra-polished Connector	-50 to -55
Angled Polished Connector	-60 to -70

[2] 16 GHz electrical receiver bandwidth.

4.3.1 Pulse shaping to mitigate crosstalk due to backreflections

In this section, the spectrally shaped channels are investigated. Through a series of experiments, the achievable receiver sensitivity for an ultra dense channel spacing (5 GHz) is determined.

This experiment involved the emulation of backreflections in an ONU through the generation of two distinct 3 GBd polarisation division multiplexed quadrature phase shift keying PDM-QPSK signals, corresponding to 10 Gbit/s with an additional 20% coding overhead for FEC. (The target BER was set to 1.5×10^{-2}, which assumes a hard decision FEC [69].)

As in the previous investigation, Fig. 4.8, QPSK was encoded on 1550 nm (λ_1) CW light from an ECL using an IQ modulator, which was driven using a Tektronix Arbitrary Waveform Generator (ArbWG) at 12 GSa/s[3]. Depending on the desired pulse shape, different digital filters were applied (see following section). Finally, PDM-QPSK was generated by passing the signal through a polarisation multiplexing emulation stage. Similarly, a second channel was generated (λ_2) spaced 5 GHz from λ_1, with the IQ modulator being driven with a second ArbWG.

The channel powers were set with a VOA before combination using a fibre coupler, and reception using a digital coherent receiver. The LO laser, also an ECL but with an amplified power of 15 dBm, was tuned to the wavelength of the channel under test. All three lasers had a linewidth of 100 kHz. The received signal was digitised using a digital sampling oscilloscope and resampled to 6 Gsamples/second (2 samples/symbol). The signal was processed offline using the DSP outlined in section 2.4, with the equaliser filter length set to 5 complex taps. The BER was measured over 2^{19} symbols.

4.3.2 Spectral shaping

As described above, RF signals were applied to a IQ modulator in order to generate optical signals modulated with QPSK while also applying pulse shaping. The data applied was a Pseudo-Random Binary Sequence (PRBS) of length $2^{15} - 1$, decorrelated by half a pattern length between in-phase and quadrature components of the signal. Where filtering was considered, two distinct pulse shapes were generated. To emulate low bandwidth electronics which might be used in a 10 Gbit/s transceiver, the ONU (upstream) signal was shaped using a 3$^{\text{rd}}$ order Bessel filter. There is an assumption that transmitters within the OLT (downstream) include digital-to-analogue converters (DAC) in order to generate multiple channels from a single source. As such, investigated was the possibility of applying a Nyquist WDM filter (a root raised cosine (RRC) filter with a rolloff factor of 0) to the PRBS to shape the optical signal.

[3]The symbol rate, 3 GBd, is the result of using integer oversampling at the transmitter.

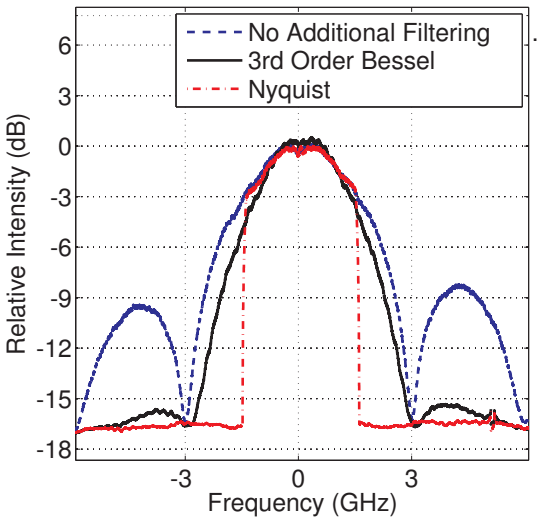

Figure 4.10: Experimentally generated spectra.

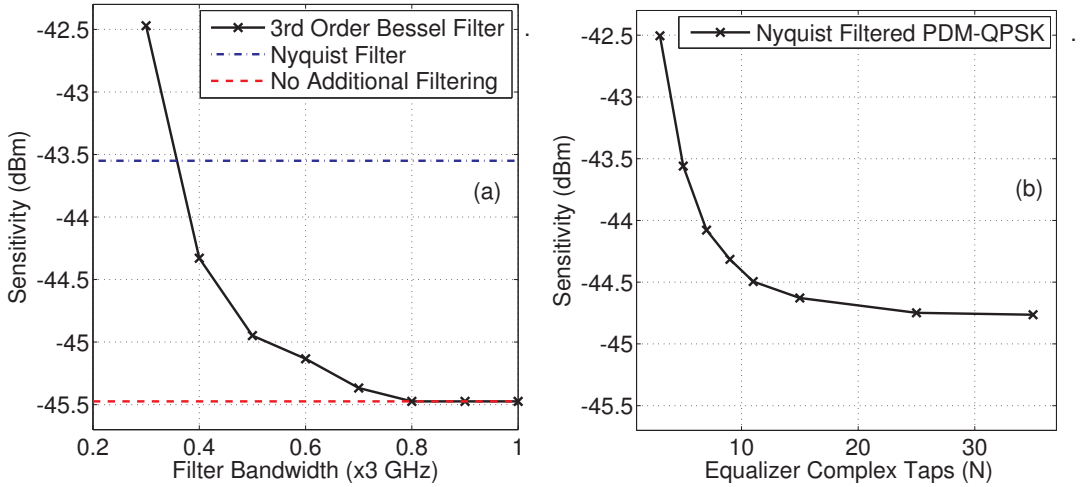

Figure 4.11: (a) Receiver sensitivity with different pulse shapes. (b) Sensitivity of Nyquist filtered pulse when the matched filter is approximated by adaptive equaliser.

It is usual to apply a RRC pulse shape at the transmitter, and then digitally at the receiver in order to achieve matched filtering. However, only the spectral shape is of interest and so, to avoid the use of more complicated receiver DSP, the RRC pulse shape was applied at the transmitter and the adaptive equaliser converged on the matched filter shape. This incurs a sensitivity penalty (see Fig. 4.11(b)), but allows for the narrowest possible spectral shape with only 1 dB sensitivity penalty for a 5-tap equaliser versus the asymptotic performance.

The receiver sensitivity when applying the filters is compared in Fig. 4.11(a). For the Bessel filtered signal, it was found that a bandwidth 50% of the symbol rate could be applied to the signal with less than 1 dB penalty, so this filter was selected for the following investigations. The resulting optical spectrum when applying these filters is shown in Fig. 4.10.

4.3.3 Experimental results and discussion

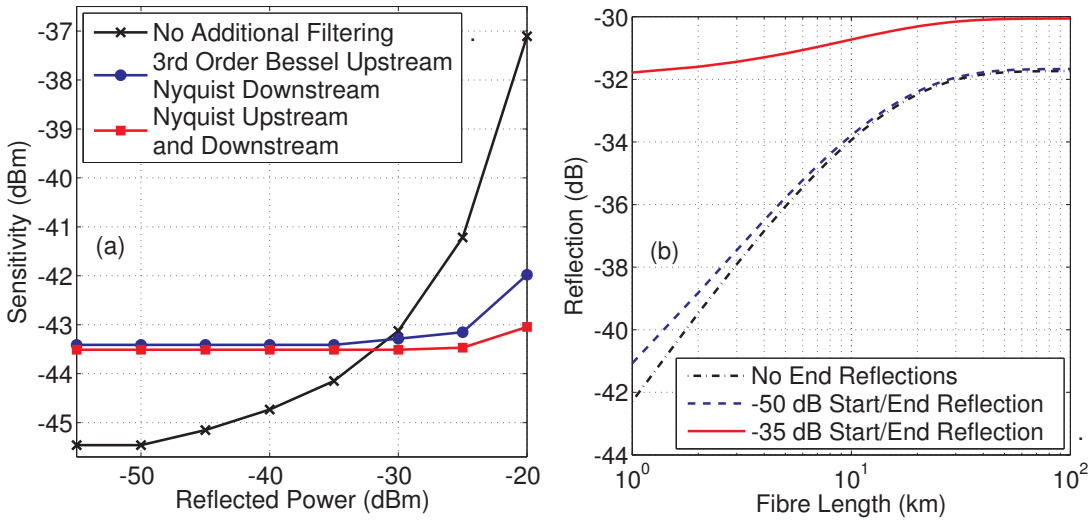

Figure 4.12: (a) Impact of backreflections from a 5 GHz spaced channel on receiver sensitivity. (b) Theoretical reflection levels due to Rayleigh backscattering when using typical FC-PC (-35 dB) and FC-APC (-50 dB) connectors [49]. The backscatter parameter is assumed to be 82 dB (SMF at 1550 nm).

Shown in Fig. 4.12(a) is a comparison of a coherent receiver tolerance to crosstalk due to backreflections with and without pulse shaping [44]. When no filtering was applied, the signal bandwidth was limited by the ArbWG electrical bandwidth (6 GHz). This wide bandwidth signal is sensitive to crosstalk, incurring a 4.2 dB sensitivity penalty in the presence of a -25 dBm reflection. When a Nyquist pulse shape is applied to the downstream, and a Bessel filter is applied to the upstream, the sensitivity penalty drops to 0.3 dB (albeit with the additional penalty shown in Fig. 4.11(a)). In the ideal case of a Nyquist pulse shape being applied to both the upstream and downstream signals, the crosstalk penalty is completely mitigated, as expected. It should be noted that there is a tradeoff between pulse shaping penalty and pulse shape. For example, a root-raised cosine filter with a non-zero rolloff factor could be used as an alternative to the Nyquist filter; constraining the bandwidth, while minimising pulse shaping penalty (this is the subject of further investigation).

In the analysis at the beginning of this section, it was assumed that the highest power reflections would come from the first connector. It is anticipated that reflections will occur also due to Rayleigh backscattering and the return loss of the end connectors, and so this analysis is expanded here. The theoretically expected reflected powers are calculated using equation (2.3), and shown in Fig. 4.12(b). The scenarios considered are: Rayleigh backscattering only, connector return loss of -50 dB and connector return loss of -35 dB; connector reflections are from the start and end of the fibre only. Assuming a 5 dBm launch power for the upstream, allowing a 512-way split over 100 km fibre, and FC-PC connectors (-35 dB return loss representing a realistic scenario), the reflected

power over 20 km single mode fibre is -25 dBm. The previous results demonstrate that pulse shaping would enable such high power reflections while incurring minimal additional penalty. If FC-APC connectors were to be used (assumed return loss -50 dB), the upstream launch power could be increased to over 7 dBm, which would enable a 1024-way split over 100 km fibre.

Nyquist pulse shaping has since been used by Shahpari *et al.* [89] to enable a coherent UDWDM-PON. Here, 2.5 GBd Nyquist-shaped (single polarisation) 16QAM signals were transmitted bidirectionally over 40 km SMF; the upstream channels being offset from downstream by the symbol rate. From Fig. 4.12, it can already be seen that 40 km transmission is beyond the worst case scenario for Rayleigh backscattering. However, due to the Nyquist pulse shaping, crosstalk due to backscatter is alleviated.

At high transmission powers, Shahpari *et al.* attribute penalty to nonlinearity, however, it is not possible to separate the impact of nonlinearity and crosstalk due to backscattering from these results. Additionally, the transmission and reception is all performed on a single polarisation; as shown previously, dual polarisation QPSK can achieve 10 Gbit/s transmission with the same bandwidth requirement. Future research could investigate the relative nonlinear and crosstalk tolerance of single polarisation 16QAM and dual polarisation QPSK for this application, although the research presented herein would suggest that dual polarisation QPSK would outperform 16QAM in this scenario, due to the sensitivity penalty when using 16QAM.

4.4 Summary

Projections of future internet use show that the coming years will see a dramatic rise in customer demand for bandwidth; a need which must be served by increasing capacity in the access network. Coherent detection schemes, although more complex than their direct detection counterparts, allow a simplification of network architecture while simultaneously increasing capacity. The key results of this work are as follows:

- Coherent detection enables long reach (100 km) optical access whilst increasing the passive split ratio by an order of magnitude compared with GPON solutions; eliminating the need for a discrete metro network
- The frequency selectivity of coherent detection allows the use of UDWDM, allowing each ONU to use a dedicated wavelength for communication
- A WDM-PON based on coherent detection can be made to operate in a colourless mode (permitting dynamic network reconfiguration)
- Bidirectional (full duplex) transmission is both feasible and practical using coherent detection without additional optical filtering

- Rayleigh backscattering reduces receiver sensitivity due to crosstalk, but pulse shaping can be used to mitigate this effect.

5

Digital signal processing for integrated coherent receivers

SHOWN already in the previous chapters is how coherent receivers can offer high receiver sensitivity without optical filtering (chapter 3) whilst achieving a high spectral efficiency (chapter 4). Additionally, and crucially for access networks, they offer frequency selectivity (chapter 4), which can be used to select an arbitrary wavelength channel simply by retuning the Local Oscillator Laser (LO) wavelength. The experimental results shown in the previous chapters demonstrate these properties using laboratory grade equipment, combined with advanced DSP algorithms typically used in long-haul transmission. This chapter addresses the possibility of using components which are suitable for mass production, and how the DSP can be altered to be both simpler, and more specific to the channel impairments typical of a PON.

5.1 Tunable light sources for coherent PON

5.1.1 Candidate lasers for coherent access

There are cost constraints when selecting components for use in an access network scenario; although costs can be minimised by selecting components which are suitable for mass production. However, there may be additional constraints due to limits on component power consumption and dissipation, physical size, resistance to physical

shock, mean time to failure, and temperature sensitivity. Recent investigations have shown that these issues can be overcome through photonic integration [90]. Therefore, it can be assumed that the 90^o optical hybrid, balanced photodiodes, and Polarisation Beam Splitters (PBSs) could all be integrated using similar techniques, as in [91]. However, only some types of lasers are suitable for this application, and so care must be taken when selecting a laser to be used as the local oscillator.

External Cavity Lasers (ECLs) are one such source which could be employed however, while they generally exhibit a low linewidth, they present issues in terms of cavity stability [92] and large form factor. Additionally, standard C-band tunable ECLs have not yet been integrated for manufacturing using a scalable production process, making them unsuitable for use in access networks.

External Cavity Lasers (ECLs) do exist with a modified tuning design based on micro-electromechanical systems (MEMS), which are continuously tunable over the full C-band and suitable for mass production [93]. Due to their smaller form factor they are less susceptible to physical shock than the conventional ECL, however, due to their reliance on mechanical tuning, vibrations on the rotary actuator lead to spectral broadening [93].

An alternative choice for LO would be a semiconductor laser, which can be produced using a scalable production process. Examples include Sampled Grating Distributed Bragg Reflector (SG-DBR) lasers, Digital Supermode Distributed Bragg Reflector (DS-DBR) lasers, tunable Vertical-Cavity Surface-Emitting Lasers (VCSELs), and Distributed Feedback (DFB) laser arrays with thermal tuning [94]. C-band tunable VCSELs are an ongoing area of research. Although such lasers have been produced which can tune continuously across the full C-band, the focus has been to develop athermal VCSELs which, again, tune using optical MEMS [95]. Although linewidth may be an issue with such tuning mechanisms, this has not yet been explored, and so future developments in this area may make such lasers useful for coherent PON.

In terms of spectral linewidth, the DFB laser array has the best properties, however there are some design challenges concerning the coupling of the laser outputs, and achieving continuous tuning over a large bandwidth, due to the difficulties associated with manufacturing DFB lasers which operate at a specific wavelength [94].

Tunable DBR lasers can be manufactured which exhibit spectral linewidths less than 1 MHz [96], which is required for low symbol rate coherent detection. Additionally, both SG-DBR and DS-DBR lasers can be tuned using electrical driving signals, making them an ideal choice for use as integrated local oscillator lasers. The feasibility of the integration of SG-DBR lasers in high bandwidth coherent receivers has been shown in [97], albeit without the integration of a PBS; such integration is also possible for DS-DBR lasers.

The disadvantage of such lasers is that noise on electrical driving circuitry can be

translated into the optical domain leading to RIN and frequency ($1/f$) noise (in addition to the intrinsic cavity linewidth) [98, 99]. This can also lead to amplitude noise (see section 5.2.2) and frequency noise on the received signal, which must be compensated. Nevertheless, if these issues can be overcome then semiconductor lasers offer great potential for coherent access networks.

Recent research has examined the use of SG-DBR lasers for the signal source in low symbol rate coherent communications, and measured the impact of low frequency phase noise when the LO is a low linewidth ECL [100]. It was found that the high phase noise and excess low frequency noise lead to difficulties with carrier recovery, including cycle slips. Additionally, in [99], DS-DBR lasers were investigated analytically and experimentally; it was found that, for these lasers, the low frequency noise is dominated by $1/f^2$ noise. Due to the low frequency noise, the performance of the Viterbi and Viterbi carrier phase estimation algorithm is impaired and so, in this work, a simplified phase estimation algorithm was proposed which performs equally well at low symbol rates. However, these analyses focus only on the phase noise of the laser. By contrast, in the following, the focus is on the use of a DS-DBR laser in a PON, where the RIN-induced amplitude noise of the LO causes conventional carrier recovery to fail. As such, the use of a variation of differential carrier recovery is proposed.

The remainder of this chapter is principally organised as follows. The characterisation of the DS-DBR laser linewidth and RIN spectrum is described in section 5.1.2. Digital signal processing techniques for overcoming the increased phase noise and RIN of the DS-DBR laser are detailed in sections 5.2.1 and 5.2.3, respectively. Finally, section 5.2.7 details the impact of LO RIN and digital RIN compensation on receiver sensitivity[1]. Following this, section 5.3 examines the feasibility of using an independent measurement of noise from the LO laser to digitally compensate both phase and intensity noise. This approach is experimentally validated by compensating the phase noise of a high linewidth LO laser. The last section of this chapter, section 5.4.1, considers possible simplifications to the digital equaliser algorithm, which dominates the receiver DSP complexity.

5.1.2 DS-DBR laser characterisation

The DS-DBR laser is a commercially available, monolithically integrated, semiconductor laser. While the laser can be quasi-continuously tuned over the C-band, it has been designed to tune on a 50 GHz grid [101]; otherwise it is typical of a laser required for coherent PON applications.

The Lorentzian linewidths of the two DS-DBR lasers (signal and LO) used in this investigation were measured using a coherent heterodyne technique with digital analysis

[1]The results in these sections have been derived, in part, from [46].

[102]. The reference laser used when measuring linewidth was an ECL (linewidth 200 kHz). These results are shown in Fig. 5.1.

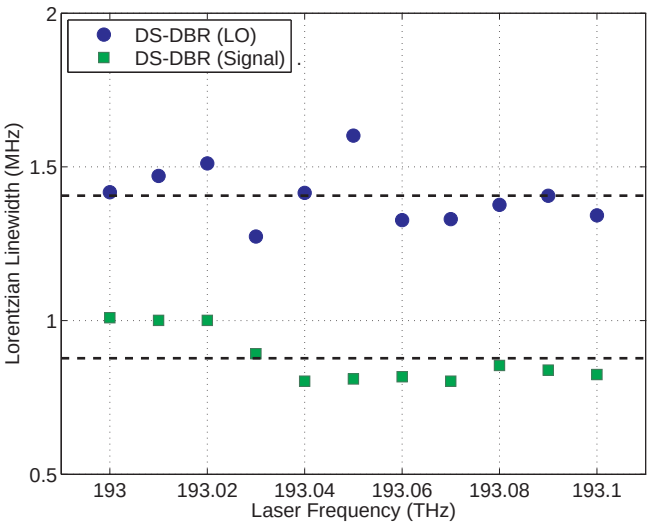

Figure 5.1: Phase noise measurement of the two DS-DBR lasers used in this work. The phase noise is defined here as the convolution between the Lorentzian component of the DS-DBR and ECL linewidths. (ECL linewidth ~200 kHz.) The mean linewidth (horizontal dashed lines) for the LO laser was 1.4 MHz, and 880 kHz for the signal laser.

The RIN of the lasers used as local oscillators was measured using a self homodyne coherent technique. Here, the power spectral density of the signal was analysed digitally to provide an estimate of the RIN spectrum; this approach enables the measurement of RIN over a large bandwidth and, importantly, at low frequencies. Due to the challenges associated with removing the noise floor from the measurement, it was not possible to estimate the absolute RIN of each laser using this technique. However, the RIN spectrum of these lasers was referenced to separate measurements taken at high frequencies using a network analyser, which automatically removed the noise floor from each measurement using the shot noise calibration technique[2]. The combined result of these approaches is in line with manufacturer specifications, and presented in Fig. 5.2.

It has previously been shown that the RIN spectrum of a semiconductor laser changes as a function of the laser's modulation response frequency [66], decreasing by 20 dB per decade; this is confirmed in Fig. 5.2.

5.2 Algorithms mitigating laser RIN and phase noise

5.2.1 Differential decoding in coherent systems

The linewidth·symbol-time product ($\Delta\nu\tau_s$) determines both the efficacy and feasibility of carrier phase estimation [63]. Assuming that the carrier phase is estimated only once

[2]For the details of this technique, see the standard method detailed in [103].

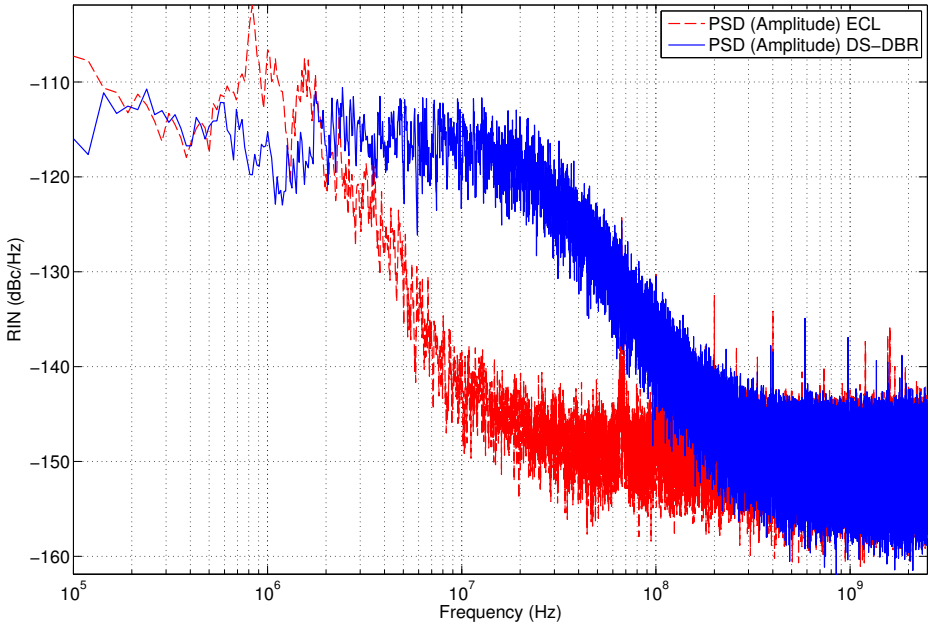

Figure 5.2: Self-homodyne RIN spectrum measurement of a DS-DBR laser and an ECL.

per symbol, then when using an ECL at the transmitter and receiver, $\Delta\nu\tau_s < 10^{-4}$; even with the low symbol-rates considered here. This permits the use of the Viterbi and Viterbi fourth power phase estimation algorithm, which is detailed in [64]. Conversely, with a DS-DBR laser at the transmitter and receiver, $\Delta\nu\tau_s$ is approximately $\sim 8 \times 10^{-4}$. The high resulting phase noise means that using fourth power phase estimation results in repeated cycle slips (section 2.4.3), whereby a succession of incorrect phase estimates lead to a $\frac{\pi}{2}$ deviation from the actual phase, invalidating subsequent data.

Differential decoding by symbol (DS) and differential detection by field (DF) can be used to overcome cycle slips. In both cases, data is encoded on the difference between the phase of two consecutive symbols (see section 2.4.4). At the receiver this data is recovered by comparing the phase of two consecutive received symbols. DS involves making a decision on the symbol before differentially decoding, and therefore requires carrier phase estimation (Fig. 5.3(a)).

DF is used in this work (Fig. 5.3(b)), which is a digital implementation of the interferometric approach applied in optical DQPSK experiments. By first digitising the signal, equalisation can be applied, making this approach more robust to chromatic dispersion and mismatched optical path lengths within the receiver while permitting polarisation multiplexing without optical polarisation tracking. Additionally, a high-power LO laser can be used, which can improve receiver sensitivity [33]. In this scenario, the carrier phase is not directly recovered, but inferred from the difference

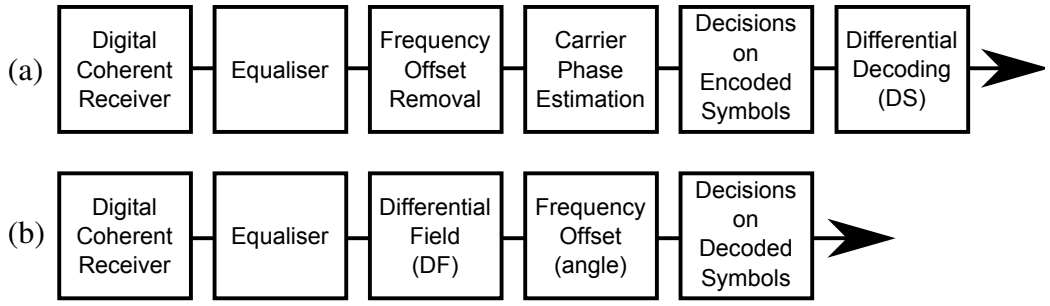

Figure 5.3: Examples of DSP chains which can be used to coherently detect and recover a differentially encoded PDM-QPSK signal. (a) Differential decoding by symbol (DS); the carrier phase must be estimated before the symbol can be recovered, and (b) differential decoding by field (DF) where the carrier recovery and differential decoding are performed by the same operation. Note that, in both cases, the equaliser is required to perform timing recovery and to separate the two orthogonal polarisation states.

between two symbols.

$$\begin{aligned} r_{s-1}^{*} r_s &= \left(e^{-j(\frac{\pi}{2}M_{s-1})}\right)\left(e^{j(\frac{\pi}{2}M_s+\omega\tau_s)}\right) \\ &= e^{-j(\frac{\pi}{2}M_{s-1})} e^{j(\frac{\pi}{2}M_s+\omega\tau_s)} \\ &= e^{-j(\frac{\pi}{2}M_{s-1}-\frac{\pi}{2}M_s-\omega\tau_s)} \end{aligned} \tag{5.1}$$

where r_s is a symbol from the equalised symbol stream, $M_s \in 0\ldots3$ is the encoded data on symbol s, and $\omega\tau_s$ is the angular offset between two adjacent symbols. The result of $\omega\tau_s$ is that any frequency offset will lead to a fixed rotation of the QPSK constellation points. To calculate the frequency offset from this result, the data must be removed using a fourth power operation. In practice, the frequency offset estimate is derived from a noisy signal so the angle of a multiple symbol average can be taken as follows.

$$\begin{aligned} \frac{1}{4}\angle\left(\sum_{s=-n}^{n}\left[r_{s-1}^{*} r_s\right]^4\right) &= \frac{1}{4}\angle e^{j(4\omega\tau_s)} \\ &= \omega\tau_s \end{aligned} \tag{5.2}$$

where the window length is $2n+1$. This is analogous to the Viterbi and Viterbi algorithm, but without the requirement of phase unwrapping (this has already been applied differentially).

Note that, even when the frequency offset is relatively small, this estimation performs two important functions. Firstly, this algorithm can track small changes in the frequency offset over time; this relaxes the constraints on the frequency stability of the LO laser. Crucially, however, from an implementation perspective, this provides a metric to feed back to the LO laser itself to ensure that the frequency offset from the signal is minimised.

In the case of DS, frequency offset estimation and carrier recovery are applied

before a hard decision on the symbol can be made; only then is differential decoding applied. DS, while less tolerant to phase noise than DF, avoids the additional SNR penalty due to the multiplication of noise terms from two adjacent symbols. Due to the duplication of errors (an error in one symbol will lead to an error in the next symbol), in an AWGN channel with high OSNR, both methods will at least double the BER [63] (see section 2.4.4).

5.2.2 Impairment due to LO RIN and receiver common mode gain

Any random variation in amplitude or phase of an optical carrier will lead to a degradation in OSNR, which can be considered to be a measure of the uncertainty of the state of a received signal. Therefore, for intensity modulation with direct detection, it is clear that the RIN of the signal laser will degrade performance, because it increases the probability of making an incorrect decision on the amplitude of the signal. The impact of RIN on coherent phase-modulated communications systems is less intuitive.

Theoretical investigations into the impact of RIN on coherent receivers showed that the RIN of the LO degrades power sensitivity due to the imperfect balancing of photodiodes [104]. Balanced photodiodes with infinite Common Mode Rejection Ratio (CMRR) ideally cancel any directly detected signal, preventing the translation of intensity noise into the digital domain. However, in practice, differential amplification is not ideal, resulting in an SNR degradation. The theoretical explanation of this impairment is as follows.

The RIN of a laser is defined as the ratio of the mean-square optical intensity fluctuation, normalised to a 1 Hz bandwidth at a fixed frequency, and the average optical power. When a laser with non-negligible RIN is used as the LO, the intensity noise will contribute to the LO/signal beating. This RIN component can be treated as an additional electric field without loss of generality and so, neglecting extrinsic noise sources, this leads to the following signal from the photodiodes

$$\begin{aligned} I_+ &\propto |E_{Sig} + (E_{LO} + E_{RIN})|^2 \\ I_- &\propto |E_{Sig} - (E_{LO} + E_{RIN})|^2 \end{aligned} \tag{5.3}$$

where $E_{Sig,LO,RIN}$ are the electric fields corresponding to the signal, LO and RIN, respectively, and $I_{+,-}$ are the electric currents from the two square-law photodiodes comprising the balanced photodetector. These signals are passed to differential amplifiers (with a finite CMRR) resulting in the final output current

$$\begin{aligned} I \propto & 2C(E_{LO}E_{Sig} + E_{RIN}E_{Sig}) \\ & +(1-C)(E_{LO}^2 + E_{Sig}^2 + E_{RIN}^2 + 2E_{LO}E_{RIN}) \end{aligned} \tag{5.4}$$

where $C/(1-C)$ is the CMRR, and C is normalised to unity ($0 < C < 1$). Assuming that E_{RIN} and E_{Sig} are both small compared with E_{LO} (justified when considering the >60 dB LO/signal ratio in chapters 3-4), then terms including E_{LO} will dominate

$$I \propto E_{LO}(CE_{Sig} + (1-C)E_{RIN}) \tag{5.5}$$

where constant terms have been removed due to the assumed AC-coupling of the differential amplifiers. As the magnitude of the signal field, E_{sig}, reduces relative to the magnitude of the RIN, E_{RIN}, the RIN term begins to dominate. Note that, while this affects all coherent receivers using any light source as a local oscillator, it is only significant when the LO laser has a sufficiently high power to overcome other noise sources, such as thermal noise or, in the case of a digital coherent receiver, quantisation noise.

With a finite CMRR, and assuming that E_{RIN} follows a white Gaussian noise process, this introduces an LO-RIN beat term which cannot be removed [104]. However, RIN from a semiconductor laser is normally manifested as 1/f noise (or 'pink noise') due to noise from driving circuitry being translated into the optical domain, and also due to the properties of the laser cavity itself [98]. For the DS-DBR laser this results in the RIN spectrum shown in Fig. 5.2.

5.2.3 Time-dependent DC offset removal

Since the RIN spectrum is not white, equation (5.5) can be used to design a digital filter which tracks changes in amplitude over time in order to compensate the effect of RIN[3]. The simplest choice, from the perspective of design and hardware implementation, is a moving average filter (hereafter 'averaging filter'), which treats $|E_{LO}E_{RIN}|^2$ as a time-dependent Direct Current (DC) offset[4]. This filter can be applied to the signal from each channel as a FIR filter in the time domain, where the filter coefficients are given by

$$x[n] = \begin{cases} 1 - 1/N & \text{if } n = N/2 \\ -1/N & \text{otherwise.} \end{cases} \tag{5.6}$$

Here, N is the number of filter taps, which determines the (high-pass) frequency response of the filter. The frequency response of this filter is not an ideal high-pass (see section 5.2.5), meaning that the ideal filter length is not just a function of the LO laser RIN spectrum, but also the signal-LO power ratio and the CMRR of each channel.

Other high pass filters exist which can be implemented using FIR filters. The

[3]Note that it is possible to cancel RIN optically [105, 106] but this approach is beyond the permissible complexity for an ONU.

[4]The implicit assumption here is that the balanced photodiodes are Alternating Current (AC)-coupled such that $\langle I \rangle = 0$.

Gaussian filter, for example, has less pass band ripple than the averaging filter, and its bandwidth can be set independently of the number of filter taps. The filter coefficients are given by

$$x[n] = \begin{cases} 1 - \exp\left(-B\left(\frac{n-1}{2}\right)\right)/T & \text{if } n = N/2 \\ \exp\left(-B\left(\frac{n-1}{2}\right)\right)/T & \text{otherwise.} \end{cases} \tag{5.7}$$

where B is the reciprocal of the variance of the Gaussian function, and the normalisation factor is evaluated as $T = \sum_{n=1}^{N} \exp\left(-B\left(\frac{n-1}{2}\right)\right)$. Both the averaging filter and the Gaussian filter described here are linear in phase, with a high-pass frequency response. However, the averaging filter can be efficiently computed using a circular buffer; the complexity would be much greater for the Gaussian filter.

5.2.4 Experimental investigation of RIN compensation

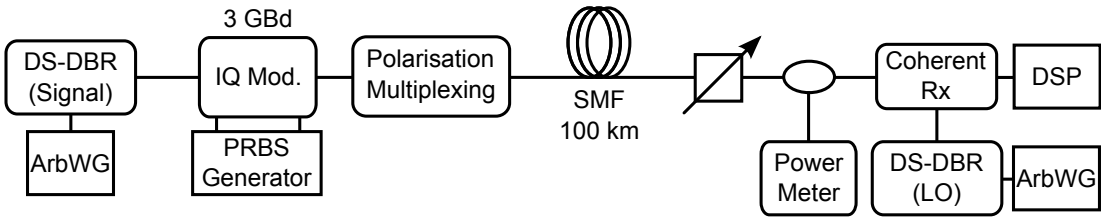

Figure 5.4: Experimental Configuration for measuring receiver sensitivity with DS-DBR lasers for signal and LO.

To demonstrate the feasibility of a coherent LR-PON incorporating DS-DBR lasers, a single-channel downstream link was implemented, based on the architecture shown in Fig. 4.5. This experimental configuration (Fig. 5.4) involved the generation, transmission and detection of 3 GBd (12 Gbit/s) PDM-QPSK. Either the DS-DBR lasers or an ECL (linewidth 200 kHz) were used for signal and LO, as indicated. The PDM-QPSK signal was generated using the process outlined in section 4.3.2 (though without pulse shaping).

To emulate the LR-PON fibre backhaul, the signal power was set to 0 dBm and transmitted over 100 km SMF. As in previous chapters, splitting loss was emulated using a variable optical attenuator between the fibre and the coherent receiver.

In this investigation, hard decision FEC is assumed such that 20% coding overhead would enable correction of a BER up to 1.1×10^{-2} to below 10^{-15} [70].

Each section of the DS-DBR lasers was driven using Arbitrary Waveform Generators (ArbWGs) to provide a variable voltage source for tuning. The DS-DBR laser has been designed to tune to a 50 GHz grid, so fine resolution wavelength adjustments were achieved using temperature controllers. As a proof of concept for UDWDM PON, the receiver sensitivity was measured over 11×10 GHz spaced channels (193.0–193.1 THz) by retuning both signal and LO lasers, although the laser could, in principle, be used to detect any channel in the C-band.

5.2.5 Filter performance

The filters outlined in section 5.2.3 aim to remove the low frequency components of a received signal in order to compensate for the low frequency distortions introduced by LO RIN. For a received signal power of -39 dBm, the effects of filtering are displayed in the constellation diagrams in Fig. 5.5.

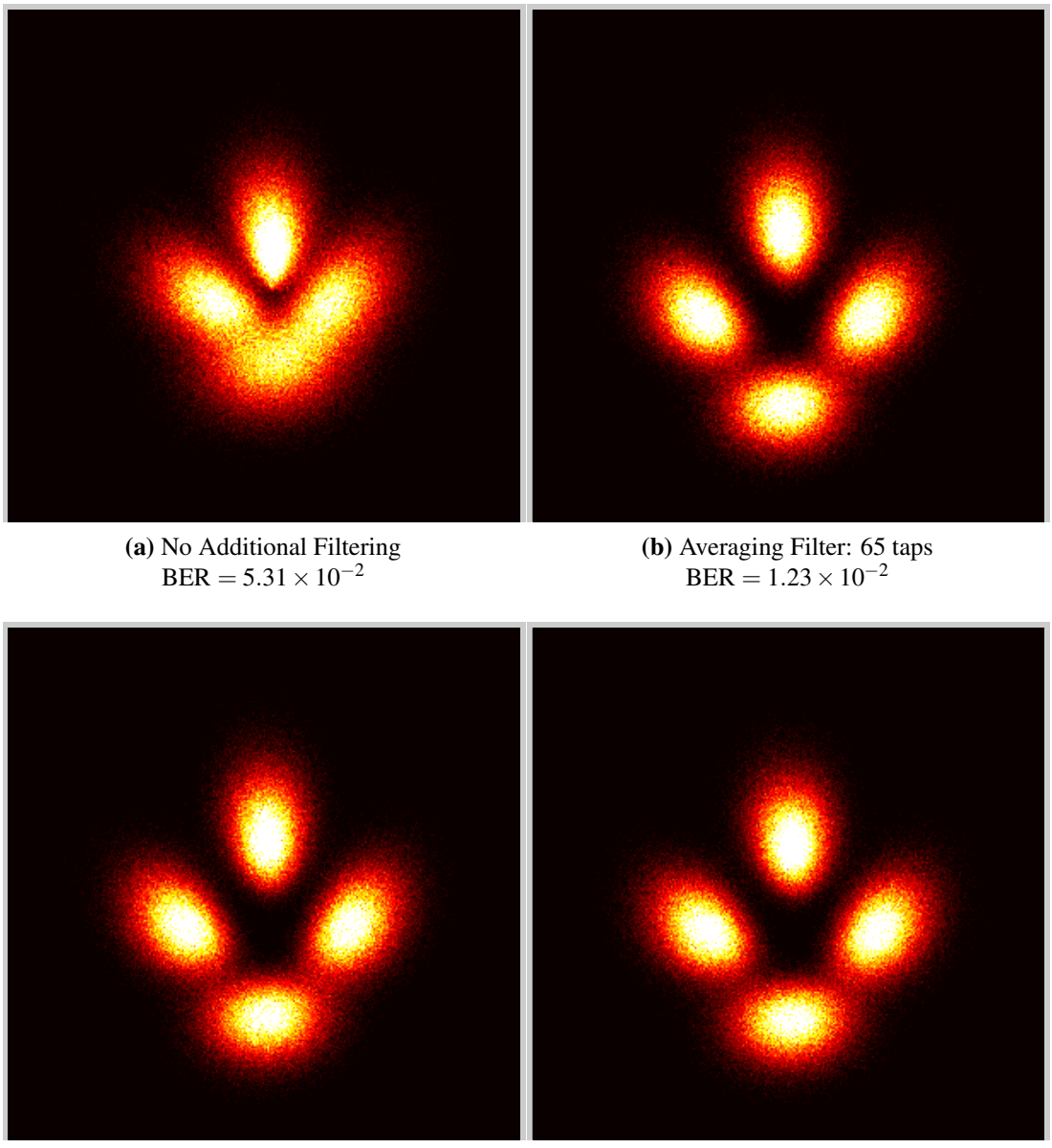

(a) No Additional Filtering
BER $= 5.31 \times 10^{-2}$

(b) Averaging Filter: 65 taps
BER $= 1.23 \times 10^{-2}$

(c) Gaussian Filter: 65 taps
BER $= 1.22 \times 10^{-2}$

(d) Gaussian Filter: 512 taps
BER $= 1.11 \times 10^{-2}$

Figure 5.5: The effect of RIN compensating filters on QPSK constellation diagrams (differential on field). The signal power is -39 dBm and the LO power is +15 dBm.

Without this digital prefiltering, Fig. 5.5(a), the received constellation (post equalisation) is heavily distorted due to RIN, with a BER of 5.31×10^{-2}. However, using the simple averaging filter, Fig. 5.5(b), the constellation is greatly improved and the

BER is reduced to 1.23×10^{-2} (just over the FEC limit). In this case, a 65 tap filter was selected in order to minimise the BER.

The result using a Gaussian filter of the equivalent length (65 taps) results in a small reduction in BER, and the constellation when using this filter is shown in Fig. 5.5(c). Finally, the constellation shown in Fig. 5.5(d) results from applying a Gaussian filter with 512 taps. As the Gaussian function has an infinite response, this long filter is used as an approximation to an ideal Gaussian filter. Here, the BER is further reduced to 1.11×10^{-2}, which is the FEC limit. (Note that when applying the Gaussian filters, the filter bandwidth was selected which minimised BER.)

Overall, there is only a small difference in BER when applying the simple averaging filter and the ideal Gaussian filter. The reason for this becomes clear when considering the frequency response of the filters shown in Fig. 5.6.

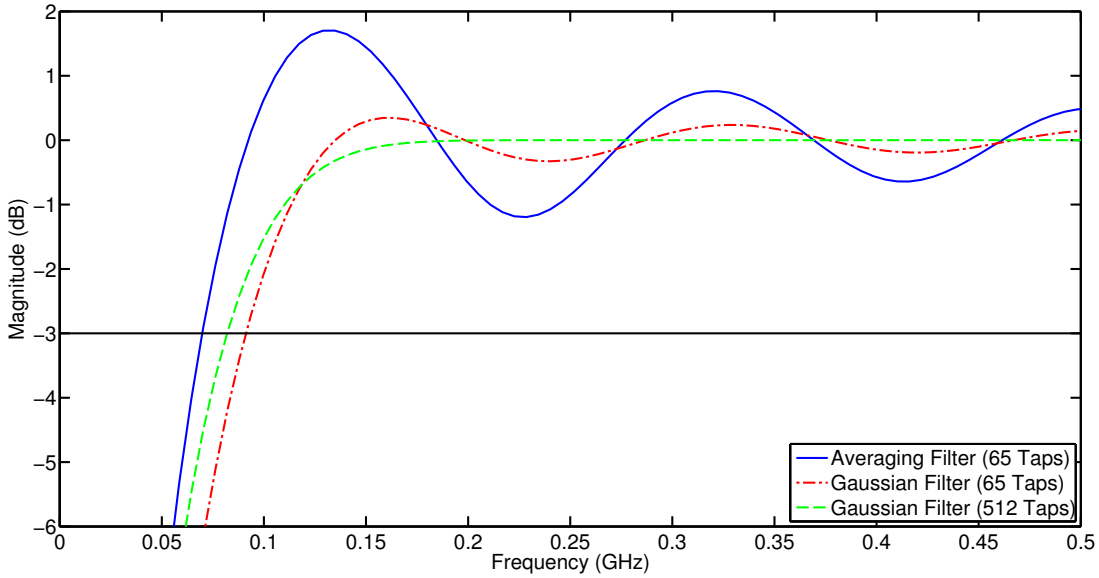

Figure 5.6: Frequency response of the averaging filter and the Gaussian filters.

While there is a small difference in cutoff frequency for which these three filters are optimised, the most notable difference is the passband ripple. The ripple of the averaging filter is 2.9 dB (defined as the difference between the first maximum and the first minimum of the magnitude). This reduces to 0.7 dB for the Gaussian filter and is negligible for the ideal Gaussian filter.

5.2.6 RIN compensation

With a high LO-signal ratio, RIN from the LO laser would be a significant noise source, reducing the sensitivity of a coherent receiver. Note that the (low power) RIN from the signal laser would have a minimal impact on receiver sensitivity. The impact of RIN is dependent on the CMRR; measured for the receiver used in this investigation to be

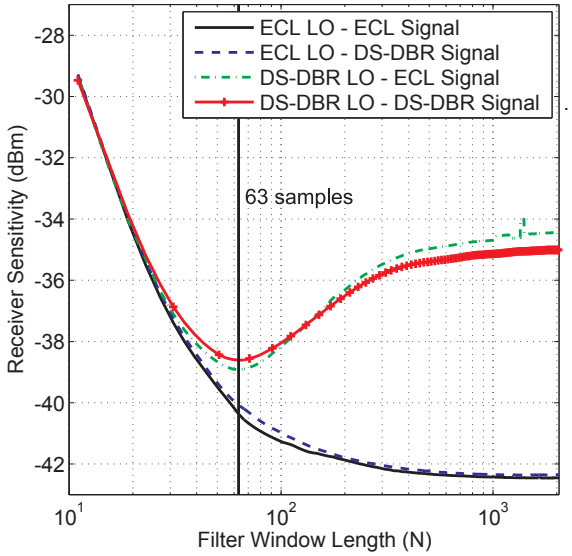

Figure 5.7: The required received power to achieve a BER below the FEC limit (1.1×10^{-2}) for different RIN compensation filter window sizes. The vertical line indicates the filter length that optimises receiver sensitivity. (These results are obtained by fitting received power against Q^2-factor.)

between 10 dB and 15 dB for all four channels (signal and LO port)[5]. Results are shown in Fig. 5.7 from a back-to-back performance characterisation of achievable receiver sensitivity when incorporating a digital RIN compensating filter within the receiver DSP. Here, the required sensitivity has been extrapolated at the FEC limit, however the complete data are shown in appendix B. To obtain these results, four combinations of the two laser types were investigated (DS-DBR and ECL as signal or LO).

When ECLs are used as both the signal and LO lasers, the receiver sensitivity improves asymptotically with increasing length of the RIN compensating filter window; up to the maximum filter length tested (2049 taps). This indicates that the DC offset of the coherently detected signal is approximately time invariant over this interval. Conversely, when DS-DBR lasers are used as the signal and LO sources, there is a particular window length which optimises filter performance for each received power, implying that low-frequency noise has been removed.

The final two curves show the performance when an ECL and DS-DBR laser are used as the signal and LO source, or LO and signal source, respectively. A comparison of these results confirms the theory that it is RIN from the LO laser that impacts on receiver sensitivity.

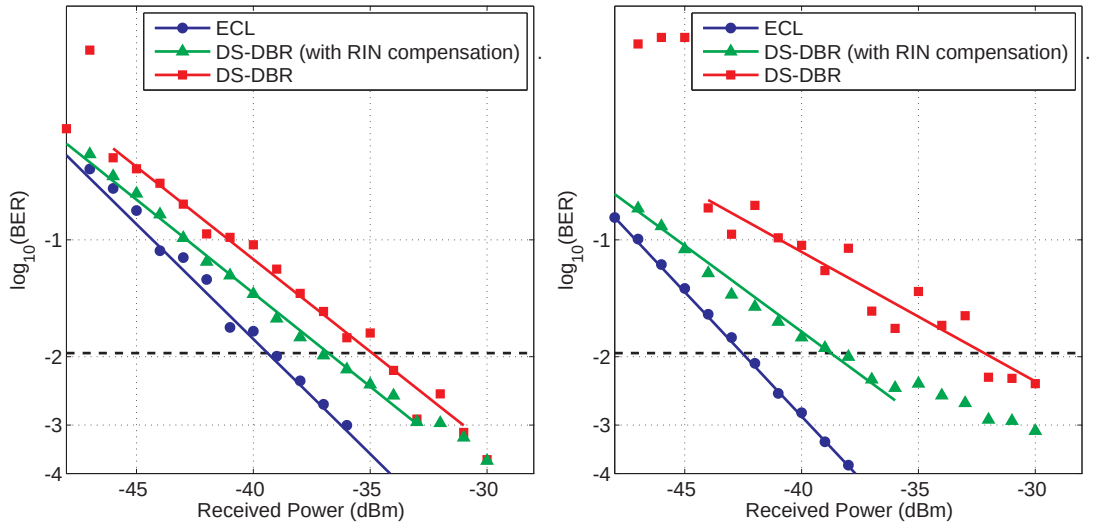

(a) 10 dBm LO Power **(b)** 15 dBm LO Power

Figure 5.8: Experimentally determined receiver sensitivity of 3 GBd PDM-QPSK after transmission over 100 km SMF. Shown is the sensitivity of the first channel (193 THz) with and without digital RIN compensation (dashed horizontal line is the 1.1×10^{-2} BER limit for FEC).

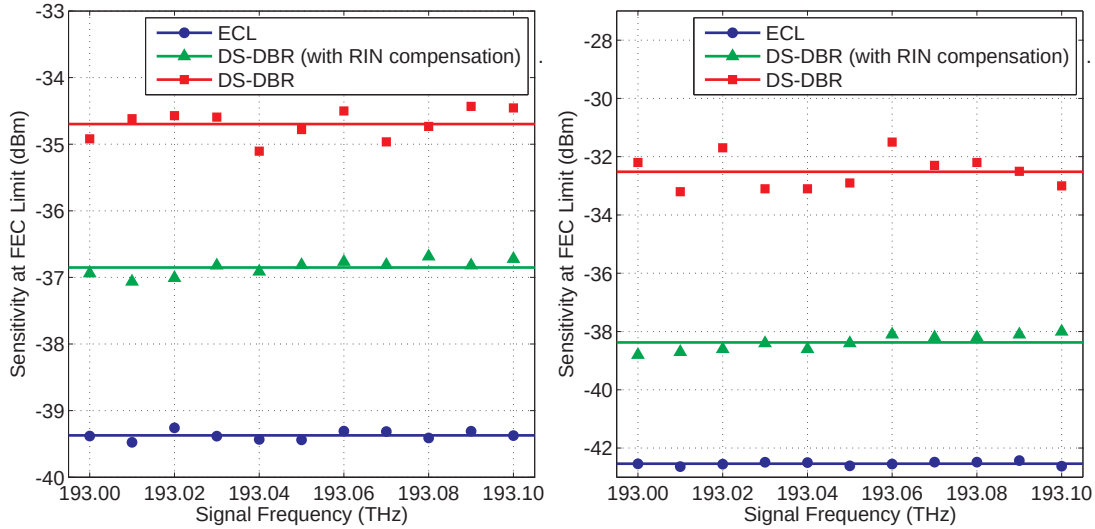

(a) 10 dBm LO Power **(b)** 15 dBm LO Power

Figure 5.9: Individual channel sensitivities, with the horizontal lines indicating the average sensitivity for each configuration. The receiver sensitivity when using ECLs is shown as a reference.

5.2.7 Transmission performance

The results in this section were obtained using the experimental configuration shown in Fig. 5.4, including transmission over 100 km SMF. Shown in Fig. 5.8 is the measured receiver sensitivity when using DS-DBR lasers at the transmitter and receiver tuned to 193 THz. The BER degrades significantly when the LO-signal ratio is around 60 dB due to the increased impact of RIN. It was found that, in the low signal power region, LO RIN lead to equaliser false locking (discarding data from one polarisation) or malconvergence, leading to significant BER degradation.

When RIN compensation was applied the receiver sensitivity improves, albeit with an error floor at higher powers. It is evident that there is an error floor when no RIN compensation is applied, so the error floor can be attributed, in this case, to the incomplete removal of RIN. The performance when using ECLs is shown for reference, and the relative penalty at the FEC limit is 3.7 dB. The achievable sensitivity for the DS-DBR configuration is -38.8 dBm, when using an LO power of 15 dBm.

Fig. 5.9 shows how receiver sensitivity varies when changing the operating frequency of the DS-DBR lasers. It was found that, when RIN compensation was applied, the variance of receiver sensitivity was negligible, indicating the suitability of this approach for UDWDM-PON. In Fig. 5.9(a), the LO power was set to 10 dBm and for Fig. 5.9(b) it was set to 15 dBm. Comparing these results further confirms the theory that a higher LO power increases the impact of LO RIN, while also showing the enhanced efficacy (and necessity) of RIN compensation. For a 10 dBm LO power, the average sensitivity improvement at the FEC limit when applying RIN compensation was 2.1 dB, while for a 15 dBm LO power this increased to 5.9 dB.

These results can be used as a basis for estimating network performance. Assuming 5 dBm/λ launch power [31], the loss budget for a 10 dBm (15 dBm) LO power is 41.9 dB (43.4 dB). For the configuration outlined in Fig. 4.5, assuming 3 dB loss per 1:2 split, this loss budget would enable transmission over 100 km with a 1:128 (1:128) way split (albeit with a 2.4 dB margin in the latter case). The aggregate network capacity in this configuration would be 1.28 Tbit/s. The total optical power at launch would be 26 dBm; comparable to the output power of a high-power EDFA.

5.2.8 Parallel signal processing

Finally, for this section, a note on the prospective hardware implementation of the DSP. A direct implementation (symbol by symbol processing without buffering) of the DSP chain shown in Fig. 5.3 would require hardware with a clock speed of 6 GHz: receiving 3 GBd PDM-QPSK at 2 samples/symbol. In CMOS, the technology used

[5]The same filter is used on each channel in this investigation. Therefore, the worst CMRR, 10 dB in this case, is the most significant.

for Application-Specific Integrated Circuits (ASICs), the power consumption increases with clock speed. For the cost-sensitive access network application, it is therefore advantageous to reduce clock speed and, consequently, power consumption.

It is possible to parallelise the implementation of filters, such that for M parallel filters (an M-symbol bus), the required clock rate is reduced by a factor of M. From the point of view of performance, this could impact on the performance of the equaliser because the taps can only be updated once per M symbols. The information from the error signal of each parallel filter can be retained by averaging the error terms over the whole bus before updating the tap weights.

Compared in Fig. 5.10 is the performance of the serial and parallel DSP algorithms. The first analysis, Fig. 5.10(a), shows the receiver sensitivity when using an ECL at the transmitter and the receiver. It is clear that, in this scenario, the bus width has no impact on receiver sensitivity. Fig. 5.10(b) shows the results from the same investigation when the ECLs are replaced by DS-DBR lasers. Even with the reduced coherence time for these lasers (Fig. 5.1), there is still a negligible impact on sensitivity when moving from serial DSP to parallel DSP with a bus width up to 1024 samples. Note that the feedback time for the CMA error term is the (symbol time)·(bus width) product. This analysis shows that the required clock speed of the receiver could be made as low as one thousandth of the sample rate, if required.

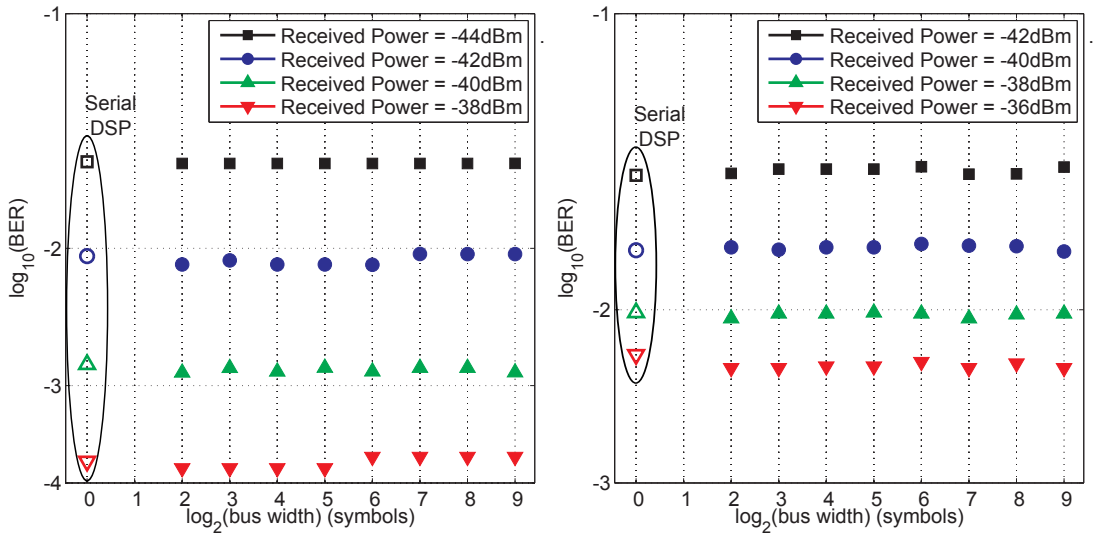

(a) ECL LO, ECL signal

(b) DS-DBR LO, DS-DBR signal

Figure 5.10: Impact of bus width on receiver sensitivity. Open markers indicate performance using serial processing for each optical power level. The difference in BER between serial and parallel DSP algorithms is negligible, and independent of the laser used.

5.3 Independent laser phase measurement for digital linewidth reduction

Up until this point, the research presented in this thesis has focussed on the technologies required to realise a 10 Gbit/s/λ UDWDM-PON. If current trends are to continue, there will be a demand for increased capacity; beyond 10 Gbit/s/λ (see chapter 1). If the LR-PON network architecture is to be upgraded, this will require the use of higher order modulation formats, which increase spectral efficiency at the cost of sensitivity. However, when using high order QAM, for example, the laser linewidth requirements are more stringent than for QPSK, due to the reduced radial distance between constellation points.

As previously noted, whilst ECLs provide a low linewidth source (ideal for the transmission of QAM), tunable semiconductor lasers are more practical for low-cost applications; although they normally exhibit a higher linewidth. Therefore, the integration of tunable semiconductor lasers into a high capacity PON scenario will require the phase noise of the laser to be tracked or compensated.

Several techniques exist for reducing the impact of phase noise on coherent receivers such as digital carrier phase estimation (for examples see [63]), carrier assisted phase estimation [107] and optical tracking of carrier phase. In the first two scenarios, the carrier phase estimate is impaired by noise from the channel, reducing the efficacy of phase estimation. Additionally, while carrier assisted phase estimation can outperform digital carrier phase estimation, it reduces spectral efficiency.

The third technique reduces the phase noise of a laser by directly measuring the laser phase with an interferometer and modulating the inverse of the phase onto the optical carrier itself [108, 109]. Although the resulting laser linewidth can be significantly reduced, it is challenging to synchronise the phase noise measurement with the feedforward phase compensation, making this technique complex to implement. The alternative, feedback approach has been demonstrated using a monolithically integrated SG-DBR laser [110], however, whilst the linewidth reduction factor is impressive (a factor of 27), the resulting linewidth (3 MHz) is still too high for low symbol rate applications.

For the access network scenario, the high linewidth laser is present in the ONU, meaning that downstream transmission performance is limited by the LO laser[6]. As such, a method for compensating only the LO phase noise is required.

A method for independently measuring and digitally compensating the phase noise of a LO laser was first proposed by Secondini *et al.* in [112], and verified for long-haul transmission in [113] (here, the process is termed 'Digital Coherence Enhancement').

[6]Note that LO linewidth also decreases sensitivity when a large amount of chromatic dispersion is compensated digitally at the receiver [111].

In these works, the process is demonstrated for a DFB laser. Additionally, this work considers only the use of differential QPSK. Arguably, the power of this technique comes from the fact that it is independent of modulation format, and that the phase noise being compensated does not follow any particular distribution. In the following sections, the technique is outlined, and the concept is demonstrated for high order QAM using a DS-DBR laser as the local oscillator.

Section 5.3.1 describes the scheme for measuring, and compensating, the phase noise of a local oscillator laser in a digital coherent receiver. Section 5.3.2 describes the experimental approach taken to measure phase noise, as well as proof of concept experiments. Section 5.3.3 describes the experimental technique used to generate and simulate a 6 GBd PDM-64QAM transceiver using LO phase noise compensation, and experimental validation of these results.

5.3.1 Laser phase measurement scheme

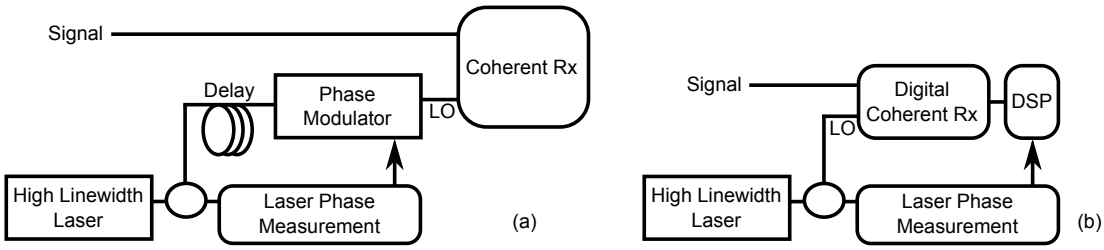

Figure 5.11: Schematic for local oscillator phase noise measurement. (a) The linewidth reduction method described in [108] applied to an LO in a coherent receiver. (b) The method used herein [112], digitally compensating LO linewidth.

The LO phase noise mitigation scheme consists of an optical measurement of differential phase, followed by digital signal processing (DSP) to calculate the laser phase noise, and is illustrated in Fig. 5.11. The output of a high linewidth LO is split into three paths. One path is sent to the LO port of a coherent receiver to provide a phase reference for a data carrying signal, while the remaining two paths are passed into a 90° optical hybrid, with the addition of an optical delay line in one of the arms. The delay line (time delay, τ) acts in a similar way to an interferometer, with the delay line length determining the maximum frequency, $1/\tau$, which can be discriminated between the two arms.

The signal received after the 90° optical hybrid is defined as $I(t) \propto E(t)E^*(t-\tau)$, where $I(t)$ is the combined photodiode currents (in-phase and quadrature) and $E(t)$ is the LO electric field. Direct detection terms are minimised by using balanced photodiodes. Assuming constant intensity, the argument of the signal can be reduced to a difference

between two time instants

$$\arg\left[E(t)E^*(t-\tau)\right] = \phi(t) - \phi(t-\tau) \approx \tau\frac{d\phi(t)}{dt} \tag{5.8}$$

for small τ (i.e. $\lim_{\tau\to 0}$). This is then numerically integrated[7] to calculate $\phi(t)$.

$$\phi(t) = \int_0^t \frac{d\phi(t)}{dt}\,dt = \frac{1}{\tau}\int_0^t \arg\left[I(t)\right]\,dt \pmod{2\pi} \tag{5.9}$$

Once this phase noise is measured, it is used to digitally compensate the combined data and LO signals that are received using a separate digital coherent receiver. This process removes the phase noise contribution of the LO from the data carrying signal.

5.3.2 FM noise spectrum and linewidth reduction

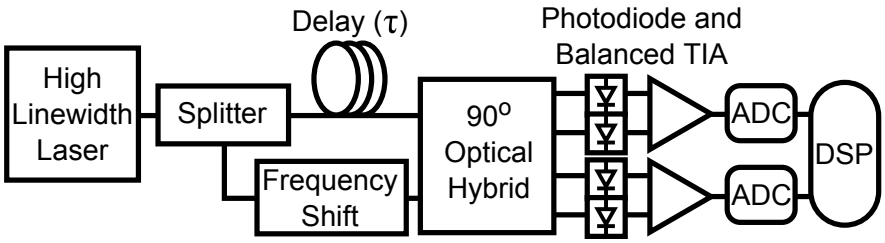

Figure 5.12: Experimental configuration for laser phase noise measurement.

To quantify the possible linewidth reduction using this technique, the experimental configuration shown in Fig. 5.12 was used. For this initial investigation, the high linewidth laser was first emulated by modulating phase noise onto CW light from an ECL (intrinsic linewidth 10 kHz) as in [114]. Phase noise was applied to the CW light using an IQ modulator) driven by an ArbWG operating at 12 GSa/s. The modulated phase was then compared with the phase estimated using this technique (Fig. 5.13).

For the phase noise compensation stage, the interferometer bandwidth was set to 550 MHz, allowing a practical implementation with 1.1 GSa/s ADCs. A 35 MHz frequency shift was applied to one arm using an Acousto-Optical Modulator (AOM) to overcome AC-coupling from balanced TIAs; this shift was later removed digitally. (Note that the frequency shift would not be required if balanced photodiodes were used, as in [112].) The signal from the photodiodes was digitised and resampled to 12 GSa/s. The performance of the linewidth measurement is limited by the interferometer bandwidth, the receiver bandwidth, and the temperature dependent variation in interferometer length.

Fig. 5.13(a) compares the spectrum of the applied FM noise with the spectrum of the phase noise after compensation (residual) for a 10 MHz laser linewidth. Though the

[7] Assuming the time step to be at the Nyquist limit, this integration can be computed in hardware using a cumulative sum to update a fixed resolution buffer.

interferometer bandwidth is 550 MHz, the phase noise compensation is flat only up to 30 MHz. Within the bandwidth DC-30 MHz, the phase noise is reduced significantly, with an estimate of the resulting linewidth shown in Fig. 5.13(b). For a 10 MHz input linewidth, the effective linewidth can be reduced to below 100 kHz.

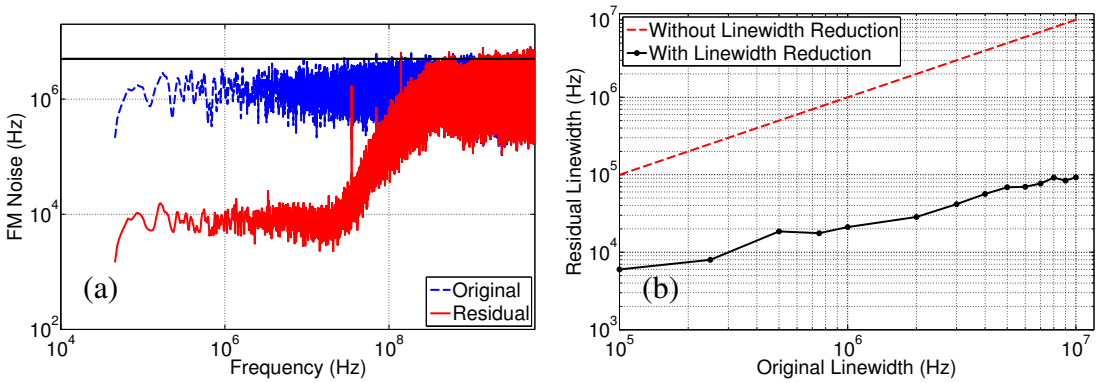

Figure 5.13: (a) FM noise spectra before and after compensation of 10 MHz linewidth. (b) Residual linewidth after phase noise compensation (in compensation bandwidth).

It is of primary interest for this thesis to evaluate the possible phase noise reduction when using the DS-DBR laser; an LO laser with a non-Lorentzian linewidth. The laser used in this investigation exhibits an excess low frequency noise as well as a high Lorentzian linewidth (1.4 MHz). To estimate the uncompensated FM noise spectrum, a coherent heterodyne technique was employed as described in [102], using a 10 kHz linewidth reference laser, Fig. 5.14. The compensated spectrum was estimated by comparing the phase noise measured using the heterodyne technique, and the phase noise measured using digital coherence enhancement. The resulting FM noise spectrum is also shown in Fig. 5.14. The low frequency phase noise is reduced by an order of magnitude.

5.3.3 Simulation and experimental validation

The following details an experimental investigation into the technique, where the phase noise is digitally removed from a combined LO and modulated signal. In contrast to the previous sections, in this experiment the BER was measured as a function of OSNR, rather than received optical power. This isolates the penalty due to LO RIN (see section 5.2.2) from the penalty due to LO laser linewidth. To set the OSNR, the noise from an EDFA (with no input) was attenuated using a VOA, and coupled into the signal path immediately before the coherent receiver. The OSNR in a 0.1 nm bandwidth was measured using an Optical Spectrum Analyser (OSA).

When applying phase noise compensation, the high frequency FM noise is uncompensated as it falls outside the interferometer bandwidth. To evaluate the impact of these frequency components on the residual phase noise, high order QAM signals were gen-

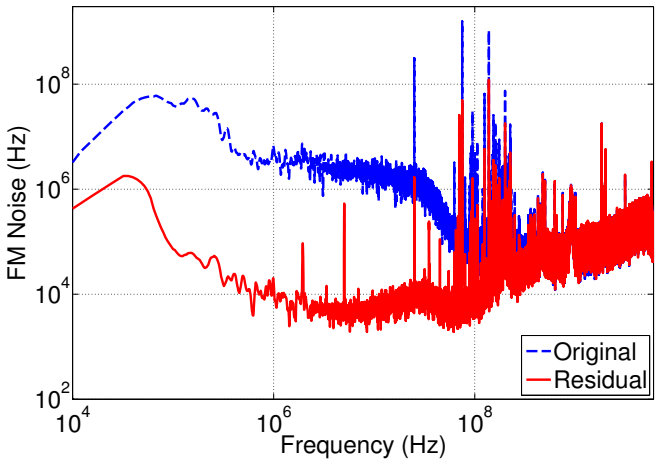

Figure 5.14: FM noise spectra before and after compensation of a high linewidth semiconductor tunable laser. Despite the non-Lorentzian laser linewidth, the phase noise can still be compensated.

erated and detected. The transmitter laser was an ECL (wavelength 1554 nm, linewidth 10 kHz), the LO was a DS-DBR laser (linewidth 1.4 MHz). Optical 6 GBd 64QAM was generated using an ArbWG operating at 12 GSa/s, driving an IQ modulator. As in previous experiments, polarisation multiplexing was achieved by splitting the signal into two arms of a delay line stage (200 symbols delay) before recombination using a polarisation beam combiner.

At the receiver, signals were detected using a phase- and polarisation-diverse coherent receiver, and digitally sampled using a digital storage oscilloscope, before being resampled to 2 samples/symbol. The received signals were pre-equalised using the CMA, followed by a radially directed equaliser, as described in section 2.4.2. Finally, a decision directed equaliser stage was interleaved with decision directed carrier phase estimation [61], also described in section 2.4.2. The phase noise estimation stage was configured as described in section 5.3.2. In order to monitor the transmitter phase bias, and to correct for any potential imbalance, an orthogonalisation procedure was used, as described in section 2.4.4. Finally, k-means clustering was used to make final symbol decisions (also see section 2.4.4).

The PDM-64QAM transceiver structure was also studied in simulation. Here, a variable linewidth was added to the LO in order to quantify the penalty expected for a particular (linewidth)$\times$(symbol duration) product ($\Delta\nu \cdot T$). The phase noise compensation scheme was simulated to quantify the impact of residual high frequency phase noise.

The simulation results, Fig. 5.15(a), show that for uncompensated LO laser phase noise, the sensitivity penalty is 1 dB when $\Delta\nu \cdot T = 3.1 \times 10^{-5}$. Using the phase noise compensation scheme, the penalty is 1 dB for $\Delta\nu \cdot T = 3 \times 10^{-4}$. This confirms the experimental results shown in Fig. 5.15(b), where $\Delta\nu \cdot T = 2.3 \times 10^{-4}$. For this

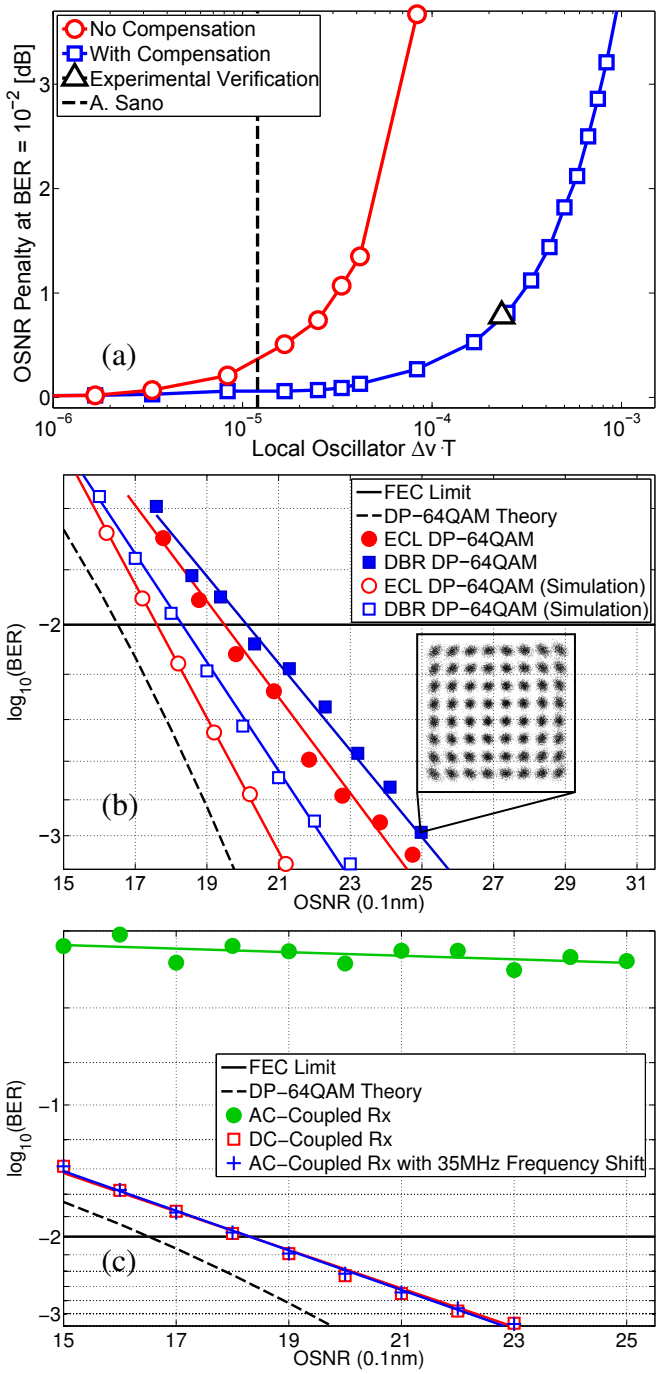

Figure 5.15: (a) Simulation showing penalty due to LO laser linewidth (c.f. [65]). The previous highest LO $\Delta\nu \cdot T$ is indicated (A. Sano, [115]). (b) Experimental results showing PDM-64QAM performance both with an ECL and with a phase noise compensated DS-DBR laser as the LO. (When using the DS-DBR laser without phase compensation, the data cannot be recovered.) (c) Simulations showing the effect of AC-coupling when measuring and compensating an LO laser linewidth of 1.4 MHz.

experimental configuration, phase noise compensation is required in order to recover the data. When applying phase noise compensation, the sensitivity penalty against using the ECL as LO laser is 0.6 dB. This represents data recovery with $\Delta\nu \cdot T = 2.3 \times 10^{-4}$ compared with the previous highest reported results $\Delta\nu \cdot T = 1.2 \times 10^{-5}$ [115].

Finally, Fig. 5.15(c) confirms that receiver AC-coupling impairs the phase estimate due to high pass filtering of the measured differential phase. Therefore, the frequency shift used in the phase measurement technique, Fig. 5.11, could be removed for DC-coupled receivers.

Note that the choice of symbol rate in this particular investigation is arbitrary as it is $\Delta\nu \cdot T$ that determines performance. As such, the performance for other modulation formats, symbol rates and laser linewidths can be extrapolated; here, using the data from [65] as a reference. Consider an upgrade to the PON discussed in chapter 4, with a target data rate of 40 Gbit/s per channel; requiring 6 GBd PDM-16QAM channels, encoding 8 bit/symbol. Based on the simulation result, the penalty for using DS-DBR lasers (assuming the best case of Lorentzian linewidth) would be approximately 1dB. Using this technique, the penalty would be completely negated.

Considering the scenario where the channel bandwidth is fixed at 3 GHz, the upgrade to 40 Gbit/s would require PDM-256QAM channels. From the perspective of required receiver sensitivity, this may be an unrealistic prospect (this is explored in chapter 6). However, looking purely at the linewidth requirements, using this compensation scheme it would be possible to recover the signal, albeit with a sensitivity penalty of approximately 2 dB.

Of most immediate significance with regards to this result is that it would enable the use of carrier phase estimation (such as the Viterbi and Viterbi algorithm) with high linewidth, potentially increasing the receiver sensitivity over those shown in section 5.2.7. However, for the case of the DS-DBR laser, it is the RIN which is the limiting factor in the use of carrier phase estimation, although this is also addressed in chapter 6.

5.4 Low complexity adaptive equalisation

It has already been noted in this chapter that it is important to reduce the complexity of receiver DSP in order to reduce power consumption. Potentially, the adaptive equaliser is the most power consuming block of the DSP (except the FEC, which is outside the scope of this research). This section details an investigation into reduced complexity equaliser filter tap updates, including an implementation of multiplier-free tap updates.

5.4.1 CMA complexity analysis

The full algorithm for filtering and updating the CMA is detailed in section 2.4.2, so will not be repeated here. However, in order to analyse the complexity of this algorithm, there are several repeated operations which are now highlighted. Consider, first the filter itself, $\mathbf{h}_{xx} \cdot \mathbf{x}_{in}$. Both the filter vector and input vector are complex numbers, and so computing this multiplication requires N complex multiplications for an N-tap filter. For each polarisation there are two such filtering operations, leading to a complexity of 4N complex multipliers[8].

The complexity of the error term calculation depends on the modulation format being equalised, however for PDM-QPSK the total complexity of this stage (both polarisations) is only four real multipliers, which is negligible for N>1.

Finally, the complexity of the tap update stage can be computed. These are reiterated below.

$$\mathbf{h}_{xx} \leftarrow \mathbf{h}_{xx} + \mu e_x \mathbf{x}_{in} x^*_{out}$$
$$\mathbf{h}_{xy} \leftarrow \mathbf{h}_{xy} + \mu e_x \mathbf{y}_{in} x^*_{out}$$
$$\mathbf{h}_{yx} \leftarrow \mathbf{h}_{yx} + \mu e_y \mathbf{x}_{in} y^*_{out}$$
$$\mathbf{h}_{yy} \leftarrow \mathbf{h}_{yy} + \mu e_y \mathbf{y}_{in} y^*_{out}$$

First, note that the perturbation to the tap updates are scaled by the learning parameter, μ. By scaling this parameter to be a power of 2, a hardware 2's complement implementation of multiplication by μ can be implemented with a simple bit shift [117]. Note also that the gradient term (the multiplication between the error and the output sample, e.g. $e_x x_{out}$) can be computed before multiplication with the input vector (a much more costly operation). The error term is a real number while the output symbol is complex, thus computing the gradient for each filter requires 2 real multipliers (8 real multipliers in total). Finally, the gradient term can be multiplied by the input vector, requiring 4N complex multipliers. These 4N complex multipliers dominate the complexity of the tap update algorithm.

It is interesting to note that the order of magnitude complexity of the filtering and the filter adaptation are both[9] $O(N)$, meaning that the tap updates contribute half the adaptive equaliser complexity using the direct implementation of convolution and, potentially, more than half the equaliser complexity when implementing convolution in the frequency domain, where the complexity is $O(\log_2(N))$ (for large N).

[8] For a large value of N, it is possible to reduce the required complex multipliers by using Fourier domain convolution, but there is no gain for N<8 [116]

[9] Big O notation, indicating, in this case, that the complexity in terms of multiplications is linear.

5.4.2 Signum tap update algorithms

In the field of wireless communications, it has been known for some time that the equaliser updates can be simplified by discarding some, or all, of the information about the magnitude of the gradient term, keeping only the sign of the gradient [118]. In order to find the sign of the gradient, the signum function is required, equation (2.35); the definition is reiterated below

$$\mathrm{sgn}(x) = \begin{cases} -1 & \text{if } x < 0 \\ 0 & \text{if } x = 0 \\ 1 & \text{otherwise} \end{cases}$$

where x is a real number. A complex signum function can be derived based on signum by treating the real and imaginary components of a complex number, z, independently

$$\mathrm{csgn}(z) = \mathrm{sgn}(\Re(z)) + j\,\mathrm{sgn}(\Im(z)) \tag{5.10}$$

The following two algorithms are for blind-adaptive filter tap weight updates, based on this principle.

Sign-data tap weight update algorithm

The initial simplification of the conventional tap weight updates can be made by first taking the complex sign of the output data symbol. This is a reasonable simplification because, at least for the CMA, the expected modulus of the data is already one. However, the error term contains only amplitude information. Information about the quadrature of the data is still required; the csgn operation retains this information, as the signal is restricted to four equidistant points on a unit circle: $\pi/4$,$3\pi/4$,$5\pi/4$ and $7\pi/4$. The algorithm is detailed below.

$\mathbf{h}_{xx} \leftarrow \mathbf{h}_{xx} + \mu e_x \mathbf{x}_{in}\,\mathrm{csgn}(x^*_{out})$
$\mathbf{h}_{xy} \leftarrow \mathbf{h}_{xy} + \mu e_x \mathbf{y}_{in}\,\mathrm{csgn}(x^*_{out})$
$\mathbf{h}_{yx} \leftarrow \mathbf{h}_{yx} + \mu e_y \mathbf{x}_{in}\,\mathrm{csgn}(y^*_{out})$
$\mathbf{h}_{yy} \leftarrow \mathbf{h}_{yy} + \mu e_y \mathbf{y}_{in}\,\mathrm{csgn}(y^*_{out})$

The complexity of this algorithm is now significantly reduced (see Table 5.1) for two reasons. First, the multiplication between the error term and the input vector requires only $2N$ real multipliers, because the error term is a real number. Second, and most significantly, the product of this intermediate result and the sign of the output symbol requires only adders.

Sign-sign tap weight update algorithm

The logical extension of this approach is to take the sign of both the error term and the output data symbol, such that only the sign of the gradient is used to update the filter taps. This is possible because incrementally updating the filter taps using the sign of the gradient will still lead to minimisation of signal error.

$$\mathbf{h}_{xx} \leftarrow \mathbf{h}_{xx} + \mu \,\mathrm{sgn}\,(e_x)\mathbf{x}_{in}\,\mathrm{csgn}(x^*_{out})$$
$$\mathbf{h}_{xy} \leftarrow \mathbf{h}_{xy} + \mu \,\mathrm{sgn}\,(e_x)\mathbf{y}_{in}\,\mathrm{csgn}(x^*_{out})$$
$$\mathbf{h}_{yx} \leftarrow \mathbf{h}_{yx} + \mu \,\mathrm{sgn}\,(e_y)\mathbf{x}_{in}\,\mathrm{csgn}(y^*_{out})$$
$$\mathbf{h}_{yy} \leftarrow \mathbf{h}_{yy} + \mu \,\mathrm{sgn}\,(e_y)\mathbf{y}_{in}\,\mathrm{csgn}(y^*_{out})$$

Here, multipliers are not required. The gradient can be computed by inverting the sign of $\mathrm{csgn}(x_{out})$ based on the sign of $\mathrm{sgn}\,(e_x)$. Further, multiplying the gradient with the input vector requires only adders, as noted previously.

A comparison of implementation complexity

There are several known ways to implement a complex multiplier in hardware. For a multiplication between two complex numbers, wz, where $w = a + jb$ and $z = c + jd$ and $a, b, c, d \in \Re$, the direct multiplication is computed as

$$wz = (ac - bd) + j(ad + bc)$$

which requires four real multipliers and two real adders. The most efficient implementation of this operation (assuming multipliers are more costly than adders) is [119]

$$wz = [d(a-b) + a(c-d)] + j[d(a-b) + b(c+d)]$$

which is sometimes called Gauss' method. Due to the repetition of the term $d(a-b)$, only three real multipliers are required in this implementation, although at the cost of an additional three real adders (five in total).

A comparison of the complexity of each of the tap weight update algorithms is shown in Table 5.1. Interestingly, although the sign algorithm would reduce the number of logic gates required in a hardware implementation, the complexity is still $O(N)$ (in terms of multipliers). The sign-sign algorithm is therefore the most attractive for a low-cost implementation, with a complexity, with respect to multipliers, of $O(1)$.

5.4.3 Simulation and experimental investigation

The performance for all three algorithms was first evaluated in simulation. 3 GBd PDM-QPSK signals were generated and noise loaded to 4 dB OSNR. It is conventional to use polarisation rotations to evaluate the equaliser's tracking performance [32]; as such, polarisation rotations were added to the signal at this stage. A balanced coherent receiver was simulated, with the receiver DSP proceeding as normal thereafter. In order

Table 5.1: IMPLEMENTATION COMPLEXITY FOR TAP WEIGHT UPDATE ALGORITHMS

	CMA (Direct Implementation)	CMA (Gauss' Method)	Sign Data	Sign-Sign
Real Multipliers	16N+4	12N+4	8N	0
Real Adders	16N	28N	16N	16N
Bit Shifts	4	4	4	4
Inverters	6	10	12N+2	12N+6
Comparators	0	0	4	6

to make a fair comparison between the equalisers, each was initialised using ideal tap weights, and each equaliser filter length was 5 complex taps.

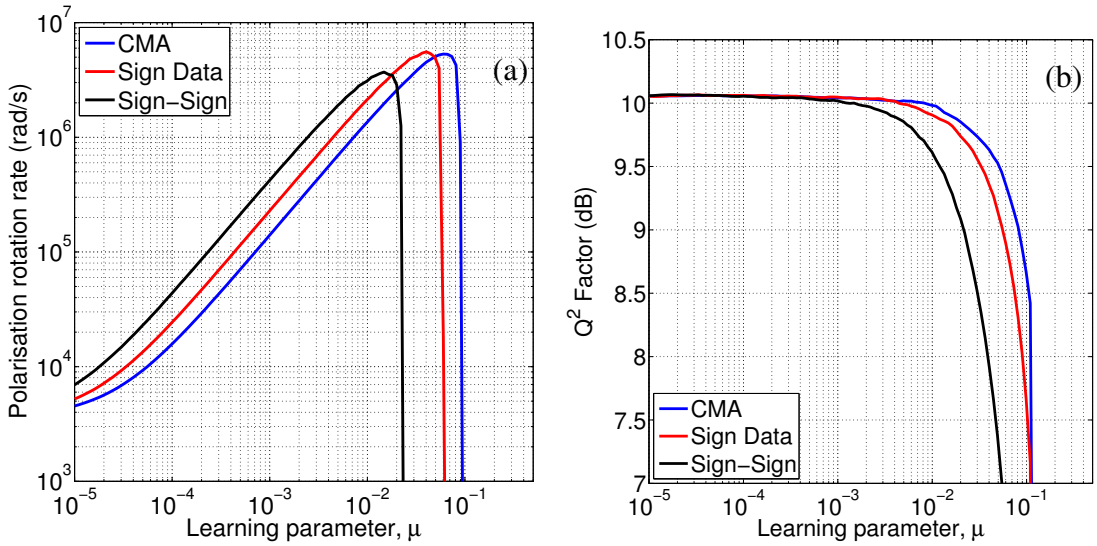

Figure 5.16: Simulation results for a 5-tap CMA equalising a 3 GBd PDM-QPSK signal, noise loaded to 4 dB OSNR. (a) Ability to track polarisation rotations (performance measured at a Q^2-factor of 8.5 dB). (b) Dependence of Q^2-factor on the learning parameter, μ, without polarisation rotations.

As shown in Fig. 5.16, all three algorithms can track polarisation rotations >1 Mrad/s. The maximum polarisation rotation rates were 5.3×10^6 (CMA), 5.6×10^6 (Sign Data), and 3.7×10^6 (Sign-Sign).

Note that taking the sign of the output data and/or the error term increases the effective value of the learning parameter, μ, leading to the maximum permissible value of μ to be lower for both the signed algorithms.

These equalisers were also investigated using the experimental data from section 3.2.2. Here, both the back-to-back and transmission performance of each algorithm was measured in order to evaluate, firstly, the benchmark performance of each equaliser and, subsequently, to evaluate the impact of the residual chromatic dispersion typical of an access network.

From Fig. 5.17, it can be seen that all three algorithms exhibit identical performance in both the back-to-back and transmission scenarios. Though the CMA and Sign-Data

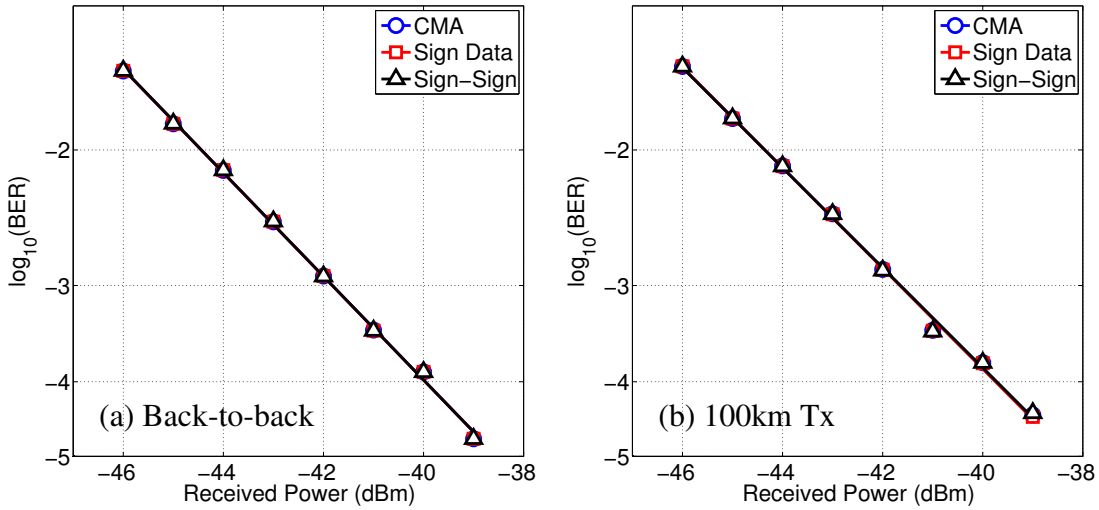

Figure 5.17: Experimental investigation of three equaliser tap update algorithms: standard CMA, sign on output data (Sign Data), and sign on output data and error term (Sign-Sign). Transmitted signal was 3.125 GBd PDM-QPSK. (a) Back-to-back configuration, and (b) transmission over 100 km SMF.

algorithms offer superior performance when tracking fast rotations, the Sign-Sign algorithm is sufficient for the impairments encountered in 100 km transmission. Therefore, based on this experimental investigation, it would appear the lowest complexity algorithm, Sign-Sign, is the best choice for a digital coherent receiver in an access network.

5.5 Summary

Coherent receivers measure the full optical field, which can be translated into the digital domain via analogue-to-digital converters. As such, digital signal processing can be used to compensate, not only for channel impairments, but also for receiver impairments. Whilst DSP can potentially relax the performance requirements of the optical front end, the DSP itself should also be simple to enable a low-power implementation suitable for an access network. The key results of this chapter are as follows:

- Digital signal processing enabling the reception of PDM-QPSK using a high-linewidth, high-RIN LO laser
- Simplified DSP algorithm for carrier recovery in the presence of LO frequency wander
- Low-complexity receiver has potential for LR-PON with 1:128 way split
- Scheme presented for directly measuring and digitally compensating the linewidth of a LO laser in a coherent receiver. This scheme enables reception of 6 GBd

PDM-64QAM with only 0.6 dB penalty at BER 10^{-2} when the LO has a 1.4 MHz linewidth (DS-DBR laser)

- Algorithm presented for multiplier-free equaliser tap weight updates Experimentally, no penalty is observed for the simplified algorithm versus the standard CMA tap weight updates.

6

Conclusions and further work

COHERENT passive optical networks have been extensively explored in this thesis, with a view to implementation in an optical access network. In this chapter, the salient results from these investigations are summarised (section 6.1). Suggestions for future direction in this work are given in section 6.2.

6.1 Summary of research

In recognition of increasing consumer demand for bandwidth, research has been undertaken to develop a network architecture and associated transceiver technology capable of economically delivering 10 Gbit/s per subscriber. Projections indicate that such high capacity access networks will be required by 2024.

Historically, passive optical networks have been viewed as an economically viable choice for access network deployments. This is because communications equipment can be located either at customer premises ONU or at the service provider premises OLT. However, the lack of midspan signal regeneration makes these networks loss-limited.

In this thesis, the use of coherent receivers was proposed, primarily due to their intrinsically high power sensitivity. However they also have several other properties which can be exploited in an access network scenario. The use of coherent receivers enabled a capacity increase through wavelength division multiplexing, due to their frequency selectivity (changing the wavelength of the local oscillator laser can select an arbitrary wavelength channel). Additionally, the use of coherent receivers enabled

the use of 'advanced' phase and polarisation based modulation schemes, which encode multiple bits per symbol. Finally, because coherent receivers capture the full optical field, digital signal processing could be used to compensate channel and transceiver impairments.

The conventional receivers used in PON architectures consist of a single photodiode measuring the envelope of the received signal. Digital coherent receivers require significantly more components, in this case an optical hybrid, polarisation beam splitters, four photodiodes, and four analogue-to-digital converters. Therefore, even with advances in photonic integration [90], coherent receivers will always be more costly than direct detection receivers with equivalent bandwidth. Access networks are inherently cost-sensitive, due to the direct correlation between the number of transceivers and the number of users supported by the PON architecture. Therefore, this thesis has sought to demonstrate the potential for coherent receivers firstly to outperform conventional receivers, and secondly to reduce the required receiver complexity.

In the sense of sheer performance, this work has demonstrated record receiver sensitivities for high data rate communications. Notably, 4 photons/bit sensitivity was demonstrated using the advanced modulation format PS-QPSK at 40 Gbit/s (although this result applies equally to 10 Gbit/s transmission required for the coherent LR-PON). High sensitivity was also achieved using the modulation format PDM-QPSK, which encodes 4 bit/symbol. The high information content per symbol means the required transceiver bandwidth can be reduced. In this case, a 10 Gbit/s transmitter was realised with only 3 GHz required electrical bandwidth.

By extending this transmission scheme to multiple wavelengths (WDM), this thesis also examined the feasibility of a PON with a passive power splitter to distribute signals to multiple ONUs (as is conventional for single wavelength channel PONs, for example GPON). Here, all WDM channels are transmitted to all ONUs, and the local oscillator laser in each ONU is tuned to demultiplex the channel of interest. This allows for full network reconfiguration, because each receiver is 'colourless'. However, the trade-off is the high loss due to the passive power splitter, although, due to the high sensitivity of coherent receivers, the permissible split ratio can still be large. In the ideal scenario, the feasibility study found that a 1:1024 way split would be achievable after 100 km transmission.

Bidirectional (full duplex) transmission was also investigated. This is of interest to reduce the total cost of network deployment as it halves the required number of fibres. It was found that Rayleigh backscattering can cause crosstalk between the upstream and downstream channels at the ONU receiver. Although some rejection of the reflected channels was possible using the coherent receiver, it was found that high power reflections dominated the received signal. By using digital pulse shaping at the ONU transceiver, it was found that almost arbitrarily high channel powers could

be reflected without penalty. This is the first time digital pulse shaping was used for mitigating crosstalk due to reflections in an access network scenario.

The capability of coherent receivers is best realised when coupled with digital signal processing, which can be used to compensate, channel and receiver impairments. In this thesis, the application of digital signal processing to PON was highlighted through a series of experimental investigations. A digital filter was designed which enabled the reception of PDM-QPSK using a high-linewidth, high-RIN LO laser. It was found that, even with a significantly reduced receiver complexity, a receiver sensitivity was achieved which showed the feasibility of a LR-PON with 1:128 way split.

Finally, it was noted herein that both the optical and electrical complexity of the receiver should be low in order to ensure the proposed network architecture is cost effective. There are several elements which make up the receiver digital signal processing, however the adaptive equalisation is the most complex to implement. Adaptive equalisation comprises two elements: the filtering, and the filter tap weight up dates. It was shown that, in terms of (real) hardware multipliers, the complexity of both the tap updates and the filter were $O(N)$, where N is the number of filter taps. By simplifying the tap weight update algorithm, the complexity of this component of the equalisation was reduced to $O(1)$.

6.2 Future Work

6.2.1 Simulations of a 1000 wavelength (10 Tbit/s) long reach PON

Investigations involving transmission over the full C-band, while the ultimate target of this work, is beyond the permissible complexity of the experimental investigations detailed herein. However, full C-band transmission could be investigated in simulation, in order to investigate the impact of

- fibre nonlinearity (what is the maximum transmission power?)
- channel spacing (what is the maximum capacity?)
- receiver CMRR.

These three parameters are mutually dependent. For example, the impact of cross phase modulation is greater for narrow channel spacing, and the number of channels entering a receiver changes the required receiver CMRR for operation without penalty (this issue is discussed, for example, in [120]).

Simulations of nonlinearity in a 64-channel UDWDM LR-PON were recently undertaken by Reis *et. al.* in [85, 86] and Rohde *et. al.* in [24], albeit using single-polarisation

QPSK. Here it was found that the dominant nonlinear impairment was four wave mixing, due to the dense channel spacing and constant power profile of the QPSK channels over 100 km fibre transmission. It would be advantageous to extend these simulations to model the network architecture discussed in chapter 4 in order to estimate the expected power budget for this network.

It would also be of interest to simulate nonlinearity in bidirectional transmission. Although this was investigated in chapter 4 and no penalty was observed, here only 5 channels were used. With >1000 wavelengths, and a greater total optical power, there is the potential to excite some nonlinear effect not seen in the proof of concept investigations.

Therefore, further work in this area would seek to confirm the results relating to maximum permissible transmission power (chapter 4) and calculate the achievable power budget for a $1024\lambda \times 10$ Gbit/s LR-PON.

6.2.2 Optical access networks beyond 10 Gbit/s

Consider Fig. 1.1, which describes projected consumer internet bandwidth requirements. A continuation of current trends suggests that a high-end user's bandwidth requirements will be 40 Gbit/s during the year 2027. Arguably, an end user may not require a fixed 40 Gbit/s connection for a single device, however the rapid growth in mobile internet bandwidth requirements [1] indicates that a single user may in the future require a high bandwidth connection to accommodate multiple devices.

There are several upgrade paths to the network described in section 4.2, which achieve 40 Gbit/s per subscriber. However, in order to keep the number of network subscribers constant, the bandwidth occupied by each channel must also remain constant. Table 6.1 details several modulation formats and, for each, the required symbol rate to achieve 48 Gbit/s (40 Gbit/s with 20% overhead for FEC). Future work would consider upgrade scenarios, and place limits on transceiver parameters, such as laser linewidth and receiver sensitivity. As an example, consider the following scenarios.

PDM-QPSK channels on a 20 GHz frequency grid

In the simplest upgrade scenario, the modulation format would not be altered (PDM-QPSK), however, in order to achieve 40 Gbit/s per subscriber, the symbol rate would need to be increased to 12 GBd, reducing the theoretical receiver sensitivity by 6 dB. Assuming the 40% ($\frac{2}{5}$ symbol rate) guard band between channels investigated in section 4.1.2, the channel spacing would now be 20 GHz; allowing a maximum capacity of 250 channels in the C-band (or 125 upstream and downstream channels, offset by 20 GHz in a bidirectional configuration).

With the capacity reduced by 75%, the split ratio could also be reduced by the same

Modulation Format	**Required Symbol Rate (GBd)**	**Theoretical Sensitivity Penalty vs. 3GBd PDM-QPSK at BER=10^{-2} (dB)** (see appendix A)
PDM-QPSK	12.00	6.0
PDM-8QAM	8.00	8.4
PDM-16QAM	6.00	9.6
PDM-32QAM	4.80	11.6
PDM-64QAM	4.00	13.6
PDM-128QAM	3.43	15.8
PDM-256QAM	3.00	18.1
PDM-512QAM	2.66	20.4
PDM-1024QAM	2.40	22.8

Table 6.1: MODULATION FORMATS AND SYMBOL RATES FOR 40 GBIT/S OPTICAL ACCESS

fraction, saving a theoretical 6 dB in power budget. The receiver side challenges here become

- the possible requirement for chromatic dispersion compensation
- the high transceiver electrical bandwidth requirements

This scheme has the advantage that the laser linewidth requirements are reduced versus the 3 GBd PDM-QPSK scenario, assuming 2 sample/symbol is still used for DSP.

3 GBd channels on a 5 GHz frequency grid

In this upgrade scenario, 40 Gbit/s can be achieved using 3 GBd PDM-256QAM. However, as shown in Table 6.1, the theoretical receiver sensitivity is reduced by 18.1 dB compared to the 3 GBd PDM-QPSK scenario, before the impact of laser linewidth [65] and ADC/Digital-to-Analogue Converter (DAC) resolution [121] are taken into account. Assuming the 18.1 dB loss, this corresponds to a reduction in split ratio by a factor of 64. Thus, increasing capacity is not possible while maintaining the symbol rate for this network architecture.

6.2.3 Nyquist channel spacing in optical access networks

The investigation in section 4.3.2 found that Nyquist pulse shaping (root raised cosine filter with a zero rolloff factor) could be used to mitigate inter-channel interference when the total power of the interfering channel is much greater than the channel of interest. It was found that, for 3 GBd PDM-QPSK channels with a channel spacing of 5 GHz, Nyquist pulse shaping completely eliminates crosstalk. This shows that an upstream/downstream pair of channel need only be separated by 5 GHz if Nyquist filtering is applied at the OLT and the ONU.

The logical next step is to investigate the impact of channel spacing on receiver sensitivity, by varying the channel spacing between 3 GHz (symbol rate) and 5 GHz (low crosstalk region). A recent paper showed the impact of ONU/OLT Nyquist pulse shaping of 2.5 GBd 16QAM channels [89]. Here, it was determined that bidirectional transmission over 40 km SMF was possible, even when upstream/downstream channels were spaced at the symbol rate. However, it was not possible to separate the noise sources in this experiment; nonlinear noise, crosstalk due to reflections, and receiver noise sources are all measured together (although the optimum transmitter power is determined, which gives some information about nonlinearity tolerance). Therefore, as noted above, future work would separately measure the impact of crosstalk on receiver sensitivity.

6.2.4 Alternative methods for RIN compensation

As shown theoretically and experimentally in section 5.3, it is possible to measure and partially compensate the linewidth of a local oscillator laser by independently measuring the evolution of the laser phase with time, and digitally applying the inverse of this measured phase to the combined LO and signal. The experimental results in section 5.3 demonstrate a high linewidth LO laser being used in an ASE-limited scenario, which would be useful in a repeated network. For the case of an access network, compensation of the LO RIN is also necessary. In principle this technique can also be used to measure and compensate LO laser impairments, such as RIN.

As shown for case of the DS-DBR laser in section 5.1.2, low frequency RIN dominates the intensity noise profile. Therefore, near-ideal compensation of RIN should be possible, even with a small interferometer bandwidth. However, there are some outstanding issues which must be resolved in order to compensate RIN.

As this measurement technique is coherent, the relative amplitude of a signal can also be determined. The intensity noise of a laser could then be measured as follows. The received signal is $S(t) = E(t)E^*(t-\tau)$, with a time-dependent amplitude component to the field.

$$\begin{aligned} |S(t)| = |E(t)E^*(t-\tau)| &= |A(t)e^{j\phi(t)}A(t-\tau)e^{-j\phi(t-\tau)}| \\ &= A(t)A(t-\tau) \end{aligned} \tag{6.1}$$

The amplitude at the two time instants can be separated using logarithms. Let $L(t) = \ln(A(t))$. This gives

$$\begin{aligned} \ln(|S(t)|) &= \ln(A(t)A(t-\tau)) = L(t) + L(t-\tau) \\ \ln(|S(t-\tau)|) &= \ln(A(t-\tau)A(t-2\tau)) = L(t-\tau) + L(t-2\tau) \end{aligned} \tag{6.2}$$

which is the sum of the signal envelope at time instances t and $t-\tau$, and $t-\tau$ and

$t-2\tau$, respectively. The corresponding time derivative of these logarithms can be found by taking the difference term, $\ln(|S(t))-\ln(|S(t-\tau)|)$, and using the method of equation (5.8)

$$\lim_{\tau\to 0}\left[\frac{1}{2\tau}(L(t)-L(t-2\tau))\right]=\frac{dL(t)}{dt} \tag{6.3}$$

giving the final integral

$$\begin{aligned}\frac{1}{2\tau}\int\left[\ln\left(|S(t)|\right)-\ln\left(|S(t-\tau)|\right)\right]dt &= \frac{1}{2\tau}\int 2\tau\frac{dL(t)}{dt}\,dt \\ &= L(t)+L_0\end{aligned} \tag{6.4}$$

The initial amplitude of the signal, $\exp(L_0)$, is not of interest as the important element for optical communications is the evolution of the amplitude[1]. Therefore, the final relationship between measured signal and amplitude is:

$$A(t)=\exp\left(\frac{1}{2\tau}\int\left[\ln\left(|S(t)|\right)-\ln\left(|S(t-\tau)|\right)\right]dt\right) \tag{6.5}$$

This analysis is valid for all $A(t)\neq 0$.

This demonstrates that the configuration proposed in section 5.3 enables a combined system for measuring both amplitude noise and phase noise. However, while the measurement of RIN is straightforward, the compensation of RIN is complicated by the need to know the exact Common Mode Rejection Ratio (CMRR) on each channel of the coherent receiver. Consider equation (5.5), which is an approximation describing how the received signal is distorted by a RIN-induced noise term.

$$I\propto C(E_{LO}(t)E_{Sig}(t))+(1-C)(E_{LO}(t)E_{RIN}(t))$$

It is therefore desirable to digitally remove the term $(1-C)(E_{LO}(t)E_{RIN}(t))$. In this analysis, E_{RIN} is defined as the amplitude noise term of the LO laser, so E_LO can be assumed constant. Additionally, $E_{RIN}(t)$ has no phase component, making it equivalent to $A(t)$ in equation (6.5). Thus, equation (5.5) simplifies as follows

$$I\propto CE_{Sig}(t)+(1-C)A(t) \tag{6.6}$$

The above demonstrates that RIN can be independently measured, and digitally removed from a detected beat signal in a digital coherent receiver, provided the CMRR is known *a priori*. Future investigations in this area would seek to confirm this theory experimentally. Additionally, these investigations would incorporate a method for determining both C, and the accuracy with which C must be estimated for this approach

[1] However, to estimate RIN it may be useful to define $\exp(L_0)$ as the first measured amplitude, in order to reference all further amplitude measurements to this value.

to be effective.

References

[1] CISCO, Cisco visual networking index: Forecast and methodology, 2011–2016 Technical report, CISCO Systems, May 2012. 15, 118

[2] CISCO, Cisco visual networking index: Forecast and methodology, 2010–2014 Technical report, CISCO Systems, June 2010. 15

[3] CISCO, Cisco visual networking index: Forecast and methodology, 2010–2015 Technical report, CISCO Systems, June 2011. 15

[4] J. Nielsen, Nielsen's law of internet bandwidth, May 2013 URL `http://www.nngroup.com/articles/law-of-bandwidth/`. 8, 16

[5] Britain's superfast broadband future Technical report, Department for Business Innovation and Skills, Dec. 2010. 8, 16

[6] UK fixed-line broadband performance, November 2012 Technical report, OFCOM, Mar. 2013. 8, 16

[7] C. Lam, *Passive Optical Networks* Academic Press, 2007. 17, 19, 74, 79

[8] C. Qiao and M. Yoo, "Optical burst switching (OBS) - A new paradigm for an optical internet," *Journal of High Speed Networks*, **8**(1), pp. 69–84, 1999. 17

[9] R. Davey, D. Grossman, M. Rasztovits-Wiech, D. Payne, D. Nesset, A. Kelly, A. Rafel, S. Appathurai, and S.-H. Yang, "Long-reach passive optical networks," *J. Lightwave Technol.*, **27**(3), pp. 273–291, Feb. 2009. 17, 20

[10] A. Saleh and J. Simmons, "Architectural principles of optical regional and metropolitan access networks," *J. Lightwave Technol.*, **17**(12), pp. 2431–2448, Dec. 1999. 8, 18

[11] APON and BPON family of recommendations ITU-T G.983, 2001-2005. 18

[12] N. Ansari and J. Zhang, *Media Access Control and Resource Allocation For Next Generation Passive Optical Networks* Springer, 2013. 18

[13] GPON family of recommendations ITU-T G.984, 2003-2008. 18

[14] XG-PON family of recommendations ITU-T G.987, 2003-2008. 19

[15] D. Shea, A. Ellis, D. Payne, R. Davey, and J. Mitchell, "10 Gbit/s PON with 100 km reach and x1024 split," In *Proceedings of European Conference on Optical Communication*, paper We.P.147, 2003. 20

[16] D. Shea and J. Mitchell, "A 10-Gb/s 1024-way-split 100-km long-reach optical-access network," *J. Lightwave Technol.*, **25**(3), pp. 685–693, Mar. 2007. 20

[17] Gigabit-capable passive optical networks (GPON): Reach extension, recommendation ITU-T G.984.6, 2008. 20

[18] Gigabit-capable passive optical networks (GPON): General characteristics, recommendation ITU-T G.984.1, 2008. 20

[19] Z. Al-Qazwini and H. Kim, "Symmetric 10-Gb/s WDM-PON using directly modulated lasers for downlink and RSOAs for uplink," *J. Lightwave Technol.*, **30**(12), pp. 1891–1899, Jun. 2012. 20

[20] K. Y. Cho, U. H. Hong, S. P. Jung, Y. Takushima, A. Agata, T. Sano, Y. Horiuchi, M. Suzuki, and Y. C. Chung, "Long-reach 10-Gb/s RSOA-based WDM PON employing QPSK signal and coherent receiver," *Opt. Express*, **20**(14), pp. 15353–15358, Jul. 2012. 21

[21] P. Ossieur, C. Antony, A. Clarke, A. Naughton, H.-G. Krimmel, Y. Chang, C. Ford, A. Borghesani, D. Moodie, A. Poustie, R. Wyatt, B. Harmon, I. Lealman, G. Maxwell, D. Rogers, D. Smith, D. Nesset, R. Davey, and P. Townsend, "A 135-km 8192-split carrier distributed DWDM-TDMA PON with $2 \times 32 \times 10$ Gb/s capacity," *J. Lightwave Technol.*, **29**(4), pp. 463–474, Feb. 2011. 21

[22] P. Ossieur, C. Antony, A. Naughton, A. Clarke, H.-G. Krimmel, X. Yin, X.-Z. Qiu, C. Ford, A. Borghesani, D. Moodie, A. Poustie, R. Wyatt, B. Harmon, I. Lealman, G. Maxwell, D. Rogers, D. Smith, S. Smolorz, H. Rohde, D. Nesset, R. Davey, and P. Townsend, "Demonstration of a 32×512 split, 100 km reach, $2 \times 32 \times 10$ Gb/s hybrid DWDM-TDMA PON using tunable external cavity lasers in the ONUs," *J. Lightwave Technol.*, **29**(24), pp. 3705 –3718, Dec. 2011. 21

[23] Alcatel-Lucent, Next-generation electro-optics technology with coherent detection Technical report, Alcatel-Lucent, 2009. 22

[24] H. Rohde, S. Smolorz, E. Gottwald, and K. Kloppe, "Next generation optical access: 1 Gbit/s for everyone," In *Proceedings of European Conference on Optical Communication*, paper 10.5.5, 2009. 22, 79, 117

[25] S. Smolorz, E. Gottwald, H. Rohde, D. Smith, and A. Poustie, "Demonstration of a coherent UDWDM-PON with real-time processing," In *Proceedings of Optical Fiber Communication Conference*, paper PDPD4, 2011. 22, 23

[26] S. Narikawa, H. Sanjoh, N. Sakurai, K. Kumozaki, and T. Imai, "Coherent WDM-PON using directly modulated local laser for simple heterodyne transceiver," In *Proceedings of European Conference on Optical Communication*, paper We3.3.2, 2005. 22, 23

[27] E. Ip, A. P. T. Lau, D. J. F. Barros, and J. M. Kahn, "Coherent detection in optical fiber systems," *Opt. Express*, **16**(2), pp. 753–791, Jan. 2008. 22

[28] M. Zhu, J. Liu, Y.-T. Hsueh, G.-K. Chang, G. Gu, and F. Zhu, "Terabit optical access networks using ultra-dense WDM and coherent technology," In *Proceedings of Photonics and Optoelectronics Meetings (POEM)*, pages 83310G–1–83310G–6, 2011. 23

[29] H. Rohde, S. Smolorz, J. Wey, and E. Gottwald, "Coherent optical access networks," In *Proceedings of Optical Fiber Communication Conference*, paper OTuB1, 2011. 23

[30] E. Ip, A. P. Lau, D. J. Barros, and J. M. Kahn, "Coherent detection in optical fiber systems: erratum," *Opt. Express*, **16**(26), pp. 21943–21943, Dec. 2008. 24

[31] D. Lavery, E. Torrengo, and S. Savory, "Bidirectional 10 Gbit/s long-reach WDM-PON using digital coherent receivers," In *Proceedings of Optical Fiber Communication Conference*, paper OTuB4, 2011. 9, 11, 24, 26, 59, 73, 78, 100

[32] S. J. Savory, "Digital filters for coherent optical receivers," *Opt. Express*, **16**(2), pp. 804–817, Jan. 2008. 24, 45, 47, 111

[33] K. Kikuchi and S. Tsukamoto, "Evaluation of sensitivity of the digital coherent receiver," *J. Lightwave Technol.*, **26**(13), pp. 1817–1822, Jul. 2008. 24, 41, 91

[34] D. S. Millar, D. Lavery, S. Makovejs, C. Behrens, B. C. Thomsen, P. Bayvel, and S. J. Savory, "Generation and long-haul transmission of polarization-switched QPSK at 42.9 Gb/s," *Opt. Express*, **19**(10), pp. 9296–9302, May. 2011. 25, 50, 67

[35] C. Behrens, D. Lavery, D. S. Millar, S. Makovejs, B. C. Thomsen, R. I. Killey, S. J. Savory, and P. Bayvel, "Ultra-long-haul transmission of 7×42.9 Gbit/s PS-QPSK and PDM-BPSK," *Opt. Express*, **19**(26), pp. B581–B586, Dec. 2011. 25

[36] C. Behrens, D. Lavery, D. Millar, S. Makovejs, B. C. Thomsen, R. Killey, S. Savory, and P. Bayvel, "Ultra-long-haul transmission of 7×42.9Gbit/s PS-QPSK and PM-BPSK," In *Proceedings of European Conference on Optical Communication*, paper Mo.2.B.2, 2011. 25

[37] D. Lavery, C. Behrens, S. Makovejs, D. Millar, R. Killey, S. Savory, and P. Bayvel, "Long-haul transmission of PS-QPSK at 100 Gb/s using digital backpropagation," *IEEE Photonics Technol. Lett.*, **24**(3), pp. 176 –178, Feb. 2012. 25

[38] D. Lavery, S. Liu, Y. Jeong, J. Nilsson, P. Petropoulos, P. Bayvel, and S. Savory, "Realizing high sensitivity at 40 Gbit/s and 100 Gbit/s," In *Proceedings of Optical Fiber Communication Conference*, paper OW3H.5, 2012. 26, 68

[39] D. Lavery, C. Behrens, and S. Savory, "A comparison of modulation formats for passive optical networks," In *Proceedings of European Conference on Optical Communication*, paper Tu.5.C.5, 2011. 9, 26, 62, 73

[40] D. Lavery, C. Behrens, and S. J. Savory, "A comparison of modulation formats for passive optical networks," *Opt. Express*, **19**(26), pp. B836–B841, Dec. 2011. 26, 65

[41] C. Behrens, D. Lavery, R. Killey, S. Savory, and P. Bayvel, "Long-haul WDM transmission of PDM-8PSK and PDM-8QAM with nonlinear DSP," In *Proceedings of Optical Fiber Communication Conference*, paper OM3A.4, 2012. 26

[42] D. Lavery, M. Ionescu, S. Makovejs, E. Torrengo, and S. J. Savory, "A long-reach ultra-dense 10 Gbit/s WDM-PON using a digital coherent receiver," *Opt. Express*, **18**(25), pp. 25855–25860, Dec. 2010. 11, 26, 73, 76

[43] D. Lavery, C. Behrens, and S. Savory, "On the impact of backreflections in a bidirectional 10 Gbit/s coherent WDM-PON," In *Proceedings of Optical Fiber Communication Conference*, paper OTh1F.3, 2012. 11, 26, 80

[44] D. Lavery, M. Paskov, and S. J. Savory, "Spectral shaping for mitigating backreflections in a bidirectional 10 Gbit/s coherent WDM-PON," In *Proceedings of Optical Fiber Communication Conference*, paper OM2A.6, 2013. 26, 84

[45] D. Lavery, R. Maher, D. Millar, B. C. Thomsen, P. Bayvel, and S. J. Savory, "Demonstration of 10 Gbit/s colorless coherent PON incorporating tunable DS-DBR lasers and low-complexity parallel DSP," In *Proceedings of Optical Fiber Communication Conference*, paper PDP5B.10, 2012. 26

[46] D. Lavery, R. Maher, D. Millar, B. C. Thomsen, P. Bayvel, and S. J. Savory, "Digital coherent receivers for long-reach optical access networks," *J. Lightwave Technol.*, **31**(4), pp. 609–620, Feb. 2013. 26, 89

[47] G. Agrawal, *Lightwave Technology* Wiley, 2005. 31, 44, 133

[48] E. Hecht and A. Zajac, *Optics* Addison-Wesley, 1977. 31

[49] F. Kapron, B. Adams, E. Thomas, and J. Peters, "Fiber-optic reflection measurements using OCWR and OTDR techniques," *J. Lightwave Technol.*, **7**(8), pp. 1234–1241, Aug. 1989. 11, 31, 84

[50] M. Karlsson and E. Agrell, "Which is the most power-efficient modulation format in optical links?," *Opt. Express*, **17**(13), pp. 10814–10819, Jun. 2009. 34, 59, 60, 134

[51] J. Proakis and M. Salehi, *Digital Communications* McGraw-Hill, 2008. 34, 41, 50, 134

[52] E. Wooten, K. Kissa, A. Yi-Yan, E. Murphy, D. Lafaw, P. Hallemeier, D. Maack, D. Attanasio, D. Fritz, G. McBrien, and D. Bossi, "A review of lithium niobate modulators for fiber-optic communications systems," *IEEE J. Sel. Top. Quantum Electron.*, **6**(1), pp. 69–82, Jan.-Feb. 2000. 36

[53] I. Kaminow, T. Li, and A. Willner, *Optical Fiber Telecommunications V-B* Academic Press, 2013. 36

[54] M. Taylor, "Coherent detection method using DSP for demodulation of signal and subsequent equalization of propagation impairments," *IEEE Photonics Technol. Lett.*, **16**(2), pp. 674–676, Feb. 2004. 38

[55] S. Bottacchi, *Noise and Signal Interference in Optical Fiber Transmission Systems* Wiley, 2008. 41

[56] J. R. Treichler, C. R. Johnson, and M. G. Larimore, *Theory and Design of Adaptive Filters* Prentice Hall, 2001. 46, 48

[57] D. Godard, "Self-recovering equalization and carrier tracking in two-dimensional data communication systems," *IEEE Trans. Commun.*, **28**(11), pp. 1867–1875, Nov. 1980. 46

[58] D. S. Millar and S. J. Savory, "Blind adaptive equalization of polarization-switched QPSK modulation," *Opt. Express*, **19**(9), pp. 8533–8538, Apr. 2011. 47

[59] M. Yan, Z. Tao, H. Zhang, W. Yan, T. Hoshida, and J. Rasmussen, "Adaptive blind equalization for coherent optical BPSK system," In *Proceedings of European Conference on Optical Communication*, 2010. 48

[60] S. J. Savory, G. Gavioli, R. I. Killey, and P. Bayvel, "Electronic compensation of chromatic dispersion using a digital coherent receiver," *Opt. Express*, **15**(5), pp. 2120–2126, Mar. 2007. 48

[61] I. Fatadin, D. Ives, and S. Savory, "Blind equalization and carrier phase recovery in a 16-QAM optical coherent system," *J. Lightwave Technol.*, **27**(15), pp. 3042–3049, Aug. 2009. 48, 49, 51, 106

[62] W. T. Silfvast, *Laser Fundamentals* Cambridge University Press, 2nd edition, 2008. 49

[63] M. Taylor, "Phase estimation methods for optical coherent detection using digital signal processing," *J. Lightwave Technol.*, **27**(7), pp. 901–914, Apr. 2009. 49, 51, 52, 90, 93, 102

[64] A. Viterbi and A. Viterbi, "Nonlinear estimation of PSK-modulated carrier phase with application to burst digital transmission," *IEEE Trans. Inf. Theory*, **29**(4), pp. 543–551, Jul. 1983. 50, 91

[65] T. Pfau, S. Hoffmann, and R. Noe, "Hardware-efficient coherent digital receiver concept with feedforward carrier recovery for M-QAM constellations," *J. Lightwave Technol.*, **27**(8), pp. 989 –999, Apr. 2009. 13, 51, 107, 108, 119

[66] K. Ho, *Phase Modulated Optical Communications Systems* Springer, 2005. 52, 90

[67] C. Xie, Y. Zhao, Z. Xiao, D. Chang, and F. Yu, "FEC for high speed optical transmission," In *Proceedings of Asia Communications and Photonics Conference (ACP)*, pages 83091R–1–83091R–4, 2011. 53

[68] Forward error correction for high bit-rate DWDM submarine systems, recommendation G. 975.1, 2004. 53

[69] F. Chang, K. Onohara, and T. Mizuochi, "Forward error correction for 100 G transport networks," *IEEE Commun. Mag.*, **48**(3), pp. S48 –S55, Mar. 2010. 53, 54, 70, 82

[70] B. Li, K. Larsen, D. Zibar, and I. Monroy, "Over 10 dB net coding gain based on 20% overhead hard decision forward error correction in 100G optical communication systems," In *Proceedings of European Conference on Optical Communication*, paper Tu.6.A.3, 2011. 53, 95

[71] T. Mizuochi, K. Ouchi, T. Kobayashi, Y. Miyata, K. Kuno, H. Tagami, K. Kubo, H. Yoshida, M. Akita, and K. Motoshima, "Experimental demonstration of net coding gain of 10.1 dB using 12.4 Gb/s block turbo code with 3-bit soft decision," In *Proceedings of Optical Fiber Communication Conference*, pages PD21–1, 2003. 53, 54, 70

[72] S. Dave, L. Esker, F. Mo, W. Thesling, J. Keszenheimer, and R. Fuerst, "Soft-decision forward error correction in a 40-nm asic for 100-Gbps OTN applications," In *Proceedings of Optical Fiber Communication Conference*, paper JWA14, 2011. 53, 70

[73] I. Fatadin, S. Savory, and D. Ives, "Compensation of quadrature imbalance in an optical QPSK coherent receiver," *IEEE Photonics Technol. Lett.*, **20**(20), pp. 1733–1735, Oct. 2008. 54

[74] S. Lloyd, "Least squares quantization in PCM," *IEEE Trans. Inf. Theory*, **28**(2), pp. 129–137, Mar. 1982. 55

[75] S. Makovejs, D. S. Millar, D. Lavery, C. Behrens, R. I. Killey, S. J. Savory, and P. Bayvel, "Characterization of long-haul 112Gbit/s PDM-QAM-16 transmission with and without digital nonlinearity compensation," *Opt. Express*, **18**(12), pp. 12939–12947, Jun. 2010. 55

[76] D. O. Caplan, "Laser communication transmitter and receiver design," *Journal of Optical and Fiber Communications Reports*, **4**(4-5), pp. 225–362, 2007. 10, 60, 70

[77] A. Phillips, R. Cryan, and J. Senior, "Optically preamplified pulse-position modulation for fibre-optic communication systems," *IEE Proceedings: Optoelectronics*, **143**(2), pp. 153–159, 1996. 61

[78] X. Liu, T. Wood, R. Tkach, and S. Chandrasekhar, "Demonstration of record sensitivity in an optically pre-amplified receiver by combining PDM-QPSK and 16-PPM with pilot-assisted digital coherent detection," In *Proceedings of Optical Fiber Communication Conference*, paper PDPB1, 2011. 10, 61, 70

[79] X. Liu, T. Wood, R. Tkach, and S. Chandrasekhar, "Demonstration of record sensitivities in optically preamplified receivers by combining PDM-QPSK and M-ary pulse-position modulation," *J. Lightwave Technol.*, **30**(4), pp. 406–413, Feb. 2012. 10, 61, 70

[80] M. Karlsson and E. Agrell, "Generalized pulse-position modulation for optical power-efficient communication," In *Proceedings of European Conference on Optical Communication*, paper Tu.6.B.6, 2011. 61

[81] D. J. Geisler, T. M. Yarnall, W. E. Keicher, M. L. Stevens, A. M. Fletcher, R. R. Parenti, D. O. Caplan, and S. A. Hamilton, "Demonstration of 2.1 photon-per-bit sensitivity for BPSK at 9.94-Gb/s with rate-$\frac{1}{2}$ FEC," In *Proceedings of Optical Fiber Communication Conference*, paper OM2C.6, 2013. 10, 70

[82] S. J. Savage, B. S. Robinson, D. O. Caplan, J. J. Carney, D. M. Boroson, F. Hakimi, S. A. Hamilton, J. D. Moores, and M. A. Albota, "Scalable modulator for frequency shift keying in free space optical communications," *Opt. Express*, **21**(3), pp. 3342–3353, Feb. 2013. 70

[83] B. S. Robinson, A. J. Kerman, E. A. Dauler, R. J. Barron, D. O. Caplan, M. L. Stevens, J. J. Carney, S. A. Hamilton, J. K. Yang, and K. K. Berggren, "781 Mbit/s photon-counting optical communications using a superconducting nanowire detector," *Opt. Lett.*, **31**(4), pp. 444–446, Feb. 2006. 70

[84] G. Agrawal, *Nonlinear Fiber Optics* Academic Press, 2001. 75

[85] J. Reis, P. Monteiro, and A. Teixeira, "Fiber nonlinear impact on hybrid ultra-dense WDM based optical networks," In *Proceedings of International Conference on Transparent Optical Networks (ICTON)*, paper Th.A1.5, 2010. 79, 117

[86] J. Reis, D. Neves, and A. Teixeira, "Physical impairments on high aggregate data rate passive coherent optical networks," In *In Proceedings on International Microwave Optoelectronics Conference (IMOC)*, pages 366–370, 2011. 79, 117

[87] P. Bohn and S. Das, "Return loss requirements for optical duplex transmission," *J. Lightwave Technol.*, **5**(2), pp. 243–254, Feb. 1987. 79

[88] A. Yoshida and T. Asakura, "Crosstalk-limited transmission distance in bidirectional fibre optic systems," *Pure and Applied Optics: Journal of the European Optical Society Part A*, **2**(6), pp. 701, 1993. 79

[89] A. Shahpari, J. D. Reis, R. Ferreira, D. M. Neves, M. Lima, and A. Teixeira, "Terabit+ (192 $\times$ 10 Gb/s) Nyquist shaped UDWDM coherent PON with upstream and downstream over a 12.8 nm band," In *Proceedings of Optical Fiber Communication Conference*, paper PDP5B.3, 2013. 85, 120

[90] M. Wale, "Photonic integration challenges for next-generation networks," In *Proceedings of European Conference on Optical Communication*, paper 1.7.4, 2009. 88, 116

[91] A. Beling, N. Ebel, A. Matiss, G. Unterborsch, M. Nolle, J. K. Fischer, J. Hilt, L. Molle, C. Schubert, F. Verluise, and L. Fulop, "Fully-integrated polarization-diversity coherent receiver module for 100g dp-qpsk," In *Proceedings of Optical Fiber Communication Conference*, paper OML5, 2011. 88

[92] K. Piyawanno, M. Kuschnerov, M. Alfiad, B. Spinnler, and B. Lankl, "Effects of mechanical disturbance on local oscillators and carrier synchronization," In *Proceedings of OptoeElectronics and Communications Conference (OECC)*, pages 124–125, 2010. 88

[93] J. Berger, Y. Zhang, J. Grade, H. Lee, S. Hrinya, H. Jerman, A. Fennema, A. Tselikov, and D. Anthon, "Widely tunable external cavity diode laser using a MEMS electrostatic rotary actuator," In *Proceedings of European Conference on Optical Communication*, paper TuA3.2, 2001. 88

[94] J. Buus, "Tunable laser sources for (D)WDM," *SPIE, Volume 5280 Materials, Active Devices, and Optical Amplifiers*, pages 172–181, 2004. 88

[95] F. Koyama, "Advances of vcsel photonics," In *Semiconductor Laser Conference (ISLC), 2012 23rd IEEE International*, pages 4–5, 2012. 88

[96] A. Ward, D. Robbins, G. Busico, E. Barton, L. Ponnampalam, J. Duck, N. Whitbread, P. Williams, D. C. J. Reid, A. Carter, and M. Wale, "Widely tunable DS-DBR laser with monolithically integrated SOA: design and performance," *IEEE J. Sel. Top. Quantum Electron.*, **11**(1), pp. 149–156, Jan.-Feb. 2005. 88

[97] M. Lu, H.-C. Park, A. Sivananthan, J. Parker, E. Bloch, L. Johansson, M. Rodwell, and L. Coldren, "Monolithic integration of a high-speed widely tunable optical coherent receiver," *IEEE Photonics Technol. Lett.*, **25**(11), pp. 1077–1080, Jun. 2013. 88

[98] L. Coldren and S. Corzine, *Diode Lasers and Photonic Integrated Circuits* Wiley-Interscience, 1995. 89, 94

[99] I. Fatadin, D. Ives, and S. J. Savory, "Differential carrier phase recovery for QPSK optical coherent systems with integrated tunable lasers," *Opt. Express*, **21** (8), pp. 10166–10171, Apr. 2013. 89

[100] T. N. Huynh, F. Smyth, L. Nguyen, and L. P. Barry, "Effects of phase noise of monolithic tunable laser on coherent communication systems," *Opt. Express*, **20** (26), pp. B244–B249, Dec. 2012. 89

[101] Spectral grids for WDM applications: DWDM frequency grid, recommendation ITU-T G.694.1, 2010. 89

[102] R. Maher and B. Thomsen, "Dynamic linewidth measurement technique using digital intradyne coherent receivers," *Opt. Express*, **19**(26), pp. B313–B322, Dec. 2011. 90, 105

[103] M. C. Cox, N. J. Copner, and B. Williams, "High sensitivity precision relative intensity noise calibration standard using low noise reference laser source," *IEE Proceedings: Science, Measurement and Technology*, **145**(4), pp. 163–165, 1998. 90

[104] B. Zhang, C. Malouin, and T. J. Schmidt, "Design of coherent receiver optical front end for unamplified applications," *Opt. Express*, **20**(3), pp. 3225–3234, Jan. 2012. 93, 94

[105] M. A. Newkirk and K. J. Vahala, "Large (14.5 dB) reduction of intensity noise from a semiconductor laser by amplitude-phase decorrelation," *Appl. Phys. Lett.*, **60**(11), pp. 1289–1291, Mar. 1992. 94

[106] L.-S. Fock, A. Kwan, and R. Tucker, "Reduction of semiconductor laser intensity noise by feedforward compensation: experiment and theory," *J. Lightwave Technol.*, **10**(12), pp. 1919–1925, Dec. 1992. 94

[107] M. Morsy-Osman, Q. Zhuge, L. R. Chen, and D. V. Plant, "Feedforward carrier recovery via pilot-aided transmission for single-carrier systems with arbitrary M-QAM constellations," *Opt. Express*, **19**(24), pp. 24331–24343, Nov. 2011. 102

[108] F. Aflatouni and H. Hashemi, "Light source independent linewidth reduction of lasers," In *Proceedings of Optical Fiber Communication Conference*, paper OW1G.6, 2012. 12, 102, 103

[109] I. Kim, O. Vassilieva, P. Palacharla, and M. Sekiya, "Feed-forward optical carrier phase noise compensation in m-qam transmitter," In *Proceedings of Opto-Electronics and Communications Conference*, pages 148–149, 2012. 102

[110] A. Sivananthan, H. chul Park, M. Lu, J. S. Parker, E. Bloch, L. A. Johansson, M. J. Rodwell, and L. A. Coldren, "Monolithic linewidth narrowing of a tunable sg-dbr laser," In *Proceedings of Optical Fiber Communication Conference*, paper OTh3I.3, 2013. 102

[111] I. Fatadin and S. J. Savory, "Impact of phase to amplitude noise conversion in coherent optical systems with digital dispersion compensation," *Opt. Express*, **18**(15), pp. 16273–16278, Jul. 2010. 102

[112] M. Secondini, G. Meloni, T. Foggi, G. Colavolpe, L. Poti, and E. Forestieri, "Phase noise cancellation in coherent optical receivers by digital coherence enhancement," In *Proceedings of European Conference on Optical Communication*, paper P4.17, 2010. 12, 102, 103, 104

[113] M. Secondini, G. Meloni, G. Berrettini, and L. Potì, "How to use a low-cost DFB local oscillator in ultra-long-haul uncompensated coherent systems," In *Proceedings of European Conference on Optical Communication*, paper Th.2.C.5, 2012. 102

[114] Z. Zan and A. J. Lowery, "Experimental demonstration of a flexible and stable semiconductor laser linewidth emulator," *Opt. Express*, **18**(13), pp. 13880–13885, Jun. 2010. 104

[115] A. Sano, T. Kobayashi, S. Yamanaka, A. Matsuura, H. Kawakami, Y. Miyamoto, K. Ishihara, and H. Masuda, "102.3-Tb/s (224 x 548-Gb/s) C- and extended L-band all-Raman transmission over 240 km using PDM-64QAM single carrier FDM with digital pilot tone," In *Proceedings of Optical Fiber Communication Conference*, 2012. 13, 107, 108

[116] M. S. Faruk and K. Kikuchi, "Adaptive frequency-domain equalization in digital coherent optical receivers," *Opt. Express*, **19**(13), pp. 12789–12798, Jun. 2011. 109

[117] H.-M. Chin, D. Millar, and S. Savory, "Fixed point precision requirements of the cma for digital coherent access," In *Proceedings of IEEE Photonics Conference*, pages 453–454, 2012. 109

[118] A. D. Poularikas and Z. M. Ramadan, *Adaptive Filtering Primer with MATLAB* Taylor and Francis, 2006. 110

[119] A. Wenzler and E. Luder, "New structures for complex multipliers and their noise analysis," In *IEEE International Symposium on Circuits and Systems*, volume 2, pages 1432–1435 vol.2, 1995. 111

[120] L. Nelson, X. Zhou, R. Isaac, Y. Lin, J. Chon, and W. I. Way, "Colorless reception of a single 100Gb/s channel from 80 coincident channels via an intradyne coherent receiver," In *Proceedings of IEEE Photonics Conference*, pages 240–241, 2012. 117

[121] P. Winzer, "High-spectral-efficiency optical modulation formats," *J. Lightwave Technol.*, **30**(24), pp. 3824–3835, Dec. 2012. 119

[122] E. Ip and J. Kahn, "Carrier synchronization for 3- and 4-bit-per-symbol optical transmission," *J. Lightwave Technol.*, **23**(12), pp. 4110–4124, Dec. 2005. 134

A

Sensitivity formulae

In the work described herein, it has been necessary to produce a theoretical relationship between BER and OSNR or received optical power (which is directly related to OSNR). This relationship is defined for all the modulation formats used in the above figures in terms of Q-function, which in turn is described in terms of the complementary error function as:

$$Q(x) = \frac{1}{2}\operatorname{erfc}\left(\frac{x}{\sqrt{2}}\right) \tag{A.1}$$

for arbitrary real x. In the following, OSNR is denoted in terms of $\frac{\mathcal{E}_{bavg}}{N_0}$, where N_0 is the total noise power and $\mathcal{E}_{bavg}$ is the average energy per bit. $\mathcal{E}_b$ is used where all possible symbols have equivalent energy.

Receiver sensitivity when using IM-DD

Intensity modulation with direct detection (IM-DD) is a transceiver scheme where optical OOK is modulated and transmitted over fibre, and a simple square-law photodiode is employed at the receiver. This non-coherent scheme was included for comparison in this work, as it is currently used in optical access networks such as the GPON.

The probability of a bit error, P_b, for this format is as follows [47]

$$P_{b,\text{IM-DD}} = \frac{1}{2}\exp\left(-N_p\right) \tag{A.2}$$

where N_p is the received photons in each '1' level bit. (Note, however, that this limit assumes that all out of band receiver noise sources are rejected, which is not the case for any practical receiver.)

Receiver sensitivity when using M-PSK

The formulae in this section are from reference [51]. For arbitrary M-*ary* PSK, the Symbol Error Rate (SER)-OSNR relationship is as follows

$$P_{e,MPSK} \approx 2Q\left(\sqrt{(2\log_2 M)sin^2\left(\frac{\pi}{M}\right)\frac{\mathcal{E}_b}{N_0}}\right) \tag{A.3}$$

For QPSK, this reduces to

$$P_{e,QPSK} = 2Q\left(\sqrt{\frac{2\mathcal{E}_b}{N_0}}\right)\left[1-\frac{1}{2}Q\left(\sqrt{\frac{2\mathcal{E}_b}{N_0}}\right)\right] \tag{A.4}$$

and for BPSK, this is

$$P_{b,BPSK} = P_e = Q\left(\sqrt{\frac{2\mathcal{E}_b}{N_0}}\right) \tag{A.5}$$

The approximation used to calculate BER from SER is $P_b \approx P_e/\log_2(M)$. Note that BPSK and QPSK have the same BER-OSNR relationship.

Receiver sensitivity when using M-QAM

The following formulae are from reference [51]. They apply to all M-*ary* QAM where M is a square number.

$$\begin{aligned} P_{e,MQAM} = 4\left(1-\frac{1}{\sqrt{M}}\right)Q\left(\sqrt{\frac{3\log_2 M}{M-1}\frac{\mathcal{E}_{bavg}}{N_0}}\right) \\ \times\left(1-\left(1-\frac{1}{\sqrt{M}}\right)Q\left(\sqrt{\frac{3\log_2 M}{M-1}\frac{\mathcal{E}_{bavg}}{N_0}}\right)\right) \end{aligned} \tag{A.6}$$

Once again, the approximation used for calculating BER is $P_b \approx P_e/\log_2(M)$. Note that the BER-OSNR relationship for 8-QAM, as it is not Gray-coded, requires an iterative solution, which is obtained using the procedure outlined in reference [122].

Receiver sensitivity when using PS-QPSK

The following formulae are taken directly from [50], and pertain to the modulation format PS-QPSK. First, the SER-OSNR relationship:

$$P_{e,PS-QPSK} = Q\left(\sqrt{2\frac{\mathcal{E}_{savg}}{N_0}}\right) + \frac{1}{\sqrt{\pi}}\int_0^\infty (3-3\,\mathrm{erfc}\,x+\mathrm{erfc}^2 x)\,\mathrm{erfc}(x)e^{-\left(x-\frac{\mathcal{E}_{savg}}{N_0}\right)^2}dx \tag{A.7}$$

This needs to be evaluated numerically; achieved in this work using the *quadgk* function in MATLAB. It is possible to approximate the BER from the SER as

$$P_{b,PS-QPSK} \approx P_{e,PS-QPSK}/2 \tag{A.8}$$

however, this approximation includes only the six most likely of the seven possible symbol errors. The actual theoretical BER limit is given by the following

$$P_{e7,PS-QPSK} = \frac{1}{2} - \frac{1}{2\sqrt{(\pi)}} \int_{-\infty}^{\infty} (1 - \mathrm{erfc}\, x)^3 \exp^{-\left(x - \sqrt{\frac{\mathcal{E}_{savg}}{N_0}}\right)} dx \tag{A.9}$$

and this is the formula used herein. Note that, the seventh bit error does not significantly contribute to the BER, with the result from equation (A.8) deviating from equation (A.9) by only 10^{-4} dB at a BER of 10^{-2}.

Coherent Pulse Position Modulation

In chapter 3, reference is made to the high sensitivity modulation format pulse position modulation (PPM). Here, details of pulse position modulation are given, to explain both the high sensitivity of this format, and the bandwidth expansion factor.

This format is a form of orthogonal signalling in the time domain as shown in Fig. A.1. For M-*ary* PPM, a burst of photons is transmitted in one of M time slots, encoding $\log_2(M)$ bits of information across M slots. With an increase in M, there is an increase in transmitter and receiver bandwidth requirements for a fixed data rate, however, the receiver sensitivity also improves. The reason for the improved receiver

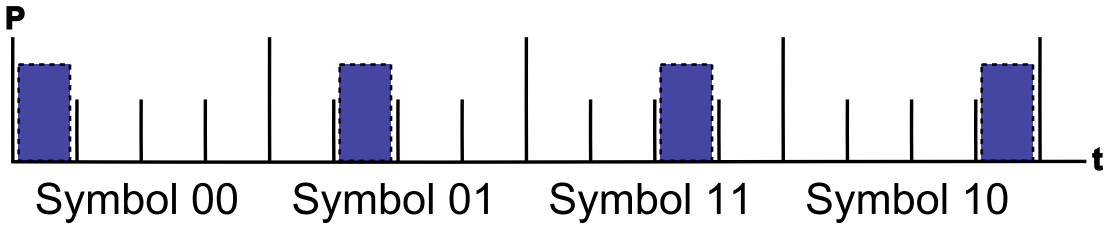

Figure A.1: Example of the bit mapping for 4-PPM. In each symbol, there are 4 slots of which only one will contain power.

sensitivity is in part due to the low average power of the signal (signal power is averaged over the symbol) but also that the peak slot power carries all the information of the symbol.

Aside from the reduced data rate per unit bandwidth, PPM presents practical issues such as difficulties with equalisation, slot synchronisation, and false alarms (wrong-slot error). Nevertheless, if the overall data rate is not a factor of a system's design (as is often the case in deep-space communications), then PPM is a good choice of modulation format, as it can be combined with FEC and direct detection receivers to maximise sensitivity whilst minimising system complexity.

B

Additional RIN Compensation Results

These graphs, Fig. B.1 and the equivalent contour plots Fig. B.2, represent the full experimentally obtained data set used in chapter 5 (back-to-back configuration). When an ECL is used as the local oscillator (Fig. B.1(a,b)) the filter length is always optimised for a larger window length of the RIN compensating filter. This implies that the ideal cut-off frequency of this filter is much lower, which corroborates the theory of RIN compensation when considering the RIN spectra shown in Fig. 5.2.

Further, consider Fig. B.1(c,d), where the LO laser is a DS-DBR laser. Here, the optimum window length is dependent on the received power. This gives credence to the theory that the impact of RIN is greatest for low signal powers.

Finally, note that in all four cases, because of the particular receiver DSP employed (differential on field), the receiver performance is independent of the linewidth (and indeed the RIN) of the signal laser.

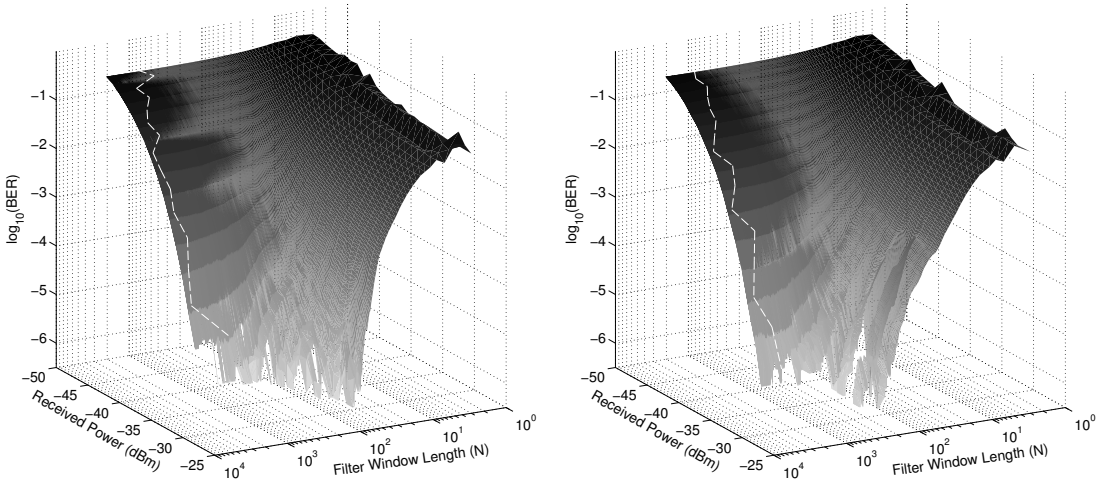

(a) ECL Signal - ECL LO

(b) DS-DBR Signal - ECL LO

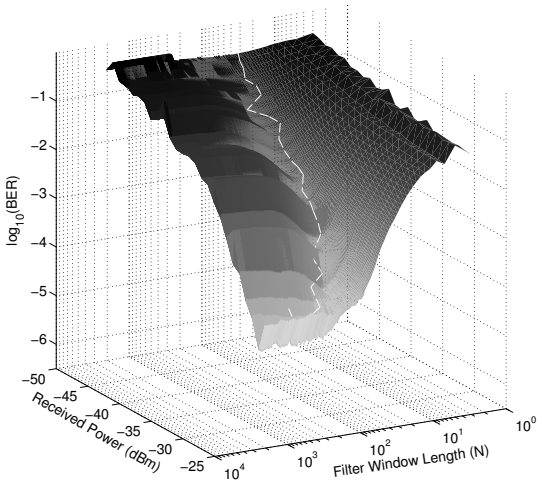

(c) ECL Signal - DS-DBR LO

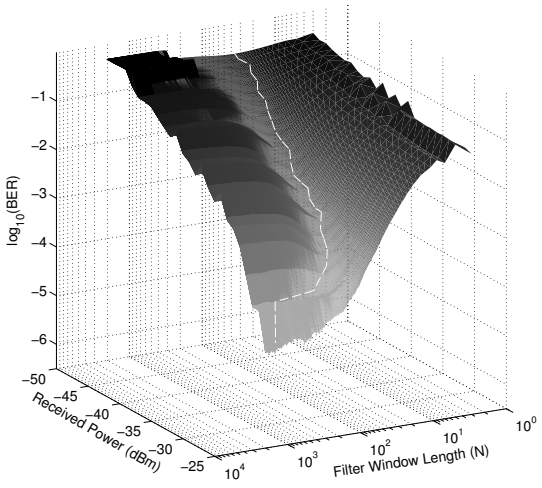

(d) DS-DBR Signal - DS-DBR LO

Figure B.1: Relationship between received power, BER, and the length of the RIN compensating filter window for 3 GBd PDM-QPSK when using different signal (transmitter) and local oscillator lasers. In each case, the white dashed line indicates the the filter length which minimises BER for each received power.

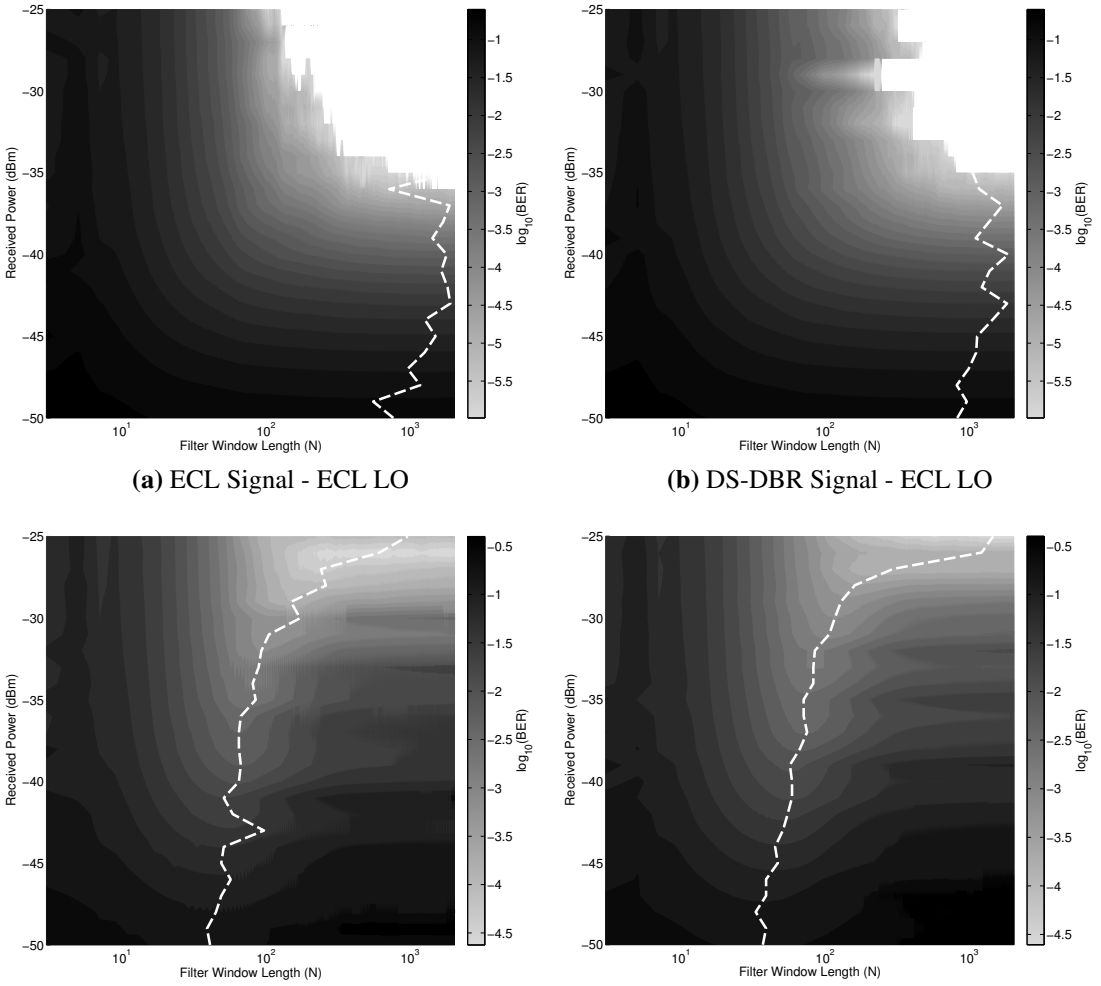

(a) ECL Signal - ECL LO

(b) DS-DBR Signal - ECL LO

(c) ECL Signal - DS-DBR LO

(d) DS-DBR Signal - DS-DBR LO

Figure B.2: Contour plots showing the relationship between received power, BER, and the length of the RIN compensating filter window for 3 GBd PDM-QPSK when using different signal (transmitter) and local oscillator lasers. In each case, the white dashed line indicates the the filter length which minimises BER for each received power.

C Acronyms

AC	Alternating Current
ADC	Analogue-to-Digital Converter
ASE	Amplified Spontaneous Emission
ASIC	Application-Specific Integrated Circuit
AOM	Acousto-Optical Modulator
AON	Active Optical Network
ArbWG	Arbitrary Waveform Generator
AWG	Arrayed Waveguide Grating
AWGN	Additive White Gaussian Noise
BER	Bit Error Rate
BPSK	Binary Phase Shift Keying
CPE	Carrier Phase Estimation
CMA	Constant Modulus Algorithm
CMRR	Common Mode Rejection Ratio
CW	Continuous Wave
DAC	Digital-to-Analogue Converter
DC	Direct Current
DD	Direct Detection

DFB Distributed Feedback

DS-DBR Digital Supermode Distributed Bragg Reflector

DSO Digital Storage Oscilloscope

DSP Digital Signal Processing

DWDM Dense Wavelength Division Multiplexing

ECL External Cavity Laser

EDFA Erbium Doped Fibre Amplifier

ENOB Effective Number of Bits

FEC Forward Error Correction

FIR Finite Impulse Response

FTTx Fibre to the Node, Curb, Building, or Home

GPON Gigabit-Capable Passive Optical Network

ISI Inter-Symbol Interference

ITU International Telecommunication Union

LO Local Oscillator Laser

LR-PON Long-Reach Passive Optical Network

MIMO Multiple Input Multiple Output

MZM Mach-Zehnder Modulator

NEXT Near End Crosstalk

OEO Optical-Electrical-Optical conversion

OLT Optical Line Terminal

ONU Optical Network Unit

OOK On-Off Keying

OSA Optical Spectrum Analyser

OSNR Optical Signal-to-Noise Ratio

PBC Polarisation Beam Combiner

PBS Polarisation Beam Splitter

PC Polarisation Controller

PDL Polarisation Dependent Loss

PDM Polarisation Division Multiplexing

PON Passive Optical Network

PPM Pulse Position Modulation

PRBS Pseudo-Random Binary Sequence

PS Polarisation Switched

PSK Phase Shift Keying

QAM Quadrature Amplitude Modulation

QPSK Quadrature Phase Shift Keying

RIN Relative Intensity Noise

RF Radio Frequency

SER Symbol Error Rate

SG-DBR Sampled Grating Distributed Bragg Reflector

SMF Single-Mode Fibre

SNR Signal-to-Noise Ratio

SOP State of Polarisation

TDM Time Division Multiplexing

TIA TransImpedance Amplifier

UDWDM Ultra Dense Wavelength Division Multiplexing

VCSEL Vertical-Cavity Surface-Emitting Laser

VOA Variable Optical Attenuator

WDM Wavelength Division Multiplexing